FLUXES OF ORGANIC POLLUTANTS FROM THE SEDIMENTS IN BOSTON HARBOR

by

Hsiao-Wen Chen

S.B., Environmental Engineering
National Cheng Kung University, 1991

Submitted to the Department of
Civil and Environmental Engineering
in Partial Fulfillment of the Requirements for the Degree of

Master of Science
in Environmental Engineering

at the

Massachusetts Institute of Technology

September 1993

Signature of Author _____
Department of Civil and Environmental Engineering
August 6, 1993

Certified by _____
Philip M. Gschwend
Professor, Department of Civil and Environmental Engineering
Thesis Supervisor

Accepted by _____
Eduardo Kausel
Chairman, Departmental Committee on Graduate Studies

FLUXES OF ORGANIC POLLUTANTS FROM THE SEDIMENTS IN BOSTON HARBOR

by

Hsiao-Wen Chen

Submitted to the Department of Civil and Environmental Engineering
on August 6, 1993 in partial fulfillment of the requirements for the degree of
Master of Science in Environmental Engineering

ABSTRACT

The sediments in Boston Harbor have been contaminated by toxic organic chemicals, such as polycyclic aromatic hydrocarbons (PAHs). The release of these pollutants to the overlying water column deteriorates the water quality of the harbor. This study reviews the transport mechanisms and desorption kinetics in sediments and develops an analytical model to calculate the fluxes of the pollutants across the sediment-water interface.

The estimated fluxes from Boston Harbor sediments range from 110 to 4300 ng/cm^2.yr for pyrene and from 10 to 280 ng/cm^2.yr for benzo[a]pyrene. The resulting loadings of pyrene and benzo[a]pyrene to the harbor water are 140 - 1400 kg/yr and 9.6 - 96 kg/yr, respectively. The results indicate that the sediment bed is the major source of organic pollutants to the Boston Harbor water.

This model also identifies the factors that critically control the release of organic pollutants from sediments. Sediments with a larger bioturbation coefficient cause a greater flux, and the flux from sediments of higher organic carbon content is smaller. The diffusive water boundary layer is another important factor; the thinner the layer is, the greater the flux is. The nature of organic pollutants also controls the flux. A chemical of lower organic carbon-water distribution coefficient has a higher tendency to leave the sediments. Furthermore, this study shows that the flux due to molecular diffusion and bioturbation (the diffusive flux) is much greater than the flux due to biological irrigation. For the diffusive flux, the resistance in the diffusive water boundary layer is more important than the resistance in the sediment bed.

Thesis Supervisor : Dr. Philip M. Gschwend
Title : Professor of Civil and Environmental Engineering

ACKNOWLEDGMENTS

The person I appreciate most is my advisor, Phil Gschwend, the most enthusiastic teacher in the world. I am grateful for his guidance and inspiration to my academic and personal life, and for his patience and understanding. The best thing that can happen to an MIT student is having an advisor like him. I would also like to thank Dr. Eric Adams for the advice on the development of the model and for his critical review of the manuscript of this thesis. Charles Wong's Master's thesis is the foundation of this thesis. I also thank him for his friendship.

This thesis would never have been done without the field data generously provided by the people involved in the investigation of the Boston Harbor sediments. The PAH data were from Susan McGroddy, and the ^{234}Th data were from Gordon Wallace. The sediment sampling was conducted by them as well as John Farrington, Hovey Clifford. I would also like to thank Charles Wong and Allison MacKay for the ^{222}Rn sorption experiments.

It has been fun to be with the research group. I especially appreciate John MacFarlance, who knows everything and can solve every problem in the laboratory. The beautiful map of Boston Harbor in this thesis was created by his "magic". Joe Ryan and Britt Holmén are the ones I look up to. I thank Örjan Gustafsson and Tom Ravens for those inspiring talks. Allison MacKay reminds me how much a smart and diligent person can achieve. Tom Carlin's tips on everything always work. I thank Mehran Islam for assisting me doing the sewage PAH analysis.

I have been very fortunate to meet many nice people. Peter and Dianne Connolly, Bruce and Cathy Jacobs have made my life half a world away from home easier. The advice from J.J. Lee and C.C. Sun has helped me survive at MIT. I appreciate the good times brought by the gang: Yi-Ching, Iris, Florence, Joey, "Prince" Huang, and "Little Tale". I particularly thank Yi-Ching Yang, the best nurse in the world, for taking good care of me when I needed it most. The friendship from the old friends on the other side of the world also has given me the strength to keep going. I thank Wen-Ching, Caesar, M.D., Frances, Jack, and other pals from National Cheng Kung University. I am deeply grateful for the support from Hsin-Yi and her mother, Mrs. Hu. Special thanks that words can not express go to my best friend Zin.

Most importantly, I would like to thank my parents, grandfather and late grandmother for their endless love and sacrifice. I also thank my sisters and brother for always being there listening to me.

This thesis was funded by EPA grant R-817145-01-0, NSF grant 8714110-CES, the National Sea Grant College Program (a part of the National Oceanic and Atmospheric Administration), and the Massachusetts Water Resources Authority.

TABLE OF CONTENTS

LIST OF TABLES

LIST OF FIGURES

CHAPTER 1

INTRODUCTION

1.1 Background

Boston Harbor has been heavily polluted by municipal and industrial sewage, which contains toxic organic chemicals, such as polycyclic aromatic hydrocarbons (PAHs), polychlorinated biphenyls (PCBs), and pesticides. Many studies of the pollution in Boston Harbor have been conducted. Battelle Ocean Sciences (1991) and Menzie-Cura & Associates (1991) studied the sources of pollutants; Shiaris and Jambard-Sweet (1986) investigated the distribution of PAHs; and the fate of the pollutants in Boston Harbor has also been studied (Chin and Gschwend 1991, 1992; Chin et al. 1991; Butman et al. 1992; Wong 1992). Shiaris and Jambard-Sweet's investigation in 1986 suggested that the major inputs of PAHs were urban runoff and the overflow of the raw sewage from the Moon Island pumping station during heavy rainfall. Similarly, the study by Menzie-Cura & Associates in 1991 concluded that the effluent and sludge from the sewage plants at Deer Island and Nut Island were the major contributors of PAHs to the harbor and that urban runoff was the second most important source.

Although now the major source of the pollutants introduced to Boston Harbor is the effluent of the sewage plants, the Massachusetts Water Resources Authority (MWRA) is changing the locations of the outfalls from Boston Harbor to Massachusetts Bay. The new outfalls will begin operation in 1995 (Butman et al. 1992). It will be interesting to

find out which pollution source will become the most important one after the discharge of effluent into Boston Harbor stops.

The release of pollutants from the sediments is one of the issues that needs to be reviewed. Because of their hydrophobic nature, many organic chemicals tend to accumulate in the sediments. If the chemical concentration of the seawater decreases, the concentration gradient from the sediment bed to the overlying seawater eventually changes from negative to positive. The chemicals accumulated in the sediments are, therefore, driven back into the overlying water. Since the sediment bed is an abundant source of organic chemicals, it is necessary to evaluate the chemical fluxes from the sediment bed across the sediment-water interface.

Wong (1992) developed a numerical model to calculate the fluxes of pyrene and benzo[a]pyrene from an disturbed sediment back to the overlying water. The model estimated the fluxes from the sediment bed, in which the dissolved concentration and the sorbed concentration were assumed to be in equilibrium, for 30 years, under various conditions. However, Wong was unable to use this numerical model to calculate the flux at the sites where the particle mixing was so extensive that the sediment-water exchange was limited by a very thin stagnant boundary layer within the overlying water (which will be discussed in Section 2.5). This caused a dilemma as to choosing the model space interval. Using a space interval larger than the thickness of this boundary layer would underestimate the flux out of the sediments; however, setting the space interval to be as small as the thickness of this boundary layer would greatly increase the number of space, and hence time, steps required for run accuracy. In addition to this limitation of the

model, Wong suggested that sorption kinetics may control the flux if transport processes are fast compared with sorption kinetics; therefore, more research concerning the sorption in sediments was needed.

1.2 Objectives

One objective of this research was to develop a model to calculate the fluxes of organic chemicals from the sediments. This model needed to be simple, but applicable to general marine environments. It also had to be able to describe the movement of organic pollutants not only dissolved in the porewater, but also associated with the colloids and sorbed in/on the solids in the sediment bed. Furthermore, it was intended to identify the transport mechanisms and the characteristics of the sediment bed that are critical for controlling the flux of organic chemicals. Therefore, people who are interested in investigating the flux of organic chemicals from sediments can recognize the most important factors limiting exchange.

Another objective of the research was to define a desorption enhancement factor. It is important to quantify the effect of desorption because a large fraction of each organic chemical is associated with the solid matrix in the sediment bed. While the fraction of the chemical dissolved in the porewater is able to directly travel into the overlying water column, the fraction of the chemical sorbed in/on the solids must first desorb. This situation may result in sorptive disequilibrium for some intervals within the bed. To maintain equilibrium, part of the sorbed fraction is released into the porewater, and, consequently, enhances the flux across the sediment-water interface.

The final objective was to use the model to calculate the organic chemical fluxes from the sediments in Boston Harbor. The goal was to compare the amount of pollutants coming out of the sediment bed with other pollution sources and thus to decide the significance of the chemical flux from the sediments after sewage releases are discontinued. These results would then contribute to decisions regarding the necessity to clean up the sediments in the harbor.

1.3 Outline of the Thesis

This thesis consists of three chapters. Chapter 2 describes the development of the flux model. First, the physical structure of the system is depicted, and the transport mechanisms, as well as the characteristics of the sediment bed, are discussed individually. Second, the governing equations of the concentrations of dissolved species, colloidal species, and sorbed species are defined. The desorption enhancement factor and the flux equation are subsequently derived. The limitation of using this model is also included. Last, a sensitivity analysis is described. The results indicate the factors that critically control the flux across the sediment-water interface.

Chapter 3 presents the application of the model; the fluxes of pyrene and benzo[a]pyrene from the sediments at the study sites are calculated using this model. First, the study sites in Boston Harbor are described in brief. Next, the determination of the parameter values is explained, followed by the calculation of the fluxes. Finally, the flux estimates from the model are then used to estimate the loadings of pyrene and benzo[a]pyrene to the water in Boston Harbor from the sediments. The results are

compared with the loadings from other sources to determine the significance of the organic pollutant fluxes from the sediments.

CHAPTER 2

FLUX MODEL FOR THE TRANSFER OF ORGANIC CHEMICALS BETWEEN BED SEDIMENTS AND THE WATER COLUMN

2.1 Review of Previous Research on Sediment-Water Exchange

Several studies of sediment-water exchange have been carried out. Some researchers directly measured chemical fluxes across the sediment-water interface by placing chambers on the sea bottom and observing the buildup of chemicals (Hale 1974; McCaffrey et al. 1980; Devol 1987; Broman et al. 1990; Archer and Devol 1992; Ciceri et al. 1992). In addition to direct measurement, most researchers developed models to describe the sediment environments. These models were based on Fick's first law of diffusion:

$$F_x = -D\frac{dC}{dx} \quad [M \cdot L^{-2} \cdot T^{-1}] \tag{2-1}$$

where F_x is the mass flux per unit area per unit time in the x direction, D [L^2 T^{-1}] is the diffusion coefficient, and dC/dx [ML^{-3}/L] is the concentration gradient along x. In order to calculate the flux, researchers took core samples from the sediment bed and analyzed the chemicals to obtain their concentration profiles (Emerson et al. 1984; Kadko and Heath 1984; Brownawell 1986; Kadko et al. 1987; Martin and Sayles 1987; Chin et al. 1991). Then the various investigators used the concentration gradients at the sediment surface to calculate the flux.

There is a serious problem in the concentration-gradient method. As indicated by Santschi et al. (1983), there is no measurable porewater gradient for situations where the resistance posed by the boundary layer above the sediment-water interface is comparable to or greater than that posed by transport within the sediment bed. The transition from the sea bottom water concentration to the equilibrium porewater concentration could occur over a distance of a few millimeters or less, which would be unresolved in core measurement. Therefore, we may underestimate the fluxes by using the concentration gradient obtained from core analysis. As for the direct measurement method, this approach can only give us the magnitude of the flux, but not help us understand the processes governing exchange.

2.2 Physical Picture of the Model

To formulate the sediment-water exchange model, first we have to define the environmental system and the transport mechanisms that drive the chemicals within the sediment bed and across the sediment-water interface. The sediment-water environment can be divided into three layers according to the transport mechanisms: the *turbulent water layer*, the *diffusive boundary water layer* over the sediment surface, and the *biologically active sediment bed* (Figure 2.1). For shallow waters ($\lesssim$ 10 m), turbulent diffusion is the dominant transport process in most of the overlying water column for vertical fluxes (Boudreau and Guinasso 1982). The turbulent motion in this layer is fast enough to homogenize chemical concentrations and, therefore, generally does not limit the vertical movement of chemicals out of the bed sediments. In contrast, in the diffusive

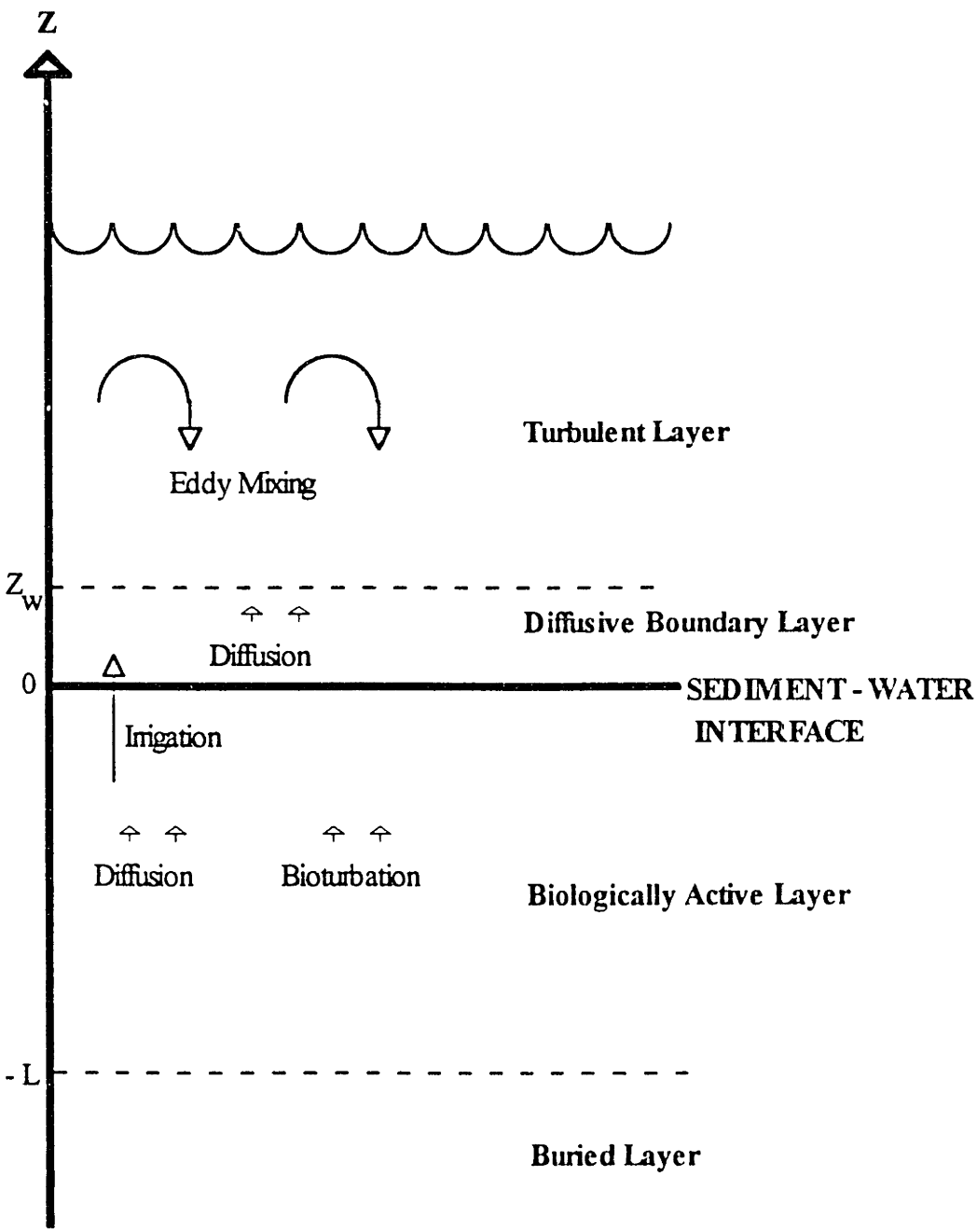

Figure 2.1 Physical picture of the environmental system

boundary layer, which is the thin layer immediately adjacent to the sediment-water interface, turbulence is suppressed by viscous forces. As a result, molecular diffusion becomes the dominant transport mechanism for dissolved species (Wimbush and Munk 1970; Thibodeaux 1979; Boudreau and Guinasso 1982; Jørgensen and Marais 1990).

The third layer is the biologically active layer in the sediment bed, where the sediments are stirred by the activities of benthic organisms. These activities are classified into two categories: *bioturbation* and *irrigation*. Bioturbation is a random mixing of sediments and the associated porewater by the feeding and burrowing behavior of benthic organisms (Goldberg and Koide 1962; Berner 1980; Brownawell 1986) and is usually quantified using a *bioturbation coefficient*, analogous to a diffusion coefficient. Irrigation is a non-local biological advective solute transport process, which allows exchange between the sediments and the overlying water column (Imboden 1981; Emerson et al. 1984; Boudreau 1986). The magnitude of the bioturbation coefficient is typically comparable to or less than a molecular diffusion coefficient; therefore, the release of a chemical from sediments is controlled, not only by bioturbation and irrigation, but also by molecular diffusion.

The model presented in this thesis is a two-box model. The environmental system of this model consists of only two of the three layers described above: the diffusive water boundary layer and the biologically active sediment bed. At this stage, the turbulent water layer is assumed to have negligible effects on sediment-water exchange for the chemicals.

2.3 Transport Mechanisms

2.3.1 Molecular diffusion in sediment beds

Molecular diffusion is an important transport mechanism in porewater because the movement of the porewater is not turbulent. The diffusivity of a chemical depends not only on the properties of the chemical but also on the condition of the porewater. Hayduk and Laudie (1974) proposed a method to estimate the aqueous solution diffusivity (D_m):

$$D_m = \frac{13.26 \times 10^{-5}}{\mu^{1.14} \cdot \bar{V}^{0.589}} \quad (cm^2/s) \tag{2-2}$$

where μ (centipoise or 10^{-2} g/cm·s) is the solution viscosity at the temperature of interest, and $\bar{V}$ is the molar volume of the liquid chemical (cm^3/mol). The molar volume of the liquid chemical can be estimated from the LeBas method (Lyman et al. 1991) using the additive volume increments listed in Table 2.1 (Reid et al. 1977).

The diffusivity of a dissolved species in a sediment bed is determined by correcting its aqueous solution diffusivity for the tortuosity and porosity of the sediments. The relationship between the sediment diffusivity (D'_m) and the aqueous diffusivity is

$$D'_m = \frac{D_m}{\theta^2} \tag{2-3}$$

where θ is the *geometric tortuosity* (Ullman and Aller 1982; Di Toro et al. 1985). The tortuosity can be expressed as

Table 2.1 Additive volume increments for calculating LeBas molar volume (Reid et al. 1977)

Atom	Increment (cm^3/mol)	Atom	Increment (cm^3/mol)
C	14.8	Br	27.0
H	3.7	Cl	24.6
O (except as noted below)	7.4	F	8.7
In methyl esters and ethers	9.1	I	37.0
In ethyl esters and ethers	9.9	S	25.6
In higher esters and ethers	11.0		
In acids	12.0	Ring	
Joined to S, P, N	8.3	3-Membered	- 6.0
		4-Membered	- 8.5
N		5-Membered	-11.5
Double bonded	15.6	6-Membered	-15.0
In primary amines	10.5	Naphthalene	-30.0
In secondary amines	12.0	Anthracene	-47.5

$$\theta^2 = \phi F \tag{2-4}$$

where ϕ is the porosity of the sediments, and F is the formation resistivity factor. Archie (1942) found an empirical relationship between the formation resistivity factor and the sediment porosity:

$$F = \phi^{-m}. \tag{2-5}$$

Therefore,

$$D_m' = D_m \phi^{(m-1)}. \tag{2-6}$$

Archie found m = 1.3 - 2 for sands and sandstones. Atkins and Smith (1961) and Atlan et al. (1969) reported m = 2.5 - 5.4 for clays. Ullman and Aller (1982) suggested that m was related to the porosity; m = 3 for $\phi \geq 0.7$, and m = 2 for $\phi < 0.7$. Thus, $D'_m = D_m \cdot \phi^2$ for $\phi \geq 0.7$, and $D'_m = D_m \cdot \phi$ for $\phi < 0.7$.

Organic chemicals in porewater include those associated with organic colloids, which include macromolecules that are comprised of both humic and labile components (Chin et al. 1991). Therefore, the diffusion of colloids also plays a role in the transport of organic chemicals in sediments. Aqueous colloidal diffusivity (D_c) is a function of the size and shape of the molecules and can be estimated using the following equation (Chin et al. 1991):

$$D_c = aM^{-b} \qquad (2\text{-}7)$$

where M is the molecular weight of the macromolecule, and a and b are empirical constants. Chin et al. (1991) estimated the aqueous colloidal diffusivity to be between 1 and 6×10^{-6} cm^2/s.

2.3.2 Biological transport processes

The activities of benthic organisms, such as ingestion and excretion, burrowing, tube building, and biodeposition, can redistribute particles in sediment beds and result in alteration of chemical gradients in the porewater (Kadko and Heath 1984; Kadko et al. 1987). Therefore, these activities can substantially facilitate the transport of chemicals within the sediment bed and across the sediment-water interface (Bosworth and Thibodeaux 1990). Green et al. (1992) used two species of marine organisms to show directly that these organisms increased solute transport. Other researchers demonstrated biological sediment reworking using ^{234}Th-^{238}U, ^{226}Ra-^{230}Th, or ^{222}Rn-^{226}Ra disequilibrium (e.g., Aller and Cochran 1976; Aller et al. 1980; Aller and DeMaster 1984; Kadko et al. 1987; Martin and Sayles 1987).

The benthic organisms that cause sediment reworking can be put into two categories: those living on top of the bed and infauna (Bosworth and Thibodeaux 1990). Organisms that live on sediment surfaces include invertebrates, such as crabs, lobsters, and snails, as well as vertebrates, for example, bottom-living fishes. Infauna are organisms that live in sediments. They include surface feeders, which feed at or above

the sediment-water interface, and subsurface feeders, which feed below the interface. Conveyer-belt feeders are special subsurface feeders which pump subsurface sediments through their bodies and deposit the sediments on the sediment surface.

BIOTURBATION

As mentioned in Section 2.2, bioturbation is a random mixing of sediments and the associated porewater by the activities of benthic organisms. Goldberg and Koide (1962) first proposed to quantify the process using a *bioturbation coefficient* D_B [$L^2 \cdot T^{-1}$], analogous to a diffusion coefficient. One way that D_B can be determined is by using radioactive tracers, for example, the disequilibrium between a natural radionuclide and its daughter, such as $^{234}Th/^{238}U$ (Aller et al. 1980; Aller and DeMaster 1984; Martin and Sayles 1987), $^{226}Ra/^{230}Th$ (Kadko and Heath 1984; Kadko et al. 1987), and $^{210}Pb/^{226}Ra$ (Nozaki et al. 1977; Peng et al. 1979; Kadko 1981; DeMaster and Cochran 1982; Kadko and Heath 1984; Cochran 1985; Brownawell 1986). In steady state, the excess activity distribution of the daughter isotope can be modeled by radioactive decay, sedimentation, and bioturbation:

$$0 = \frac{d}{dx}\left\{D_B \frac{d[(1-\phi)\rho_s A]}{dx}\right\} - \frac{d[\omega(1-\phi)\rho_s A]}{dx} - \lambda(1-\phi)\rho_s A \qquad (2\text{-}8)$$

where

x = depth below the sediment-water interface, cm,

A = excess activity of the daughter isotope over the mother isotope, dpm/g,

D_B = bioturbation coefficient, cm^2/s,

ϕ = porosity,

ω = sedimentation rate, cm/s,

ρ_s = density of dry solids, g/cm^3, and

λ = decay constant of the daughter isotope, 1/s.

When D_B, ϕ, ω, and ρ_s are constant, the solution of Equation 2-8 is

$$A = A_0 \exp\left(\frac{\omega - \sqrt{\omega^2 + 4D_B\lambda}}{2D_B} \cdot x\right) \tag{2-9}$$

where A_0 is the excess activity at $x = 0$. When sedimentation is negligible, i.e. $4D_B\lambda >> \omega^2$,

$$A = A_0 \exp\left(-\sqrt{\frac{\lambda}{D_B}} \cdot x\right). \tag{2-10}$$

Bomb-produced artificial radionuclides, such as $^{239,240}Pu$ and ^{137}Cs were also used to estimate D_B (Noshkin and Bowen 1973; Guinasso and Schink 1975; Stordal and Johnson 1982; Cochran 1985). Unlike natural radionuclides, the distribution of these artificial radionuclides cannot be assumed steady state. For a pulse input,

$$\frac{A}{A_0} = \exp\left(-\frac{x^2}{4D_B t}\right). \tag{2-11}$$

And for a continuous input,

$$\frac{A}{A_0} = \exp\left(-\frac{x^2}{4D_B t}\right) - \frac{x}{2}\sqrt{\frac{\pi}{D_B t}}\,\mathrm{erfc}\left(\frac{x}{2\sqrt{D_B t}}\right) \qquad (2\text{-}12)$$

(Cochran 1985).

McCaffrey et al. (1980) estimated D_B by measuring the ^{22}Na uptake rate. They brought cores to the laboratory and injected ^{22}Na into the overlying water of the cores. They then measured the rate at which ^{22}Na was removed by transport into porewater, as well as the vertical distribution of ^{22}Na in the sediments.

Instead of using radioactive tracers, Kadko and Heath (1984) estimated D_B by balancing dissolved and particulate diagenetic manganese fluxes. The flux balance below the precipitation level at steady state gives

$$0 = \omega Mn_{(ex)} - D'_m \frac{dC_{Mn}}{dx} - D_B \frac{dMn_{(ex)}}{dx} \qquad (2\text{-}13)$$

where

$Mn_{(ex)}$ = concentration of solid phase manganese in excess of the burial (or supply) concentration of about 2%,

C_{Mn} = concentration of dissolved manganese, and

D'_m = effective molecular diffusivity of dissolved manganese in the porewater.

And for the region above the oxidation level,

$$\ln Mn_{(ex)} = \ln Mn_{(max)} + \frac{\omega}{D_B x'} \qquad (2\text{-}14)$$

where x' is the distance from the $Mn_{(ex)}$ maximum (positive upward).

Previous estimates of D_B are: (1) on the order of 10^{-7} cm^2/s for Buzzard Bay, Massachusetts (Brownawell 1986; Martin and Sayles 1987), (2) 10^{-5} - 10^{-6} cm^2/s for Boston Harbor (Wong 1992), (3) 10^{-5} cm^2/s for Narragansett Bay, Rhode Island (McCaffrey et al. 1980), (4) from 10^{-11} to 5×10^{-8} cm^2/s for Manganese Nodule Project (MANOP) sites in the east equatorial Pacific (Kadko and Heath 1984; Cochran 1985; Kadko et al. 1987), and (5) from $<10^{-8}$ to 1.6×10^{-6} cm^2/s for Long Island Sound with most value 0.2-0.5 $\times10^{-6}$ cm^2 (Aller et al. 1980). The value of D_B mainly depends on the food supply into the sediments (Martin and Sayles 1987; Santschi et al. 1990); therefore, in the deep-sea sediments in the east equatorial Pacific, the bioturbation is slower. Aller et al. (1980) indicated that the high and low values of D_B in Long Island Sound might reflect non-steady state local accretion and erosion, respectively. Martin and Sayles (1987) found temperature was another factor that determined the biological activity in the sediments. They found a factor of three difference between the average cold season and warm season D_B.

IRRIGATION

Irrigation is a non-local advective solute transport process exchanging pore fluids between sediment beds and overlying water columns caused by the actions of tube-

dwelling benthic macrofauna (Imboden 1981; Emerson et al. 1984; Boudreau 1986; Wong 1992). These benthic organisms pump burrow water and exchange it with the overlying water to maintain the oxygen and clean water supply (Aller and Yingst 1978; Aller et al. 1983). The extent of irrigation is described by an *irrigation rate constant*, α [T^{-1}]. Similar to bioturbation, the values of the irrigation rate constant is determined by temperature and the supply of organic matter. The study by Martin and Sayles (1987) showed that the irrigation rate at their study site significantly varied with seasons. They found irrigation was unimportant during the cold season.

Like D_B, α can be determined using radioactive tracers. The disequilibrium between ^{222}Rn and ^{226}Ra has been used to estimate biological irrigation rates by many researchers (e.g., Smethie et al. 1981; Christensen et al. 1984; Hammond et al. 1985; Martin and Sayles 1987; Wong 1992). The radon excess in bottom seawater is supplied by a net flux from sediments. This flux causes a radon deficiency relative to radium emanation in the sediments (Key et al. 1979). Assuming that the amount of sorbed radon is negligible, Key et al. (1979) and Martin and Sayles (1987) formulated an equation to describe the steady-state ^{222}Rn distribution:

$$0 = D_m' \frac{d^2A}{dx^2} - \alpha_{(x)}(A - A_{ol}) - \lambda A + \lambda P \qquad (2\text{-}15)$$

where

x = depth from the interface, cm,

A = ^{222}Rn activity in the porewater, dpm/cm^3,

A_{ol} = ^{222}Rn activity in the overlying water, dpm/cm^3,

D'_m = sediment diffusivity, cm^2/s,

$\alpha_{(x)}$ = irrigation rate at depth x, 1/s,

λ = decay constant of ^{222}Rn, 1/s, and

P = ^{222}Rn production, dpm/cm^3.

The ^{222}Rn production measurement is based on the assumption that in the absence of transport process, porewater ^{222}Rn is in equilibrium with sediment ^{226}Ra (Martin and Sayles 1987):

$$P = P_\infty + \Delta P e^{-x/l} \tag{2-16}$$

where P_∞ is the asymptotic supported porewater ^{222}Rn activity, ΔP is P_∞ minus the supported ^{222}Rn activity in the porewater adjacent to the sediment-water interface, and l is the scale length for P. P_∞ , ΔP, and l are obtained from fitting the profile of the supported ^{222}Rn porewater activity.

Later Wong (1992) and Wong et al. (1992) developed a transport model for ^{222}Rn in sediments, which included sorption effects:

$$\frac{\partial C_t}{\partial t} = \frac{\partial}{\partial x}\left[D_B \frac{\partial C_t}{\partial x} + \frac{D_S + D_I}{1 + \dfrac{(1-\phi)\rho_s f_{oc} K_{oc}}{\phi}} \cdot \frac{\partial C_t}{\partial x}\right] - \frac{\alpha(x)}{1 + \dfrac{(1-\phi)\rho_s f_{oc} K_{oc}}{\phi}} \cdot C_t + \lambda (C_{supp} - C_t) \tag{2-17}$$

where

x = depth,

C_t = $\phi C_{pw} + (1-\phi) \rho_s C_s$

= total mobile radon concentration per unit volume of bulk sediments,

C_{pw} = concentration of dissolved phase radon,

C_s = concentration of sorbed phase radon,

C_{supp} = $\phi C_{supp,pw} + (1-\phi) \rho_s C_{supp,s}$

= total effective concentration of ^{226}Ra producing mobile ^{222}Rn,

$C_{supp,pw}$ = effective concentration of ^{226}Ra producing mobile ^{222}Rn in porewater,

$C_{supp,s}$ = effective concentration of ^{226}Ra producing mobile ^{222}Rn in solids,

ϕ = porosity of the sediment bed,

ρ_s = density of the dry solids,

D_B = bioturbation coefficient,

D_S = aqueous diffusion coefficient corrected for tortuosity and porosity,

D_I = enhanced bioturbation coefficient quantifying irrigation,

$\alpha(x)$ = non-local exchange term quantifying irrigation,

f_{oc} = organic carbon content of the sediment bed,

K_{oc} = organic carbon - water partition coefficient (= 23 mg/L for Rn), and

λ = decay constant of ^{222}Rn.

In this formulation, α is given

$$\alpha(x) = \frac{\lambda(C_{supp} - C_t)}{C_t} \cdot \left[1 + \frac{(1-\phi)\rho_s f_{oc} K_{oc}}{\phi}\right] . \qquad (2\text{-}18)$$

Martin and Sayles (1987) and Wong (1992) treated α as an exponentially decreasing function:

$$\alpha_{(x)} = \alpha_0 \exp\left(-\frac{x}{\alpha_1}\right) \qquad (2\text{-}19)$$

whereas Hammond et al. (1985) used three zones of constant α with discontinuous changes in α at the zone boundaries.

^{22}Na was also used to estimate irrigation rate constant by McCaffrey et al. (1980). α may be obtained from

$$\ln\left[C_s(t)\left(1+\frac{V_s}{V_p}\right) - \frac{V_s}{V_p}C_s(0)\right] = -\alpha\left(1+\frac{V_s}{V_p}\right)t \qquad (2\text{-}20)$$

where

$C_s(t)$ = normalized ^{22}Na concentration in overlying solution at time t,

$C_s(0)$ = normalized ^{22}Na concentration in overlying solution at t=0,

V_s = volume of overlying solution, and

V_p = volume of porewater.

Emerson et al. (1984) used an *in situ* ^{3}H-water experiment and dissolved silicate profiles to estimate α. They measured the rate of tritium penetration into sediments by covering the sediments with bell jars, injecting tritiated water, and then taking cores from the sediments after a period of time. The models they established were

$$\frac{\partial[^3H]}{\partial t} = D_m' \frac{\partial^2[^3H]}{\partial x^2} - \alpha \frac{[^3H] - [^3H]_0}{\phi} \qquad (2\text{-}21a)$$

and

$$0 = D_m' \frac{d^2[Si]}{dx^2} - \alpha \left([Si] - \frac{[Si]_0}{\phi} \right) + k([Si]_a - [Si]) \qquad (2\text{-}21b)$$

where

x = depth,

$[^3H]$ = concentration of dissolved ^{3}H in the porewater,

$[^3H]_0$ = concentration of dissolved ^{3}H in the overlying water,

[Si] = concentration of dissolved silicate in the porewater,

$[Si]_0$ = concentration of dissolved silicate in the overlying water,

$[Si]_a$ = asymptotic value of the silicate concentration in the porewater,

D'_m = bulk sediment diffusive coefficient corrected for tortuosity ,

α = irrigation rate constant,

ϕ = porosity, and

k = diatom dissolution rate constant.

The α values found were on the order of 10^{-6} - 10^{-7} s^{-1} for many places: Boston Harbor (Chin et al. 1991; Wong 1992), Buzzards Bay, Massachusetts (Martin and Sayles 1987), San Francisco Bay (Hammond and Fuller 1979; Hammond et al. 1985), Narragansett Bay, Rhode Island (McCaffrey et al. 1980), and Puget Sound (Emerson et al. 1984).

2.4 Desorption Kinetics in Sediment Beds

Nonpolar organic chemicals in sediment beds exist in three phases: dissolved in porewater, associated with porewater colloids, and sorbed to solids. Since only mobile organic chemicals, i.e. dissolved and colloidal phase species, can move from sediments into the overlying water, desorption may be an important process near the sediment-water interface.

The concentration of colloidal phase species, C_{col} (ng/cm^{3}pw), can be written as

$$C_{col} = C_{coc} \cdot m_{coc} \tag{2-22}$$

where C_{coc} (ng/g colloidal organic carbon) is the concentration of species associated with colloidal organic carbon, and m_{coc} (g colloidal organic carbon/cm^{3}pw) is the concentration of colloidal organic carbon in the porewater. The colloidal phase concentration can be assumed locally in equilibrium with the concentration of species dissolved in porewater, C_{pw} (ng/cm^{3}pw); therefore,

$$K_c = \frac{C_{coc}}{C_{pw}} \tag{2-23}$$

where K_c (cm^3pw/g col. org. C) is the *colloid-water distribution coefficient*. Substituting Equation 2-23 into Equation 2-22 results in

$$C_{col} = C_{pw} \cdot K_c \cdot m_{coc} \quad . \tag{2-24}$$

Sorption has been modeled as a first-order chemical reaction (Oddson et al. 1970; van Genuchten et al. 1974; Wu and Gschwend 1988):

$$\frac{dS}{dt} = -k_1 S + k_{-1} C_{pw} \tag{2-25}$$

where

S = concentration of species sorbed in/on solids, ng/g solid,

k_1 = desorption rate constant, 1/s, and

k_{-1} = sorption rate constant, cm^3 pw/g solid·s.

The mass balance relationship in the sediments gives

$$\frac{dM_s}{dt} = -\left(\frac{dM_{pw}}{dt} + \frac{dM_{col}}{dt}\right) \tag{2-26}$$

where

M_s = $S \cdot V_s \cdot \rho_s$, amount of species sorbed in/on solids,

M_{pw} = $C_{pw} \cdot V_{pw}$, amount of species dissolved in porewater,

M_{col} = $C_{col} \cdot V_{pw}$, amount of species associated with porewater colloids,

V_s = volume of the solid matrices in the sediments,

V_{pw} = volume of the porewater in the sediments, and

ρ_s = density of dry solids.

By dividing both sides of Equation 2-26 with the volume of the sediments (V_t) and substituting Equation 2-24 into Equation 2-26, Equation 2-26 becomes

$$(1-\phi)\rho_s \frac{dS}{dt} = -\left(\phi \frac{dC_{pw}}{dt} + \phi K_c m_{coc} \frac{dC_{pw}}{dt}\right) . \qquad (2\text{-}27)$$

It follows that

$$\frac{dC_{pw}}{dt} = -\frac{(1-\phi)\rho_s}{\phi(1+K_c m_{coc})} \frac{dS}{dt} . \qquad (2\text{-}28)$$

Defining $\rho = (1-\phi)\rho_s/\phi$ and substituting Equation 2-25 into Equation 2-28 yields

$$\frac{dC_{pw}}{dt} = -\frac{\rho k_{-1}}{(1+K_c m_{coc})} C_{pw} + \frac{\rho k_1}{(1+K_c m_{coc})} S . \qquad (2\text{-}29)$$

When C_{pw} and S are in equilibrium, $dS/dt = 0 = dC_{pw}/dt$, and

$$K_d = \frac{S}{C_{pw}} \tag{2-30}$$

where $K_d = f_{oc} \cdot K_{oc}$, the *solid-water distribution coefficient* (cm^3pw/g solid), in which f_{oc} is the *organic carbon content*, and K_{oc} is the *organic carbon-water partition coefficient*. Thus,

$$k_{-1} = k_1 K_d \tag{2-31}$$

And consequently,

$$\frac{dS}{dt} = k_1 (K_d C_{pw} - S) \tag{2-32}$$

$$\frac{dC_{pw}}{dt} = \frac{\rho k_1}{(1 + K_c m_{coc})} (S - K_d C_{pw}) \tag{2-33}$$

and

$$\frac{dC_{col}}{dt} = \frac{\rho k_1 K_c m_{coc}}{1 + K_c m_{coc}} \left(S - \frac{K_d C_{col}}{K_c m_{coc}} \right) \quad . \tag{2-34}$$

The desorption rate constant, k_1, can be estimated using the model developed by Wu and Gschwend (1988):

$$k_1 = \frac{\beta D_{eff}}{R^2} \tag{2-35}$$

where D_{eff} is the effective intraparticle diffusivity, R is the radius of the aggregate particle, and

$$\beta = 10.56 K_d \rho + 22.7 \tag{2-36}$$

where ρ is the solid-water ratio.

The effective intraparticle diffusivity, D_{eff}, is defined as

$$D_{eff} = \frac{D_m n^2}{(1-n)\rho_s K_d + n} \tag{2-37}$$

where n is the intra-aggregate porosity and has a typical value of 0.13 for sorbing silts (Wu and Gschwend 1986).

For a hydrophobic chemical, $\beta \approx 10.56 K_d \rho$, and $D_{eff} \approx D_m n^2/(1-n)\rho_s K_d$; therefore,

$$\begin{aligned} k_1 &\approx \frac{10.56 \rho D_m n^2}{\rho_s R^2 (1-n)} \\ &\approx \frac{0.21 \rho D_m}{\rho_s R^2} \text{ , } for\ n = 0.13 \text{ .} \end{aligned} \tag{2-38}$$

This approximation suggests that the desorption rate constant, k_1, is independent of the organic chemical's hydrophobicity.

2.5 Diffusive Boundary Layer above the Sediment-Water Interface

The thickness of the diffusive water boundary layer has been found to be 10^{-2} - 10^{0} cm (Levich 1962; Wimbush 1976; Boudreau and Scott 1978; Sarmiento 1978; Boudreau and Guinasso 1982; Santschi et al. 1983; Jørgensen and Revsbech 1985; Sweerts et al. 1989; Jørgensen and Des Marais 1990). Although it is very thin, it plays a very important role in sediment-water exchange; the flux of some chemicals across the sediment-water interface is greatly controlled by the resistance posed by this thin layer.

Near the sediment-water interface, surface friction retards the motion of the overlying fluids, and, as a result, viscosity becomes more important than turbulence. The region where eddy viscosity is smaller than molecular viscosity is referred to as the *viscous sublayer* (Figure 2.2) (e.g., Wimbush 1976; Thibodeaux 1979; Boudreau and Guinasso 1982), and the region where turbulent diffusion is smaller than molecular diffusion is called the *diffusive boundary layer.* The relationship between the thickness of the viscous sublayer (Z_v) and the thickness of the diffusive boundary layer (Z_w)is given by

$$Z_w = \frac{Z_v}{Sc^{1/3}} \qquad (2\text{-}39)$$

where Sc is the Schmidt Number, $Sc = \nu/D_m$, and ν is the kinematic viscosity (Wimbush 1976; Thibodeaux 1979). Z_v can be estimated by the following equation (Wimbush 1976):

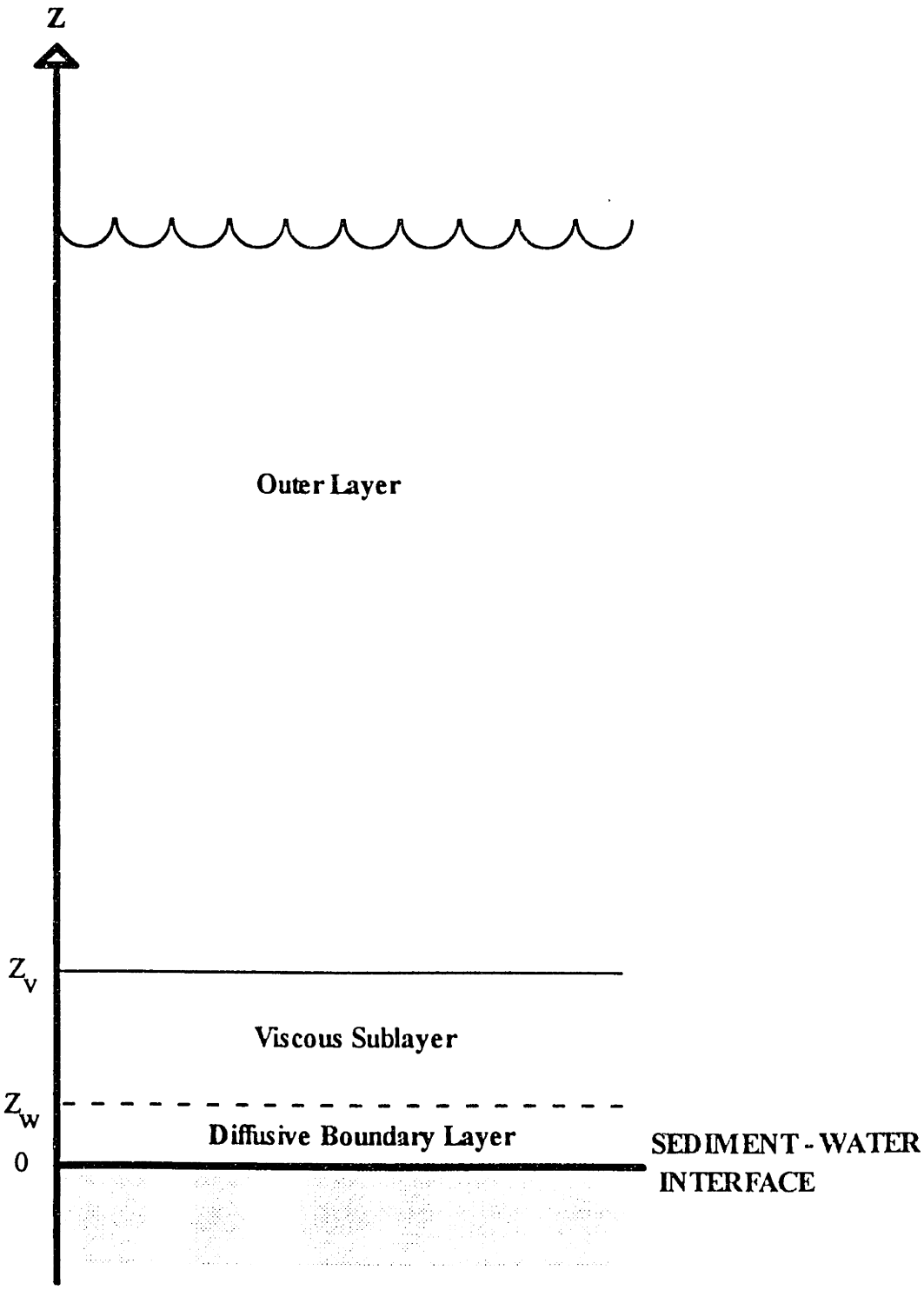

Figure 2.2 Structure of the water boundary layer

$$Z_v = \frac{12\nu}{u_*} \tag{2-40}$$

where u_* is the friction velocity due to flow of the overlying water.

Thus,

$$Z_w = \frac{12\nu^{2/3} D_m^{1/3}}{u_*} \quad . \tag{2-41}$$

The friction velocity can be estimated from the following equation (Thibodeaux 1979; Streeter and Wylie 1985):

$$u_* = \sqrt{\frac{\tau_0}{\rho}} = \sqrt{\frac{f}{8}\bar{u}} \tag{2-42}$$

where

τ_0 = shear stress exerted by the fluid onto the surface,

ρ = fluid density,

f = friction factor, a function of the roughness of the sea bottom, and

$\bar{u}$ = average flow velocity depth-wise.

From Equation 2-42 we can conclude that the thickness of the diffusive boundary layer depends on the flow velocity of the water and the roughness of the sediment bed surface (Jørgensen and Revsbech 1985; Jørgensen and Des Marais 1990).

When there is no chemical reaction within the diffusive boundary layer, the vertical flux through this layer, F_w, can be described by Fick's first law of diffusion with a linear concentration gradient:

$$F_w = D_m \frac{(C_w - C_0)}{Z_w} \tag{2-43}$$

where D_m is the diffusion coefficient, C_w is the concentration of species in bulk seawater, and C_0 is the concentration at the sediment-water interface.

2.6 Flux Model

2.6.1 Governing equations

The amount of a chemical per unit volume of bulk sediment (C_t, ng/cm^3 sediment) is the sum of the chemical dissolved in the porewater (C_{pw}, ng/cm^3 porewater), associated with the colloids (C_{col}, ng/cm^3 porewater), and sorbed in/on the solids (S, ng/g solid):

$$C_t = \phi C_{pw} + \phi C_{col} + (1-\phi)\rho_s S \tag{2-44}$$

where ϕ is the porosity of the sediment bed (cm^{3}pw/cm^{3}sed), and ρ_s is the density of the dry solids. The change of the total concentration in the sediments with time is

$$\frac{\partial C_t}{\partial t} = \frac{\partial(\phi C_{pw})}{\partial t} + \frac{\partial(\phi C_{col})}{\partial t} + \frac{\partial[(1-\phi)\rho_s S]}{\partial t} \quad . \tag{2-45}$$

Adapted from Equations 2-8, 2-15, 2-21a, 2-32, 2-33, and 2-34, and following the examples of Berner (1980) and Wong (1992), the terms on the right hand side of Equation 2-45 can be written as

$$\frac{\partial(\phi C_{pw})}{\partial t} = \frac{\partial}{\partial z}\left[D_B \frac{\partial(\phi C_{pw})}{\partial z} + \phi D_m' \frac{\partial C_{pw}}{\partial z}\right] - \alpha(\phi C_{pw} - C_w) - \frac{\partial(\phi v C_{pw})}{\partial z} - \frac{k_1(1-\phi)\rho_s}{1+K_c m_{coc}}(K_d C_{pw} - S) \quad (2\text{-}46a)$$

$$\frac{\partial(\phi C_{col})}{\partial t} = \frac{\partial}{\partial z}\left[D_B \frac{\partial(\phi C_{col})}{\partial z} + \phi D_c' \frac{\partial C_{col}}{\partial z}\right] - \alpha(\phi C_{col} - C_{col,w}) - \frac{\partial(\phi v C_{col})}{\partial z} - \frac{k_1(1-\phi)\rho_s K_c m_{coc}}{1+K_c m_{coc}}\left(\frac{K_d C_{col}}{K_c m_{coc}} - S\right) \quad (2\text{-}46b)$$

and

$$\frac{\partial[(1-\phi)\rho_s S]}{\partial t} = \frac{\partial}{\partial z}\left\{D_B \frac{\partial[(1-\phi)\rho_s S]}{\partial z}\right\} - \frac{\partial[(1-\phi)\rho_s \omega S]}{\partial z} + k_1(1-\phi)\rho_s(K_d C_{pw} - S) \quad (2\text{-}46c)$$

where

z = vertical coordinate, positive upward,

C_w = concentration of species dissolved in bulk seawater, ng/cm^{3}sw,

$C_{col,w}$ = concentration of species associated with the colloids in bulk seawater, ng/cm^{3}sw,

D_B = bioturbation coefficient, cm^2/s,

D'_m = aqueous molecular diffusivity corrected for porosity and tortuosity, cm^2/s,

D'_c = aqueous colloidal diffusivity corrected for porosity and tortuosity, cm^2/s,

α = irrigation rate constant, 1/s,

v = porewater advection rate, cm/s,

ω = sedimentation rate, cm/s,

k_1 = desorption rate constant, 1/s,

K_d = solid-water distribution coefficient, cm^{3}pw/g solid,

K_c = colloid-water distribution coefficient, cm^{3}pw/g col. org. C, and

m_{coc} = concentration of colloidal organic carbon in the porewater, g col. org. C/cm^{3}pw.

To simplify the model, it is assumed that

(1) C_w and $C_{col,w}$ are negligible compared to C_{pw} and C_{col} ;

(2) porewater advection and sedimentation are negligible;

(3) ϕ, ρ_s, D_B, D'_m, D'_c, α, k_1, K_d, K_c, and m_{coc} are constant with depth;

(4) C_{pw} and C_{col} are in equilibrium; i.e., $C_{col} = K_c \cdot m_{coc} \cdot C_{pw}$;and

(5) the concentrations of chemicals in dissolved, colloidal, and sorbed phases change so slowly that dC_{pw}/dt, dC_{col}/dt, and dS/dt are approximately zero.

Thus, the equation for mobile species is of the form:

$$
\begin{aligned}
0 \approx\ & \phi \frac{\partial C_{pw}}{\partial t} + \phi \frac{\partial C_{col}}{\partial t} \\
=\ & \phi \left[D_B (1 + K_c m_{coc}) + (D'_m + D'_c K_c m_{coc}) \right] \frac{\partial^2 C_{pw}}{\partial z^2} \\
& - \phi \alpha (1 + K_c m_{coc}) C_{pw} - k_1 (1 - \phi) \rho_s (K_d C_{pw} - S) \ .
\end{aligned}
\tag{2-47}
$$

And for sorbed species,

$$
\begin{aligned}
0 \approx\ & (1 - \phi) \rho_s \frac{\partial S}{\partial t} \\
=\ & (1 - \phi) \rho_s D_B \frac{\partial^2 S}{\partial z^2} + k_1 (1 - \phi) \rho_s (K_d C_{pw} - S) \ .
\end{aligned}
\tag{2-48}
$$

By defining $\bar{D}_B = D_B(1+K_c m_{coc})$, $\bar{D}_m = D'_m + D'_c K_c m_{coc}$, $\bar{\alpha} = \alpha(1+K_c m_{coc})$, and $\rho = (1-\phi)\rho_s/\phi$, Equations 2-47 and 2-48 can be reduced to

$$
\frac{d^2 C_{pw}}{dz^2} - \frac{\bar{\alpha} + k_1 \rho K_d}{\bar{D}_B + \bar{D}_m} C_{pw} + \frac{k_1 \rho}{\bar{D}_B + \bar{D}_m} S = 0 \tag{2-49}
$$

and

$$
\frac{d^2 S}{dz^2} - \frac{k_1}{D_B} S + \frac{k_1 K_d}{D_B} C_{pw} = 0 \ . \tag{2-50}
$$

The boundary conditions for Equations 2-49 and 2-50 are

(1) $C_{pw} = C_0$ at $z = 0$;

(2) $dS/dz = 0$ at $z = 0$;

(3) $C_{pw} = C_L$ at $z = -L$ (the depth of the biologically active layer); and

(4) $S = K_d C_{pw}$ at $z = -L$.

For most organic chemicals, it can be assumed that $\bar{\alpha} << k_1 \rho K_d$; therefore, the solutions of Equations 2-49 and 2-50 are

$$C_{pw} = C_0 + \frac{C_L - C_0}{\frac{\epsilon(\bar{D}_B + \bar{D}_m)L}{D_B \rho K_d}\coth(\epsilon L) + 1} - \frac{C_L - C_0}{L + \frac{D_B \rho K_d}{\epsilon(\bar{D}_B + \bar{D}_m)}\tanh(\epsilon L)} z - \frac{(C_L - C_0)\frac{D_B \rho K_d}{\epsilon(\bar{D}_B + \bar{D}_m)}}{L\cosh(\epsilon L) + \frac{D_B \rho K_d}{\epsilon(\bar{D}_B + \bar{D}_m)}\sinh(\epsilon L)} \sinh[\epsilon(L + z)] \quad (2\text{-}51)$$

and

$$S = C_0 K_d + \frac{(C_L - C_0)K_d}{\frac{\epsilon(\bar{D}_B + \bar{D}_m)L}{D_B \rho K_d}\coth(\epsilon L) + 1}$$

$$- \frac{(C_L - C_0)K_d}{L + \frac{D_B \rho K_d}{\epsilon(\bar{D}_B + \bar{D}_m)}\tanh(\epsilon L)} z \qquad (2\text{-}52)$$

$$+ \frac{(C_L - C_0)\frac{K_d}{\epsilon}}{L\cosh(\epsilon L) + \frac{D_B \rho K_d}{\epsilon(\bar{D}_B + \bar{D}_m)}\sinh(\epsilon L)} \sinh\left[\epsilon(L + z)\right]$$

where

$$\epsilon = \sqrt{\frac{k_1 \rho K_d}{\bar{D}_B + \bar{D}_m} + \frac{k_1}{D_B}} \quad . \qquad (2\text{-}53)$$

(See Appendix for the derivation.)

The concentration gradient at the sediment-water interface (z = 0) is

$$\left.\frac{dC_{pw}}{dz}\right|_{z=0} = - \frac{(C_L - C_0)\left(1 + \frac{K_d \rho D_B}{\bar{D}_B + \bar{D}_m}\right)}{L + \frac{K_d \rho D_B}{\epsilon(\bar{D}_B + \bar{D}_m)}\tanh(\epsilon L)} \quad . \qquad (2\text{-}54)$$

The validity of the assumption that $\bar{\alpha} << k_1 \rho K_d$ is summarized in Figure 2.3. Given Equation 2-38, $\bar{\alpha}/k_1 \rho K_d$ becomes

$$\frac{\bar{\alpha}}{k_1 \rho K_d} \approx \frac{\alpha (1 + K_c m_{coc}) \rho_s R^2}{0.2 \rho^2 D_m K_{oc} f_{oc}} . \qquad (2\text{-}55)$$

Assuming that $\bar{\alpha}$ was negligible compared with $k_1 \cdot \rho \cdot K_d$ if $\bar{\alpha}/k_1 \cdot \rho \cdot K_d = 0.1$, the values of R that made $\bar{\alpha}/k_1 \cdot \rho \cdot K_d = 0.1$ when $m_{coc} = 10^{-4}$ g col. org. C/cm^{3}pw, $\phi = 0.9$, $D_m = 3 \times 10^{-6}$ cm^2/s, and $f_{oc} = 1\%$ (R_{max}) were calculated from Equation 2-55 and shown in Figure 2-3. For sediments the aggregate radius of which is smaller than R_{max}, $\bar{\alpha} << k_1 \rho K_d$, and hence, this model is applicable. This figure is just a quick reference. For evaluation of the model applicability to sites and organic pollutants of interest, the values of $\bar{\alpha}$ and $k_1 \cdot \rho \cdot K_d$ need to be calculated.

2.6.2 Flux expressions

The total flux across the sediment-water interface (F_t) is the sum of the diffusive flux (F_D) and the irrigational flux (F_I): $F_t = F_D + F_I$.

DIFFUSIVE FLUX

The diffusive flux from the sediment bed across the sediment-water interface is

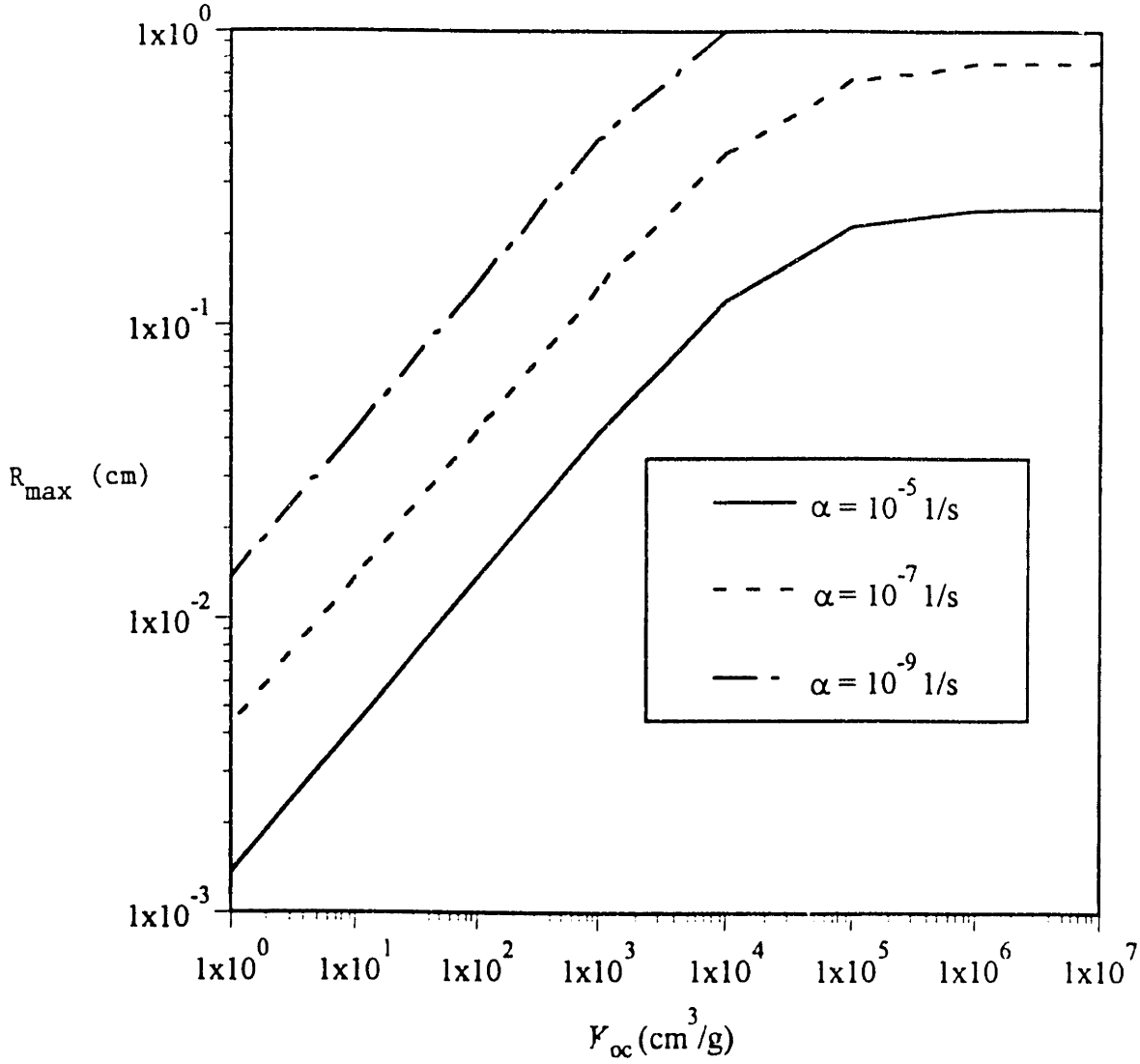

Figure 2.3 Examination of the model applicability. For sediments the aggregate radius of which is smaller than R_{max}, this model is applicable.

$$F_D = -\phi(\bar{D}_B + \bar{D}_m)\left.\frac{dC_{pw}}{dz}\right|_{z=0} \quad . \tag{2-56}$$

Substituting Equation 2-54 into Equation 2-56 yields

$$F_D = \frac{\phi(\bar{D}_B + \bar{D}_m)(C_L - C_0)\left(1 + \dfrac{K_d \rho D_B}{\bar{D}_B + \bar{D}_m}\right)}{L + \dfrac{K_d \rho D_B}{\epsilon(\bar{D}_B + \bar{D}_m)} \tanh(\epsilon L)} \quad . \tag{2-57}$$

This expression indicates that the flux of a sorptive chemical is enhanced by desorption. For a non-sorptive chemical (i.e., $K_d = 0$), the diffusive flux within the sediment bed (F'_D) is

$$F'_D = \phi(D_B + D'_m)\frac{C_L - C_0}{L} \quad . \tag{2-58}$$

The magnitude of the sorption enhancement is the ratio of F_D to F'_D :

$$ENHANCEMENT = \frac{F_{sorptive}}{F_{non\text{-}sorptive}} = \frac{F_{D(z=0)}}{F'_{D(z=0)}}$$

$$= \frac{\bar{D}_B + \bar{D}_m}{D_B + D'_m} \cdot \frac{1 + \dfrac{K_d \rho D_B}{\bar{D}_B + \bar{D}_m}}{1 + \dfrac{K_d \rho D_B}{\epsilon L(\bar{D}_B + \bar{D}_m)} \tanh(\epsilon L)} \quad . \tag{2-59}$$

Defining

$$\psi = \frac{1 + \dfrac{K_d \rho D_B}{\bar{D}_B + \bar{D}_m}}{1 + \dfrac{K_d \rho D_B}{\epsilon L(\bar{D}_B + \bar{D}_m)} \tanh(\epsilon L)} \tag{2-60}$$

$$= \frac{\epsilon L(\bar{D}_B + \bar{D}_m) + K_d \rho D_B \epsilon L}{\epsilon L(\bar{D}_B + \bar{D}_m) + K_d \rho D_B \tanh(\epsilon L)}$$

and substituting into Equation 2-59 gives

$$F_D = \phi \frac{\bar{D}_B + \bar{D}_m}{L} (C_L - C_0) \psi \quad . \tag{2-61}$$

Since $\epsilon L >> 1$, $\tanh(\epsilon L) = 1$. The ψ equation can be simplified:

$$\psi = \frac{\bar{D}_B + \bar{D}_m + K_d \rho D_B}{\bar{D}_B + \bar{D}_m + \dfrac{K_d \rho D_B}{\epsilon L}} \quad . \tag{2-62}$$

Here we assume chemical concentration profile is in steady state; therefore, the diffusive chemical flux in the sediments must be equal to that in the diffusive boundary layer (F_w), in which

$$F_w = (D_m + D_c m_{coc,w} K_c) \frac{C_0 - C_w}{Z_w} \quad . \tag{2-63}$$

Let $D_w = D_m + D_c m_{coc,w} K_c$; hence,

$$F_D = \phi \frac{\bar{D}_B + \bar{D}_m}{L} (C_L - C_0) \psi = \frac{D_w}{Z_w} (C_0 - C_w) = F_w \quad . \tag{2-64}$$

This yields

$$C_0 = \frac{\frac{\phi \psi (\bar{D}_B + \bar{D}_m)}{L} C_L + \frac{D_w}{Z_w} C_w}{\frac{\phi \psi (\bar{D}_B + \bar{D}_m)}{L} + \frac{D_w}{Z_w}} \quad . \tag{2-65}$$

Letting $C_L = S_L/K_d$ and substituting Equation 2-65 into Equation 2-64 gives

$$F_D = F_w = \frac{\frac{S_L}{K_d} - C_w}{\frac{Z_w}{D_w} + \frac{L}{\phi \psi (\bar{D}_B + \bar{D}_m)}} \quad . \tag{2-66}$$

In this flux expression, the denominator can be interpreted as the total resistance of the mass transfer across the sediment-water interface, which is the inverse of the total mass transfer velocity (v_{tot}). This total resistance consists of the resistance in the biologically active layer ($1/v_s$) and that in the diffusive boundary layer ($1/v_w$):

$$\frac{1}{v_{tot}} = \frac{1}{v_s} + \frac{1}{v_w} \tag{2-67}$$

in which

$$\frac{1}{v_s} = \frac{L}{\phi\psi(\bar{D}_B + \bar{D}_m)} \tag{2-68}$$

and

$$\frac{1}{v_w} = \frac{Z_w}{D_w} \quad . \tag{2-69}$$

If $1/v_w >> 1/v_s$, $1/v_{tot} \approx 1/v_w$, which means the transfer is dominated by the diffusive water boundary layer. If $1/v_w << 1/v_s$, the transfer is dominated by the biologically active sediment layer.

In the case that desorption in sediments is very fast, that is, $k_1 \rightarrow \infty$ (i.e., $\varepsilon \rightarrow \infty$), the concentration of dissolved species and the concentration of sorbed species are about in equilibrium, and an *equilibrium desorption enhancement factor* can be derived from Equation 2-62:

$$\psi_{eq} = \frac{\bar{D}_B + \bar{D}_m + \rho K_d D_B}{\bar{D}_B + \bar{D}_m} . \qquad (2\text{-}70)$$

The sediment resistance becomes

$$\frac{1}{v_{s_{eq}}} = \frac{L}{\phi(\bar{D}_B + \bar{D}_m + K_d \rho D_B)} . \qquad (2\text{-}71)$$

And the diffusive flux under this equilibrium condition is

$$F_{D_{eq}} = \frac{\frac{S_L}{K_d} - C_w}{\frac{Z_w}{D_w} + \frac{L}{\phi(\bar{D}_B + \bar{D}_m + K_d \rho D_B)}} . \qquad (2\text{-}72)$$

Equation 2-72 is less complicated than the non-equilibrium flux equation (Equation 2-66). If simple estimation of the diffusive flux is desired, Equation 2-72 can be used to predict the upper limit of the diffusive flux, and the ratio ψ/ψ_{eq},

$$\frac{\psi}{\psi_{eq}} = \frac{\bar{D}_B + \bar{D}_m}{\bar{D}_B + \bar{D}_m + \frac{K_d \rho D_B}{\epsilon L}} , \qquad (2\text{-}73)$$

helps evaluate the simplification.

From Equations 2-51, 2-52, and 2-65, the theoretical concentration profiles of the dissolved species and the species sorbed in the solids of sediments can be calculated, and those are generally illustrated in Figure 2.4. The concentration profile of the dissolved species calculated in this way is similar to those reported earlier by Boudreau and Guinasso (1982) (Figure 2.5). The sediment layer in which the concentration of dissolved species and the concentration of sorbed species are out of equilibrium is only a small fraction of the entire sediment bed. The thickness of this layer is approximately as large as L/ψ.

IRRIGATIONAL FLUX

The irrigational flux across the sediment-water interface is

$$\begin{aligned} F_I &= \phi\alpha\int_{-L}^{0}(C_{pw_{(z)}} - C_w)\,dz + \phi\alpha\int_{-L}^{0}(C_{col_{(z)}} - C_{col,w})\,dz \\ &= \phi\alpha(1+m_{coc}K_c)\int_{-L}^{0}C_{pw_{(z)}}\,dz - \phi\alpha(1+m_{coc,w}K_c)C_wL \end{aligned} \tag{2-74}$$

in which

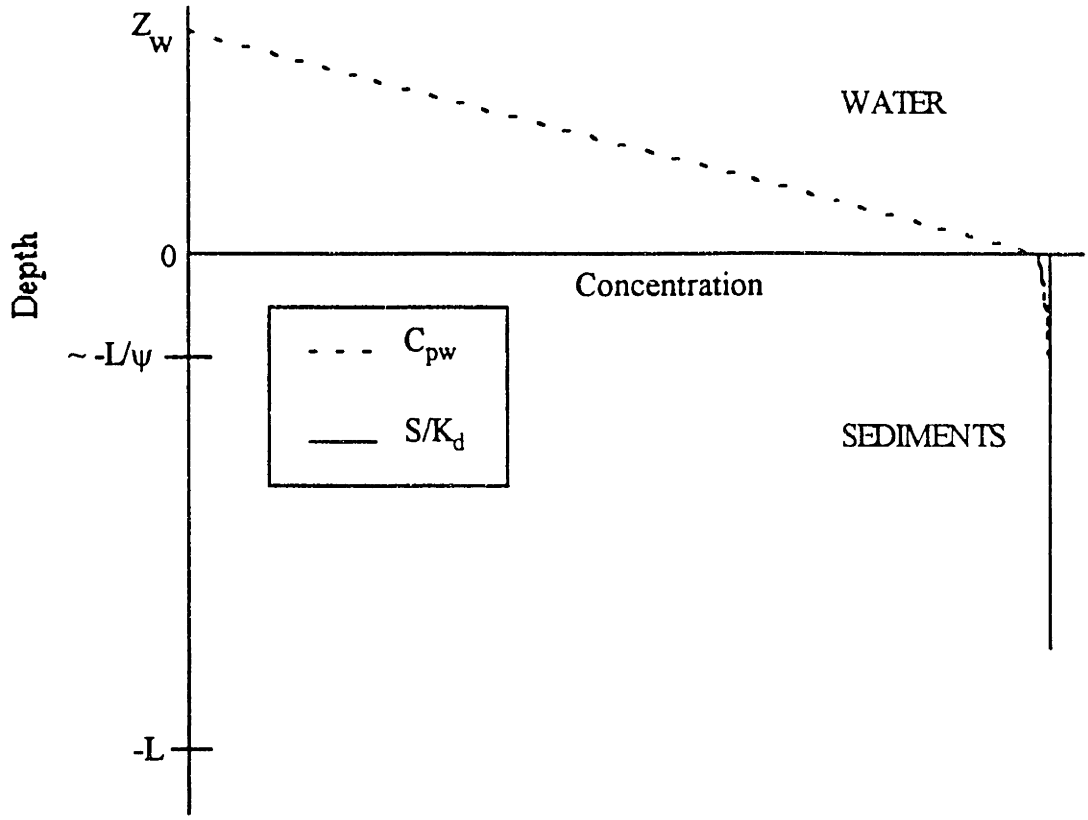

Figure 2.4 Concentration profiles of dissolved species and sorbed species predicted from the model

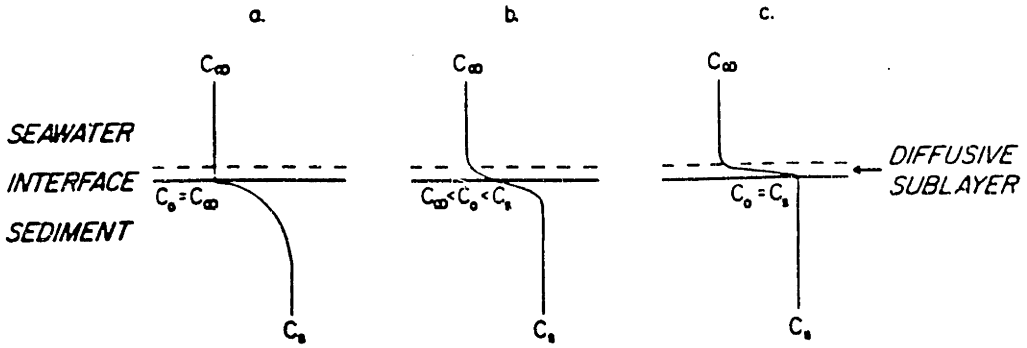

Figure 2.5 Schematic representation of the concentration gradient of a species diffusing from the sediments: (a) internally controlled regime: the resistance of the diffusive water boundary layer is much less than the resistance within the sediments; (b) intermediate regime; (c) external diffusion regime: the resistance of the diffusive water boundary layer is much greater than the resistance in the sediment bed (Boudreau and Guinasso 1982).

$$\int_{-L}^{0} C_{pw}\,dz = -\frac{(C_L - C_0)K_d\rho D_B}{\epsilon^2 L(\bar{D}_B + \bar{D}_m)} + C_0 L$$

$$+ \frac{(C_L - C_0)LK_d\rho D_B}{\epsilon L(\bar{D}_B + \bar{D}_m) + K_d\rho D_B} \qquad (2\text{-}75)$$

$$+ \frac{(C_L - C_0)L^2\epsilon(\bar{D}_B + \bar{D}_m)}{2[\epsilon L(\bar{D}_B + \bar{D}_m) + K_d\rho D_B]}$$

under the assumption that $\cosh(\varepsilon L) \rightarrow \infty$, $\tanh(\varepsilon L) = 1$, $\coth(\varepsilon L) = 1$, and $\mathrm{sech}(\varepsilon L) = 0$.

From Equations 2-74 and 2-75, we can know that the irrigational flux increases with a thicker biologically active layer (i.e., L increases), but decreases with a higher overlying water concentration (C_w). Therefore, the extent of irrigation is controlled not only by the quality of the sediment bed, but also by the quality of the overlying water. The effect of colloids on the irrigational flux is not significant, which will be discussed in Section 2.7.

2.7 Sensitivity Analysis

A sensitivity analyses was conducted to identify the model parameters that are critical for controlling the flux of organic chemicals across the sediment-water interface. The parameter values used for this analysis are listed in Table 2.2, and the results are shown as Figures 2.6 to 2.15. The sensitivities of the ratio of the resistance in sediments to the total resistance (r_s) and the ratio of the resistance in the diffusive water boundary layer to the total resistance (r_w) are also demonstrated in these figures.

Table 2.2 Parameter values for the sensitivity analysis

PARAMETER	BASE VALUE	LOWER LIMIT	UPPER LIMIT	FIGURE NUMBER	TABLE NUMBER
f_{oc}	4.2%	1.0%	10.0%	2.6	2.3
ϕ	0.80	0.01	0.99	2.7	2.4
R (cm)	0.01	$1x10^{-5}$	$1x10^{0}$	2.8	2.5
L (cm)	20	1	100	2.9	2.6
Z_w (cm)	0.015	$1x10^{-3}$	$1x10^{0}$	2.10	2.7
D_B (cm^2/s)	$1x10^{-5}$	$1x10^{-11}$	$1x10^{-4}$	2.11	2.8
α (1/s)	$5x10^{-7}$	$1x10^{-10}$	$1x10^{-5}$	2.12	
m_{coc} (g COC/cm^3)	$1x10^{-6}$	$1x10^{-10}$	$1x10^{-4}$	2.13	2.9
$m_{coc,w}$ (g COC/cm^3)	$1x10^{-6}$	$1x10^{-10}$	$1x10^{-4}$	2.14	2.10
D_m (cm^2/s)	$4.1x10^{-6}$ (pyrene)	$1x10^{-6}$	$1x10^{-5}$	2.15	2.11
	$3.7x10^{-6}$ (b[a]p)				
K_{oc} (cm^3/g)	$1.7x10^{5}$ (pyrene)	$1x10^{0}$	$1x10^{7}$	2.15	2.11
	$3.9x10^{6}$ (b[a]p)				
K_c (cm^3/g COC)	$5.2x10^{4}$ (pyrene)	*	*		
	$1.2x10^{6}$ (b[a]p)				
D_c (cm^2/s)	$3x10^{-6}$				
ρ_s (g/cm^3)	2.5				
S_L (ng/g)	1000				
C_w (ng/cm^3)	0				

* It is assumed $K_c = 0.3K_{oc}$.

For sediments rich in organic matter, a large fraction of each organic chemical is sorbed to the solids. On the one hand, the desorption enhancement is extensive (Table 2.3) because of the abundant source of each chemical from the solids to the porewater. As a result, the resistance in the sediment bed is lessened as f_{oc} is increased. On the other hand, the fraction of mobile chemical, i.e. the fraction of chemical that is able to travel across the sediment-water interface, is diminished with greater organic matter contents. Since the water resistance is more important than the sediment resistance, the net effect is that the diffusive flux only decreases somewhat as the sediment organic carbon content increases (Figure 2.6). The irrigational flux also decreases due to the decreasing amount of mobile chemicals.

For sediment of higher porosity, the fraction of mobile chemical is larger; however, the desorption enhancement becomes less significant. The degree of the decrease of the desorption enhancement is larger than the increase of porosity (Table 2.4). As a result, the resistance in the sediments increases as the porosity increases. When the water resistance, which does not change with the porosity, is much more important than the sediment resistance, the diffusive flux is not sensitive to porosity (Figure 2.7). For porosity larger than 0.9, desorption decreases to a greater extent, and the sediment resistance becomes more significant. Therefore, the diffusive flux decreases as the porosity decreases. In contrast, the irrigational flux is not controlled by the resistances. The more the mobile chemical is, the larger the irrigational flux is. However, the irrigational flux is insignificant compared to the diffusive flux. The sensitivity of the total flux to porosity is consistent with the sensitivity of the diffusive flux to porosity.

Table 2.3 Sensitivities of the enhancement factor (ψ) and resistances to the organic carbon content (f_{oc}) of sediments

PYRENE

f_{oc}	ψ	$1/v_s$ s/cm	$1/v_w$ s/cm	$1/v_{tot}$ s/cm
1%	730	2600	3400	6000
2%	1400	1300	3400	4700
3%	2100	910	3400	4300
4%	2700	700	3400	4100
5%	3300	570	3400	4000
6%	3900	480	3400	3900
7%	4400	420	3400	3800
8%	5000	370	3400	3800
9%	5600	340	3400	3700
10%	6100	310	3400	3700

BENZO[A]PYRENE

f_{oc}	ψ	$1/v_s$ s/cm	$1/v_w$ s/cm	$1/v_{tot}$ s/cm
1%	6800	140	2000	2200
2%	12000	76	2000	2100
3%	17000	55	2000	2100
4%	22000	43	2000	2100
5%	26000	36	2000	2100
6%	30000	32	2000	2100
7%	33000	28	2000	2100
8%	37000	25	2000	2100
9%	40000	23	2000	2100
10%	44000	21	2000	2100

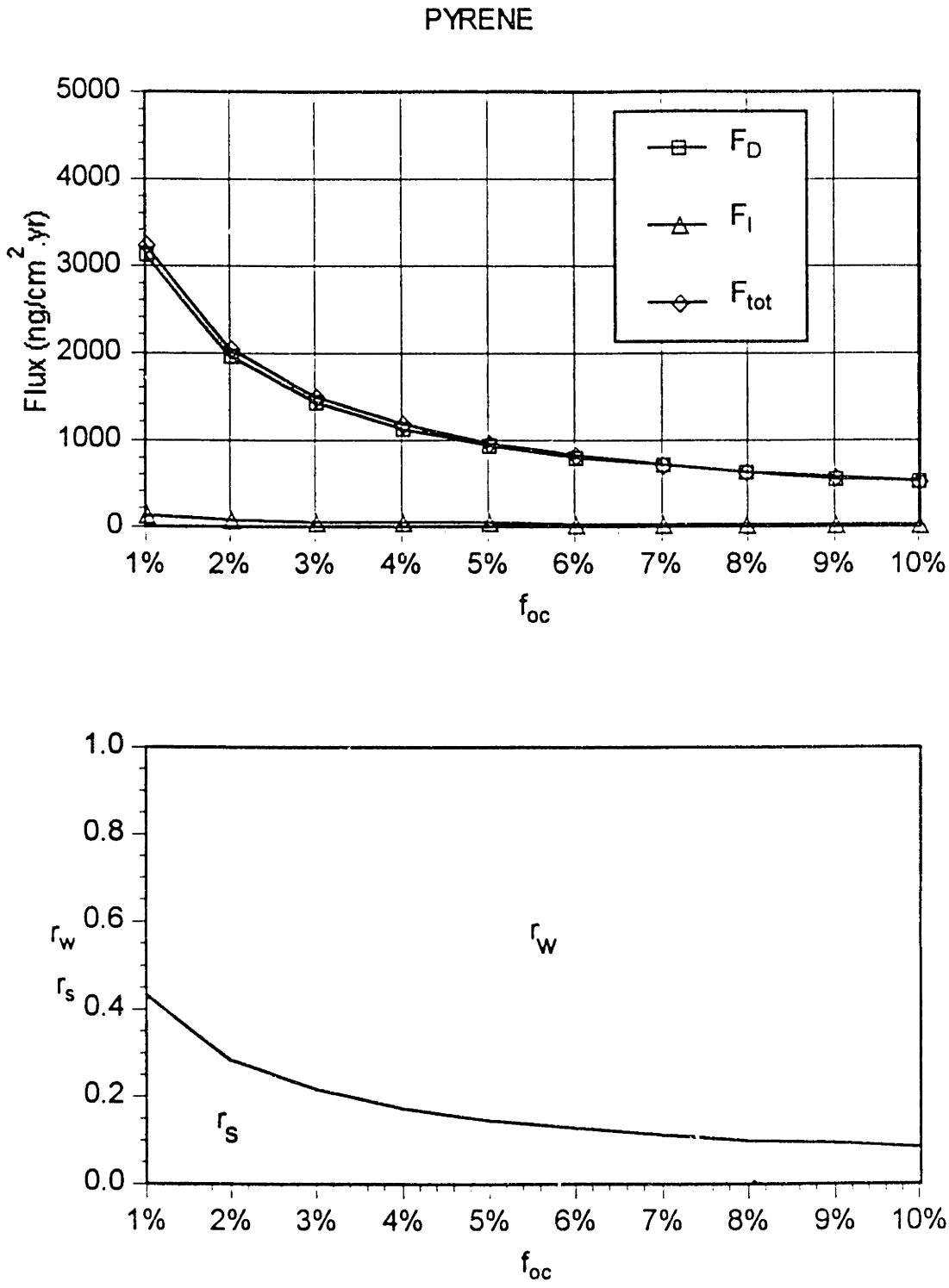

Figure 2.6a Sensitivities of fluxes and resistances to the organic carbon content (f_{oc}) of sediments for pyrene

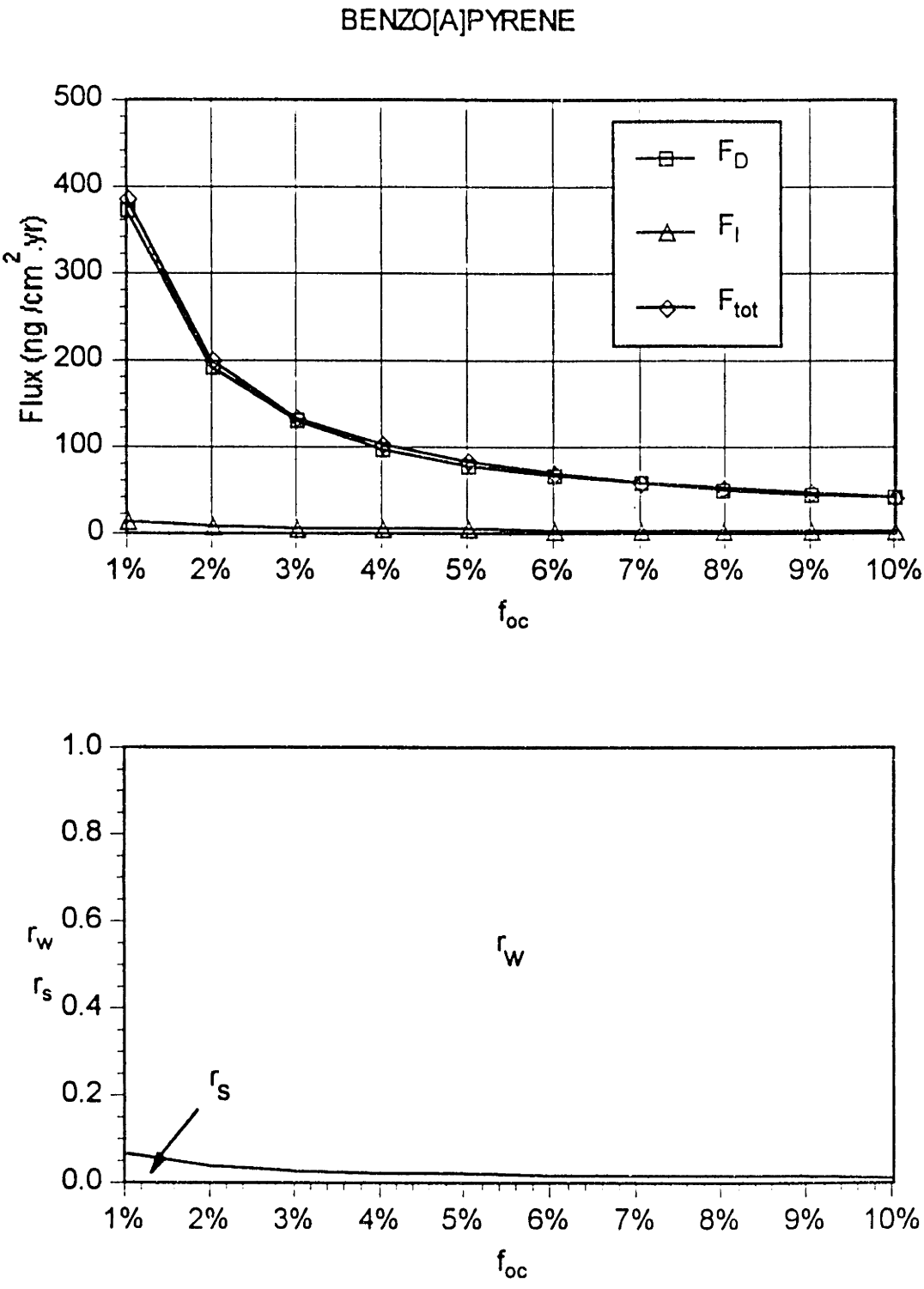

Figure 2.6b Sensitivities of fluxes and resistances to the organic carbon content (f_{oc}) of sediments for benzo[a]pyrene

Table 2.4 Sensitivities of the enhancement factor (ψ) and resistances to porosity (ϕ)

PYRENE

ϕ	ψ	$1/v_s$ s/cm	$1/v_w$ s/cm	$1/v_{tot}$ s/cm
0.1	120000	150	3400	3500
0.2	55000	170	3400	3600
0.3	31000	200	3400	3600
0.4	20000	230	3400	3600
0.5	13000	270	3400	3700
0.6	8200	340	3400	3700
0.7	5000	450	3400	3800
0.8	2800	670	3400	4100
0.9	1200	1300	3400	4700
0.99	103	13000	3400	17000

BENZO[A]PYRENE

ϕ	ψ	$1/v_s$ s/cm	$1/v_w$ s/cm	$1/v_{tot}$ s/cm
0.1	940000	10	2000	2100
0.2	420000	11	2000	2100
0.3	240000	12	2000	2100
0.4	150000	14	2000	2100
0.5	99000	17	2000	2100
0.6	64000	21	2000	2100
0.7	40000	28	2000	2100
0.8	23000	42	2000	2100
0.9	9700	83	2000	2100
0.99	850	820	2000	2900

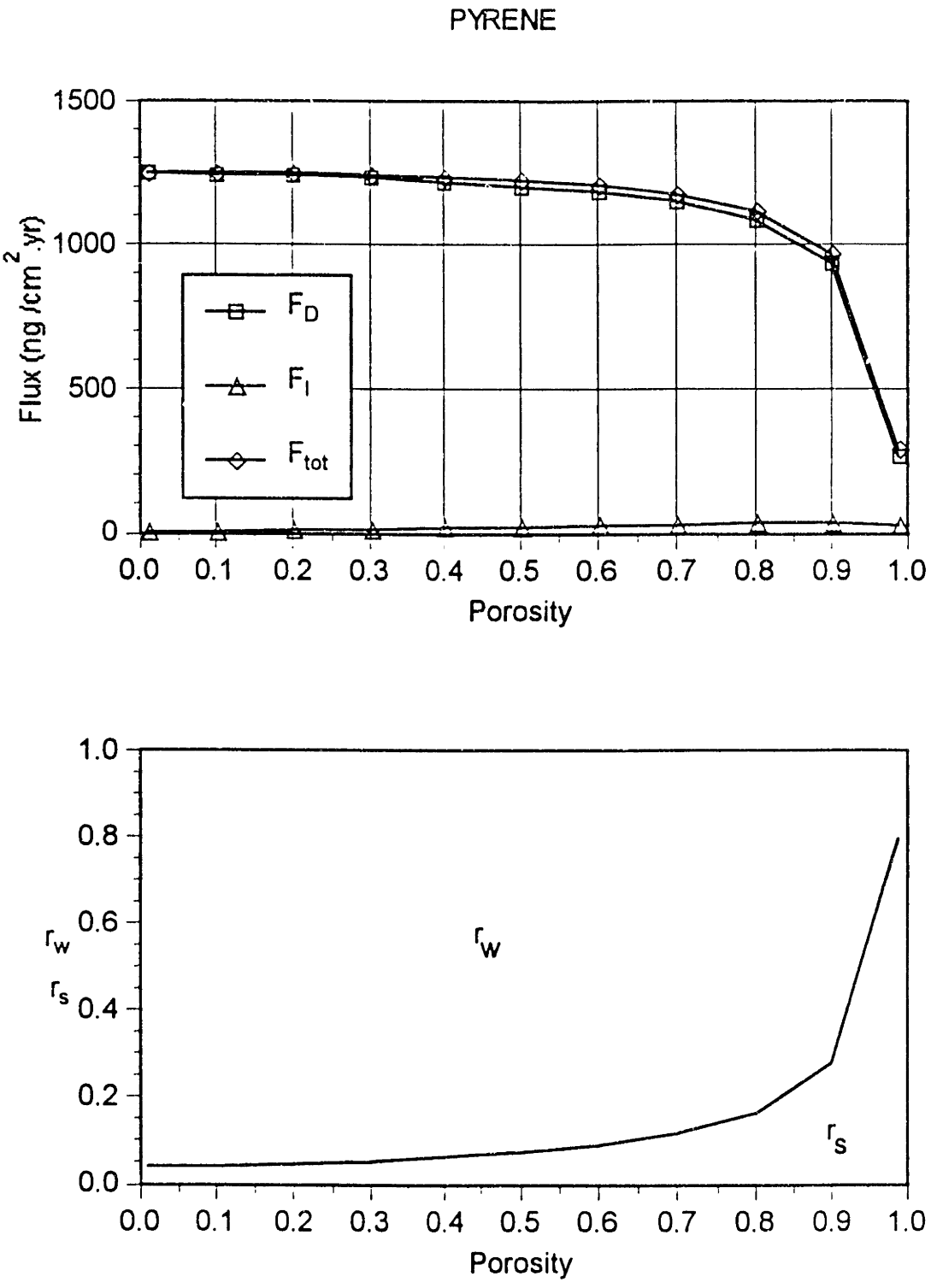

Figure 2.7a Sensitivities of fluxes and resistances to porosity (ϕ) for pyrene

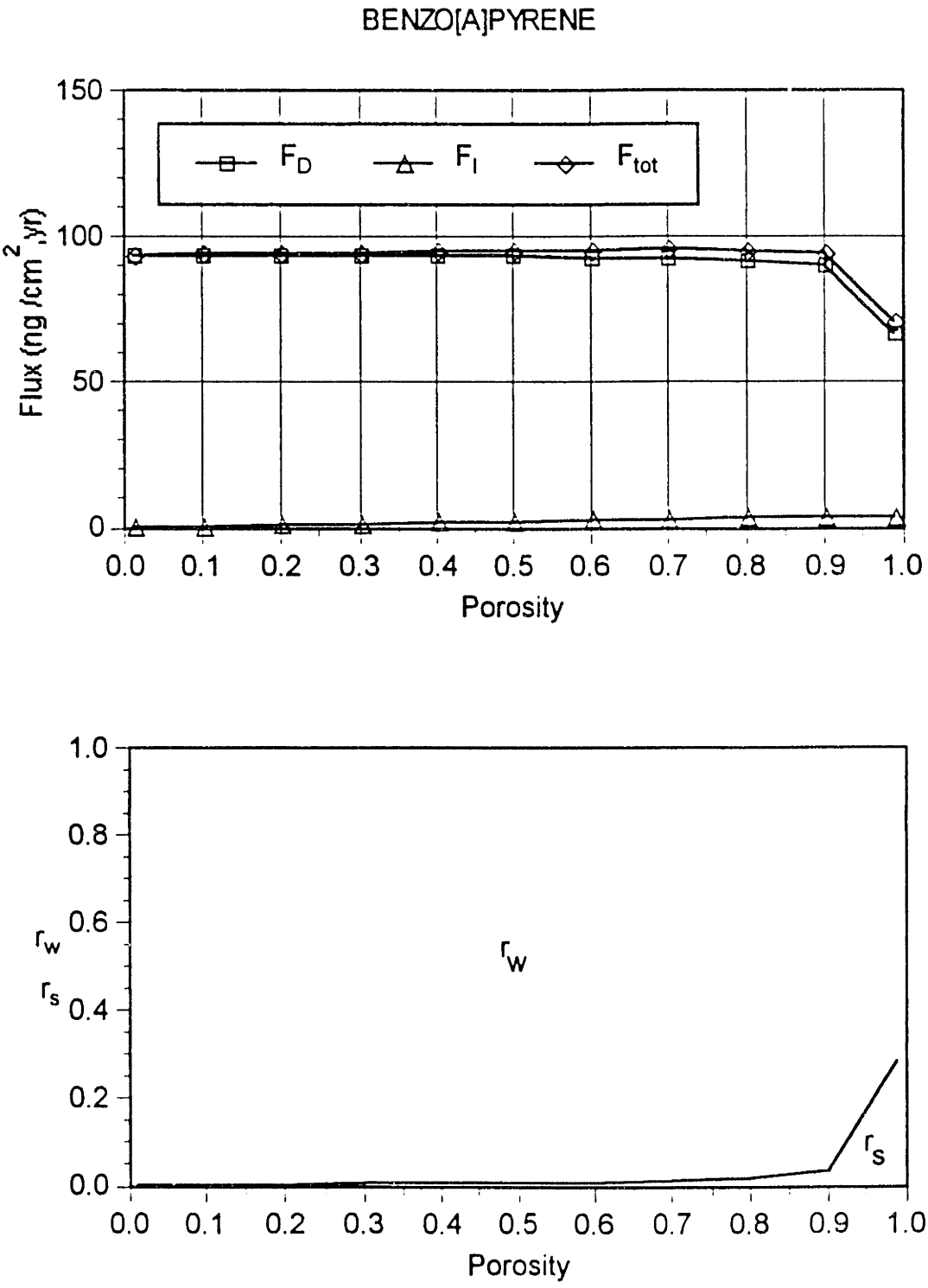

Figure 2.7b Sensitivities of fluxes and resistances to porosity (ϕ) for benzo[a]pyrene

The desorption of a chemical in the sediments depends on the size of the aggregates; for larger aggregates, the desorption rate decreases. Consequently, the desorption enhancement is smaller, and the resistance in sediments becomes more extensive (Table 2.5). For aggregates smaller than 10^{-2} cm, the sediment resistance is much less important than the water resistance; therefore, the flux is not sensitive to the aggregate size (Figure 2.8). For aggregates larger than 10^{-2} cm, the sediment resistance becomes more important, and the flux decreases as the aggregate size increases.

For diffusive fluxes, the resistance in the sediments becomes larger when the pollutants need to travel a longer distance (Table 2.6). However, this effect is counterbalanced by the desorption enhancement, which increases as the thickness of the biologically active layer (L) is increased. The desorption enhancement for a highly hydrophobic chemical, such as benzo[a]pyrene, is greater than that for a more soluble chemical, such as pyrene. As a result, for a more hydrophobic chemical, the sediment resistance becomes less important, and the diffusive flux is not as sensitive to L as that is for a soluble chemical (Figure 2.9). In contrast to the diffusive flux, the irrigational flux is proportional to L for both hydrophobic and soluble chemicals. The sensitivity of the total flux to L depends on the competition of the diffusive flux with the irrigational flux. Generally, under the conditions modeled here, the irrigational flux F_I is small relative to its counterpart diffusive flux F_D (Figure 2.9).

The thickness of the diffusive water boundary layer (Z_w) determines the magnitude of the resistance in this layer (Table 2.7). For the Z_w values reported in the studies cited in Section 2.5 (10^{-2} to 10^{0} cm), the water resistance, which is increased for thicker water

Table 2.5 Sensitivities of the enhancement factor (ψ) and resistances to the aggregate size (R)

PYRENE

R		ψ	$1/v_s$	$1/v_w$	$1/v_{tot}$
cm			s/cm	s/cm	s/cm
10^{-5}	(100 nm)	3300	560	3400	3900
10^{-4}	(1 μm)	3300	560	3400	3900
10^{-3}	(10 μm)	3300	570	3400	4000
10^{-2}	(100 μm)	2800	670	3400	4100
10^{-1}	(1 mm)	1100	1700	3400	5000
10^{0}	(1 cm)	160	11000	3400	15000

BENZO[A]PYRENE

R		ψ	$1/v_s$	$1/v_w$	$1/v_{tot}$
cm			s/cm	s/cm	s/cm
10^{-5}	(100 nm)	38000	24	2000	2100
10^{-4}	(1 μm)	38000	25	2000	2100
10^{-3}	(10 μm)	36000	26	2000	2100
10^{-2}	(100 μm)	23000	42	2000	2100
10^{-1}	(1 mm)	4800	200	2000	2200
10^{0}	(1 cm)	540	1800	2000	3800

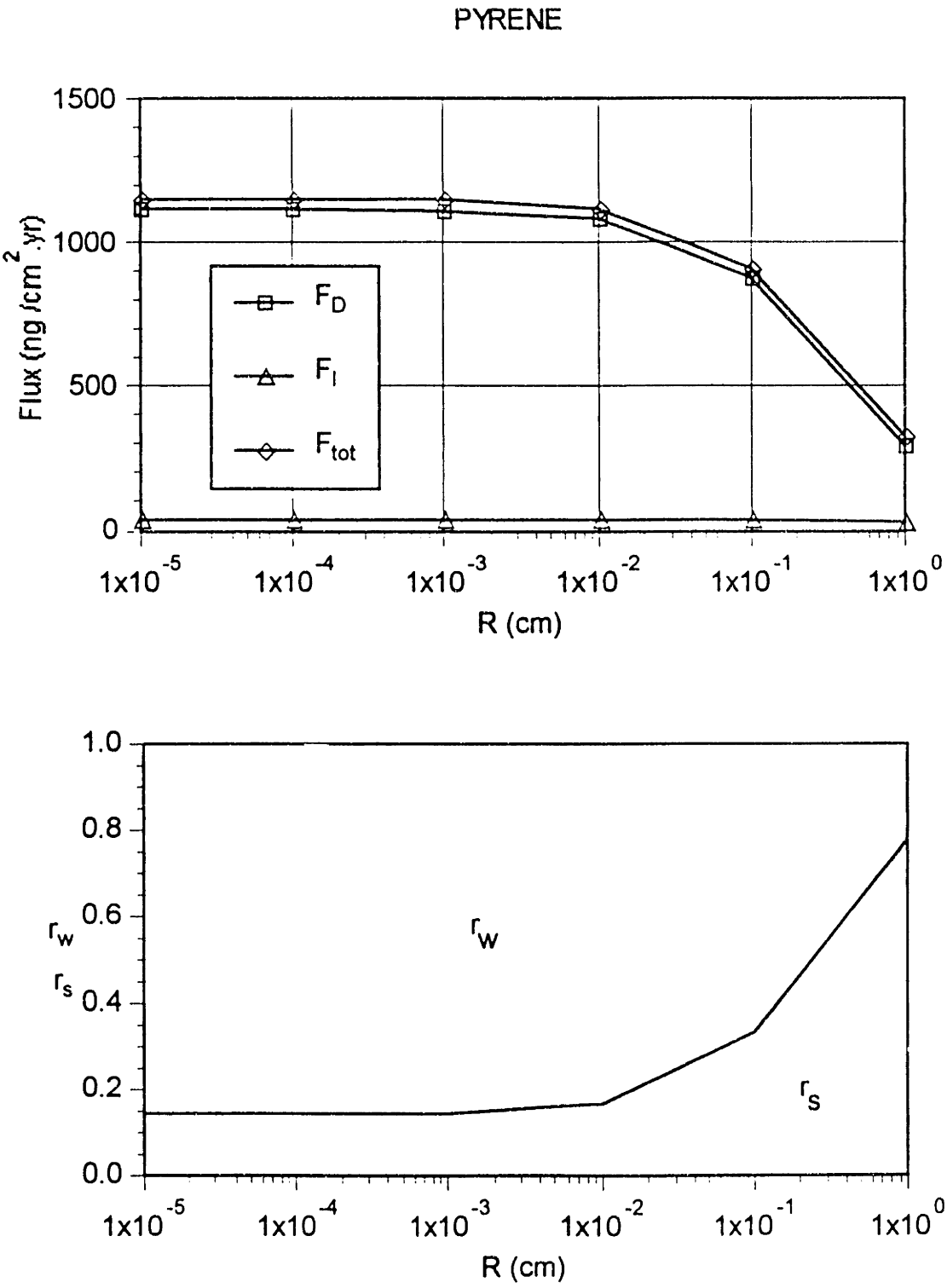

Figure 2.8a Sensitivities of fluxes and resistances to the aggregate size (R) for pyrene

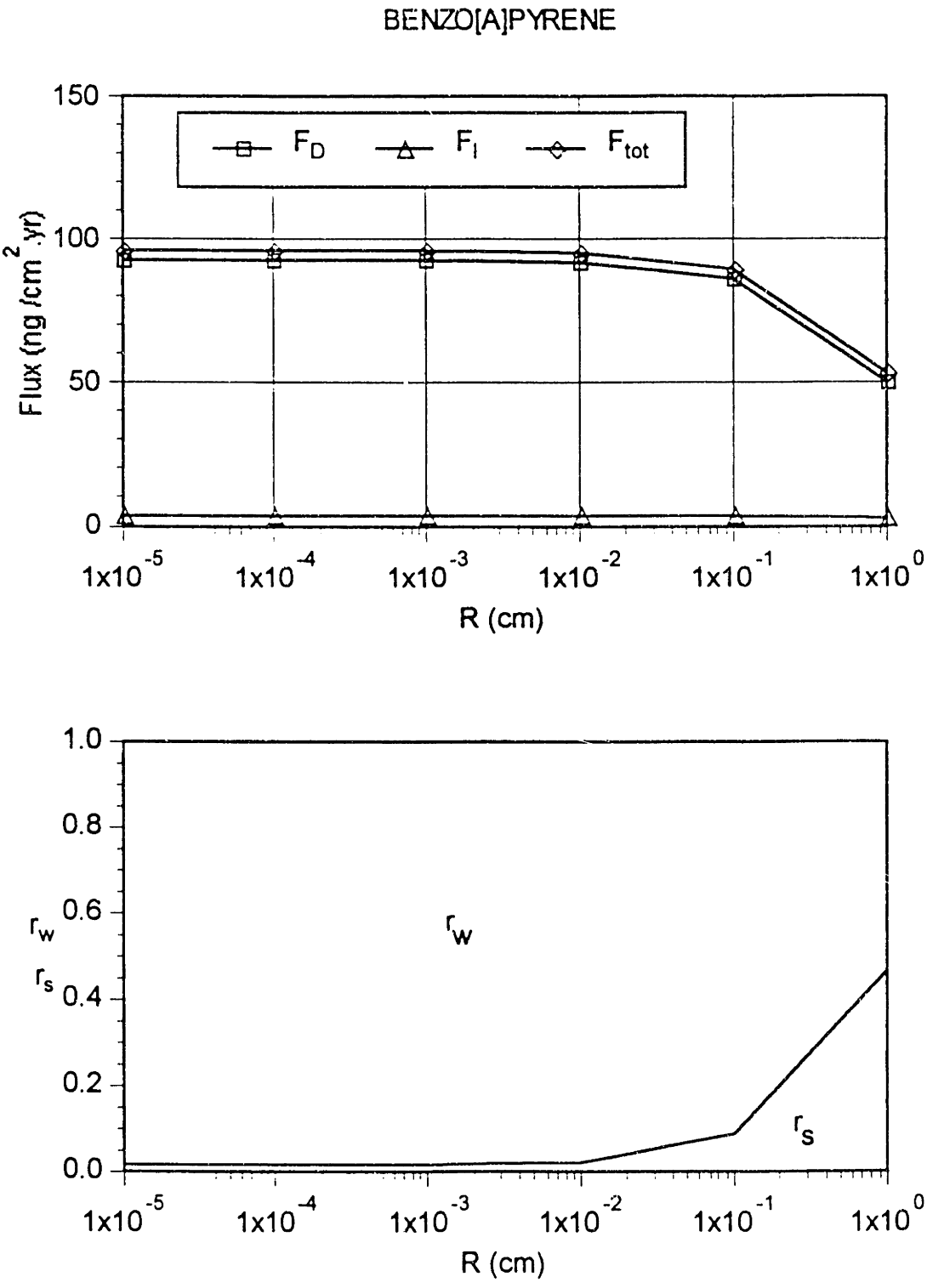

Figure 2.8b Sensitivities of fluxes and resistances to the aggregate size (R) for benzo[a]pyrene

Table 2.6 Sensitivities of the enhancement factor (ψ) and resistances to the thickness of the biologically active layer (L)

PYRENE

L	ψ	$1/v_s$	$1/v_w$	$1/v_{tot}$
cm		s/cm	s/cm	s/cm
1	680	140	3400	3500
10	2400	390	3400	3800
20	2800	670	3400	4100
50	3100	1500	3400	4900
70	3200	2100	3400	5500
100	3200	2900	3400	6300

BENZO[A]PYRENE

L	ψ	$1/v_s$	$1/v_w$	$1/v_{tot}$
cm		s/cm	s/cm	s/cm
1	2500	29	2000	2100
10	16000	30	2000	2100
20	23000	42	2000	2100
50	30000	78	2000	2100
70	32000	100	2000	2200
100	34000	140	2000	2200

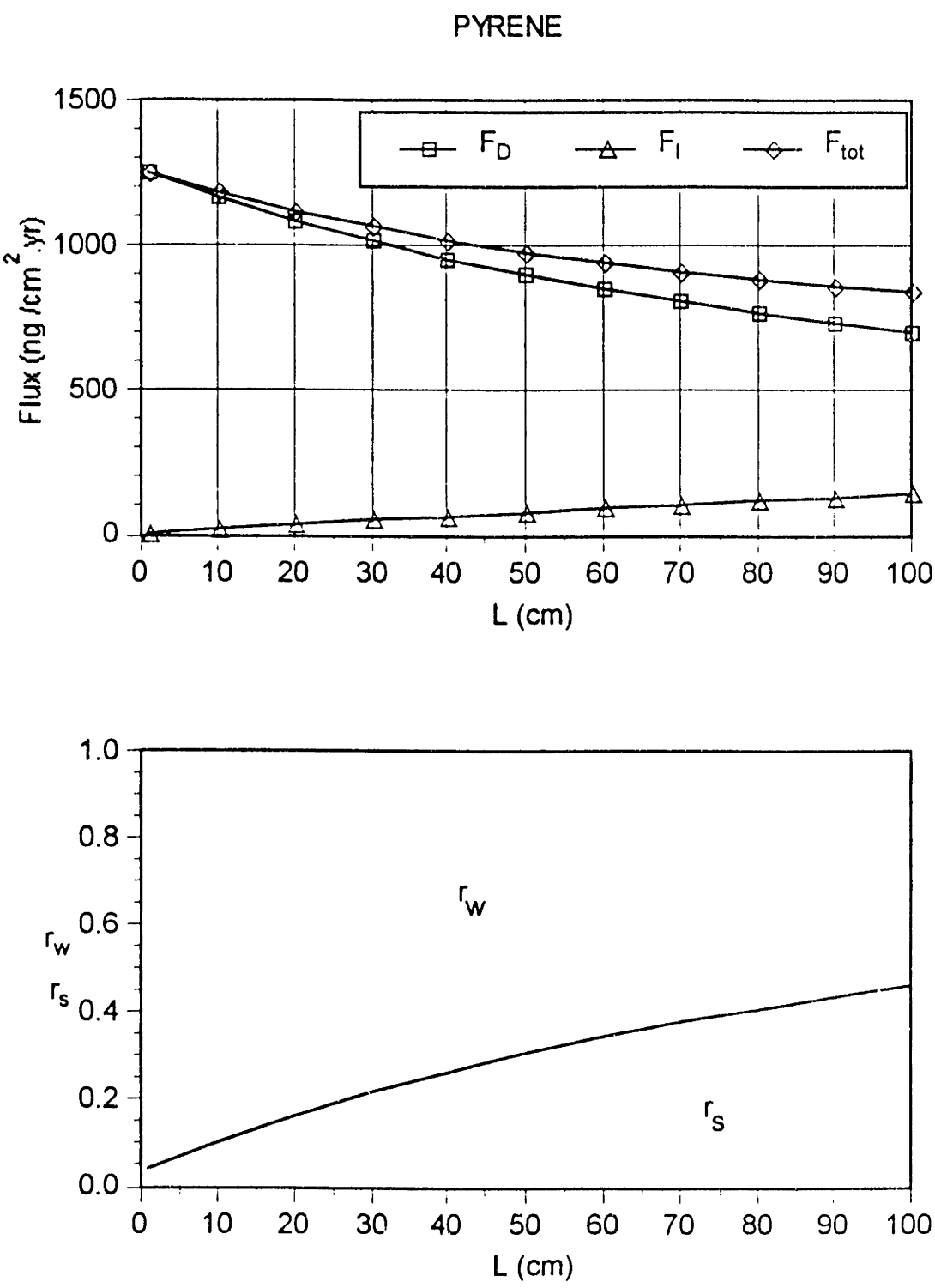

Figure 2.9a Sensitivities of fluxes and resistances to the thickness of the biologically active layer (L) for pyrene

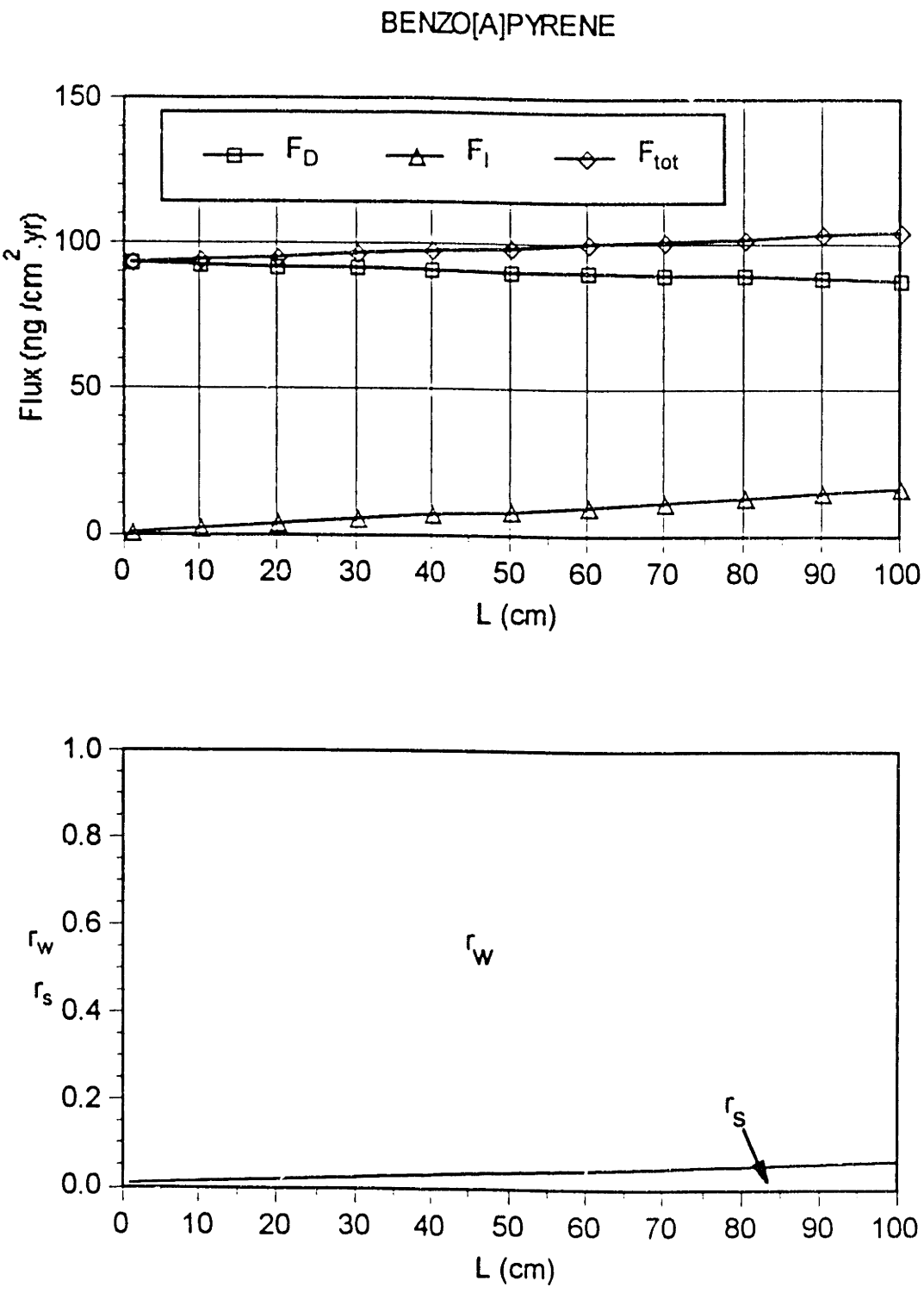

Figure 2.9b Sensitivities of fluxes and resistances to the thickness of the biologically active layer (L) for benzo[a]pyrene

Table 2.7 Sensitivities of the enhancement factor (ψ) and resistances to the thickness of the diffusive water boundary layer (Z_w)

PYRENE

	Z_w	ψ	$1/v_s$	$1/v_w$	$1/v_{tot}$
cm			s/cm	s/cm	s/cm
10^{-3}	(10 μm)	2800	670	230	900
10^{-2}	(100 μm)	2800	670	2300	2900
10^{-1}	(1 mm)	2800	670	23000	23000
10^{0}	(1 cm)	2800	670	230000	230000

BENZO[A]PYRENE

	Z_w	ψ	$1/v_s$	$1/v_w$	$1/v_{tot}$
cm			s/cm	s/cm	s/cm
10^{-3}	(10 μm)	23000	42	140	180
10^{-2}	(100 μm)	23000	42	1400	1400
10^{-1}	(1 mm)	23000	42	14000	14000
10^{0}	(1 cm)	23000	42	140000	140000

boundary layers, is more significant than the sediment resistance. Therefore, the decrease of the diffusive flux is very sensitive to the increase of Z_w (Figure 2.10; note the use of logarithmic scales of the flux diagram). In contrast, the irrigational flux increases when Z_w increases, because when Z_w is larger, the amount of chemicals released from the sediments is smaller, and, consequently, the concentration difference between the chemicals in the sediments and the chemicals in the overlying water column is larger.

Bioturbation facilitates the chemical exchange across the sediment-water interface. However, when bioturbation is much slower than molecular diffusion ($D_B << D'_m$), molecular diffusion is the only transport mechanism within the sediments. The transport in the sediments becomes so slow that the sediment resistance is much more significant than the water resistance. Therefore, molecular diffusion is the dominating transport factor controlling the diffusive flux, and consequently the diffusive flux is not sensitive to such slow bioturbation (Figure 2.11). When bioturbation becomes comparable to molecular diffusion, the sediment resistance is decreased with faster bioturbation (Table 2.8), and the diffusive flux becomes sensitive to bioturbation.

As indicated in Section 2.6.1, irrigation has negligible effect on the vertical distribution of the chemical concentration. Therefore, the diffusive flux is not sensitive to the irrigation rate α (Figure 2.12). The irrigational flux is proportional to the irrigation rate. However, for commonly reported irrigation rates (10^{-6} ~ 10^{-7} 1/s), the irrigational flux is not significant, so the total flux is not sensitive to irrigation.

When there are more organic colloids in the porewater, the fraction of organic chemicals that can travel across the sediment-water interface is larger. However, this

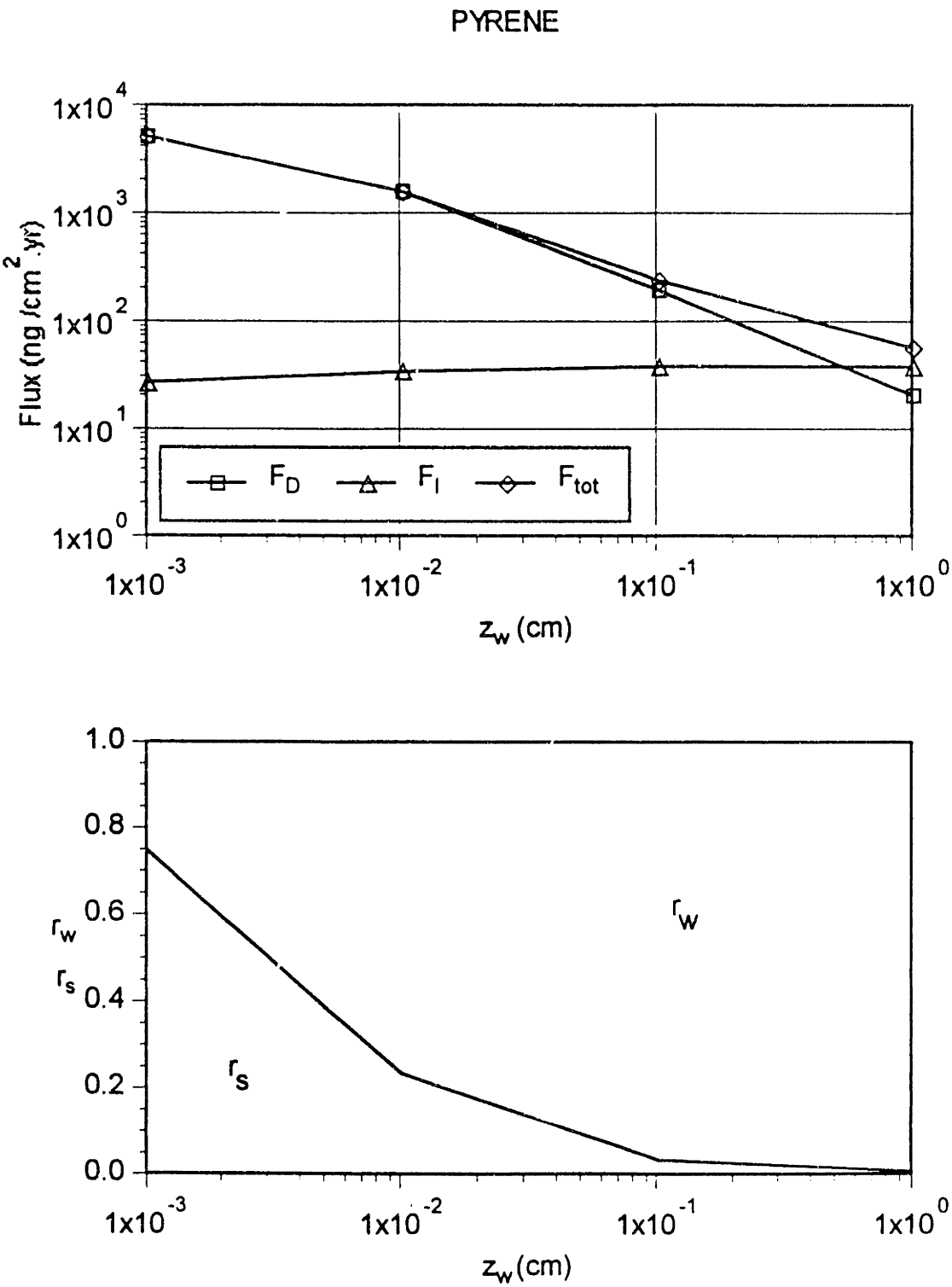

Figure 2.10a Sensitivities of fluxes and resistances to the thickness of the diffusive water boundary layer (Z_w) for pyrene

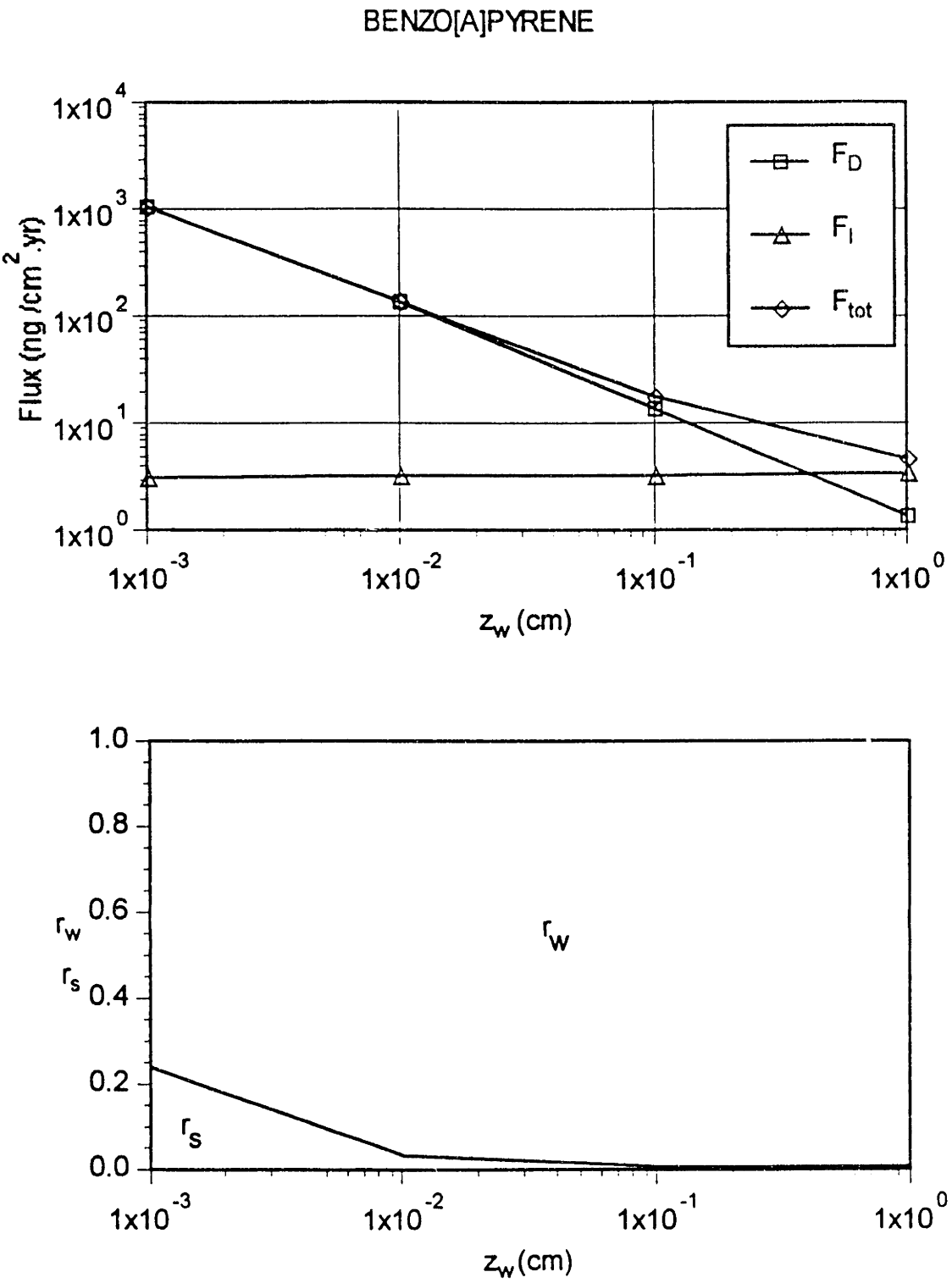

Figure 2.10b Sensitivities of fluxes and resistances to the thickness of the diffusive water boundary layer (Z_w) for benzo[a]pyrene

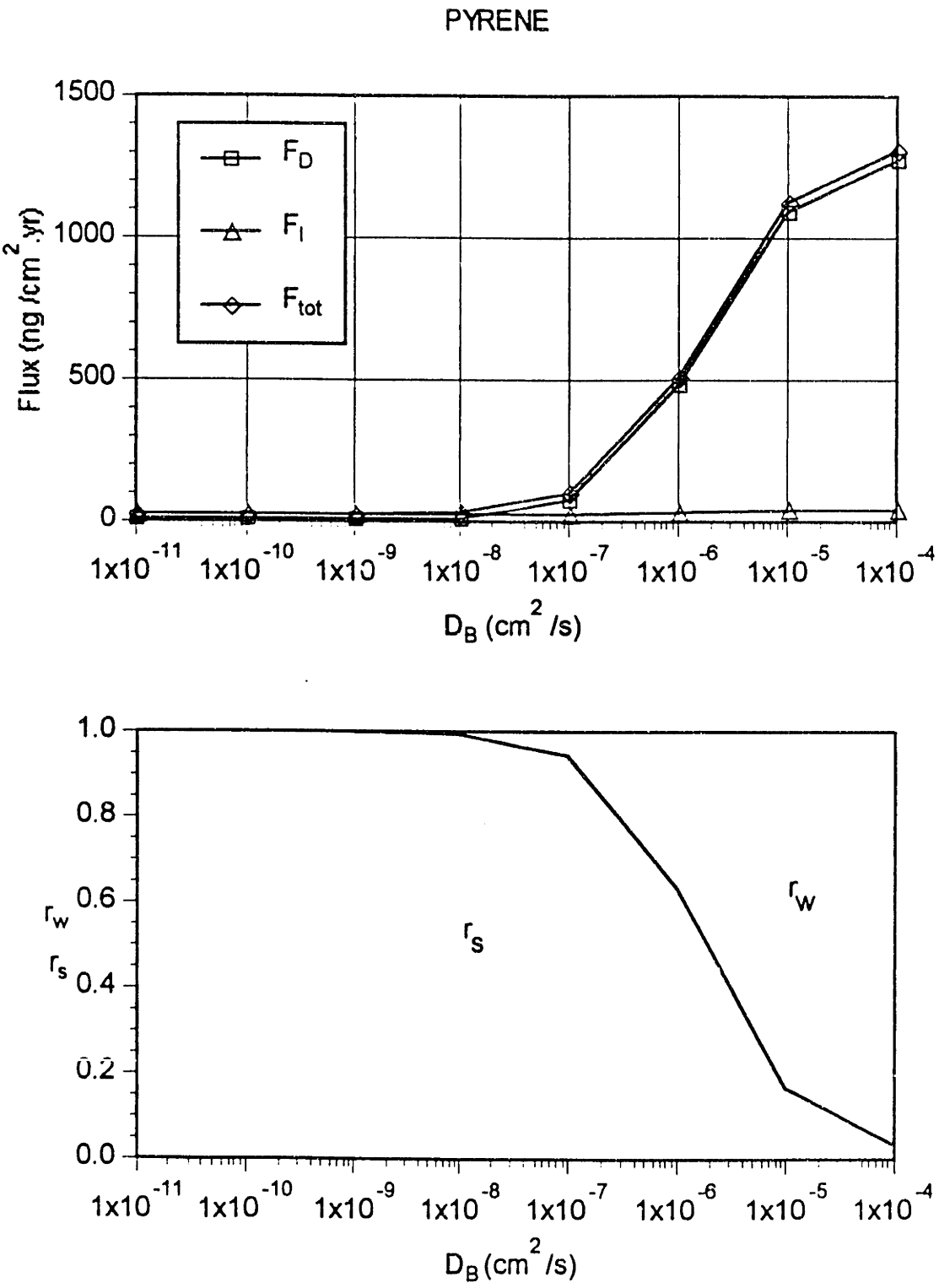

Figure 2.11a Sensitivities of fluxes and resistances to the bioturbation coefficient (D_B) for pyrene

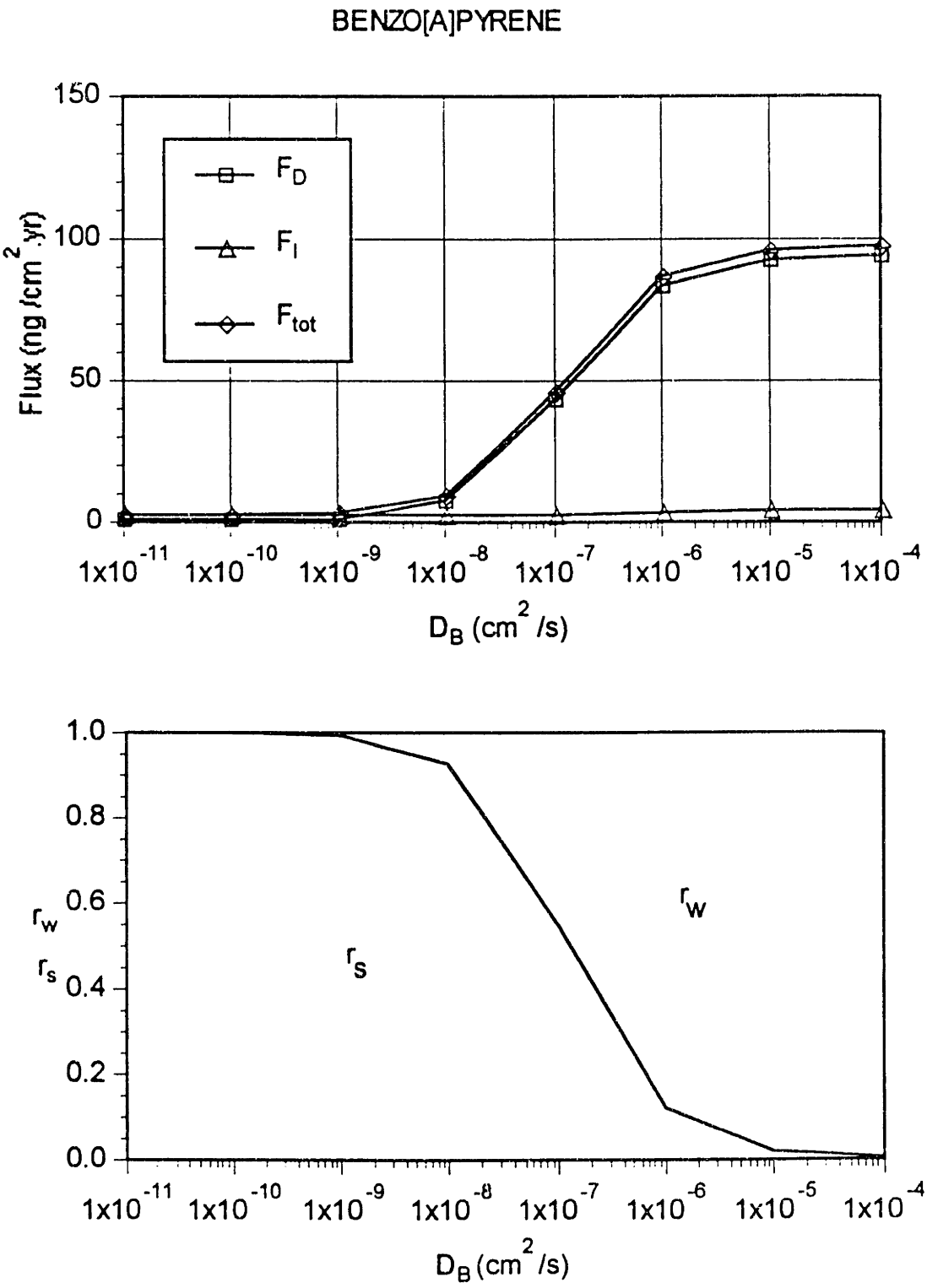

Figure 2.11b Sensitivities of fluxes and resistances to the bioturbation coefficient (D_B) for benzo[a]pyrene

Table 2.8 Sensitivities of the enhancement factor (ψ) and resistances to the bioturbation coefficient (D_B)

PYRENE

D_B	ψ	$1/v_s$	$1/v_w$	$1/v_{tot}$
cm^2/s		s/cm	s/cm	s/cm
10^{-11}	1.0	8700000	3400	8700000
10^{-10}	1.2	7600000	3400	7600000
10^{-9}	2.6	3400000	3400	3400000
10^{-8}	17	530000	3400	530000
10^{-7}	150	56000	3400	59000
10^{-6}	1100	5800	3400	9200
10^{-5}	2800	670	3400	4100
10^{-4}	2500	94	3400	3500

BENZO[A]PYRENE

D_B	ψ	$1/v_s$	$1/v_w$	$1/v_{tot}$
cm^2/s		s/cm	s/cm	s/cm
10^{-11}	1.2	4400000	2000	4400000
10^{-10}	3.2	1700000	2000	1700000
10^{-9}	23	230000	2000	240000
10^{-8}	220	24000	2000	26000
10^{-7}	2000	2500	2000	4500
10^{-6}	13000	280	2000	2300
10^{-5}	23000	42	2000	2100
10^{-4}	13000	8.4	2000	2100

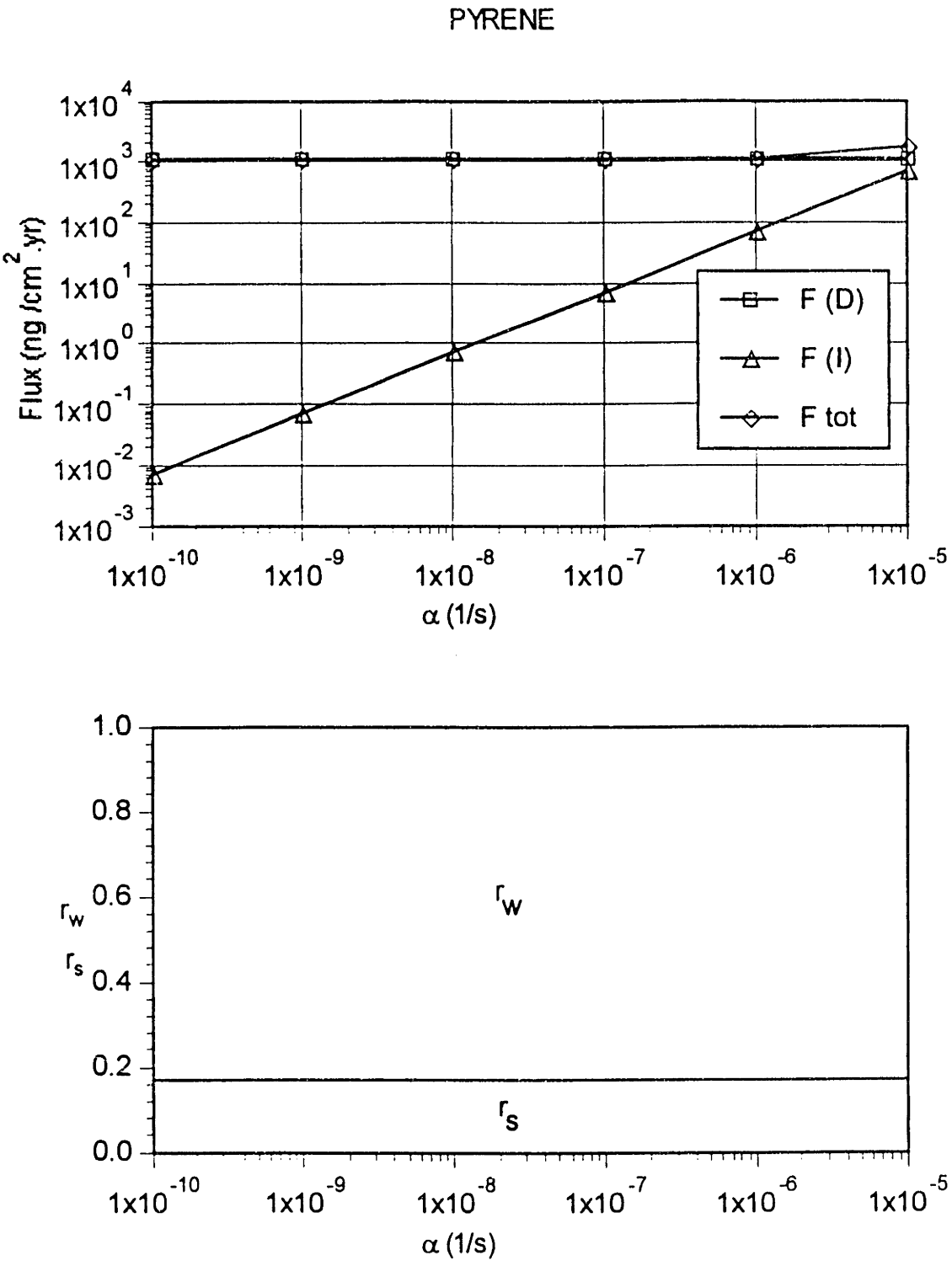

Figure 2.12a Sensitivities of fluxes and resistances to the irrigation rate constant (α) for pyrene

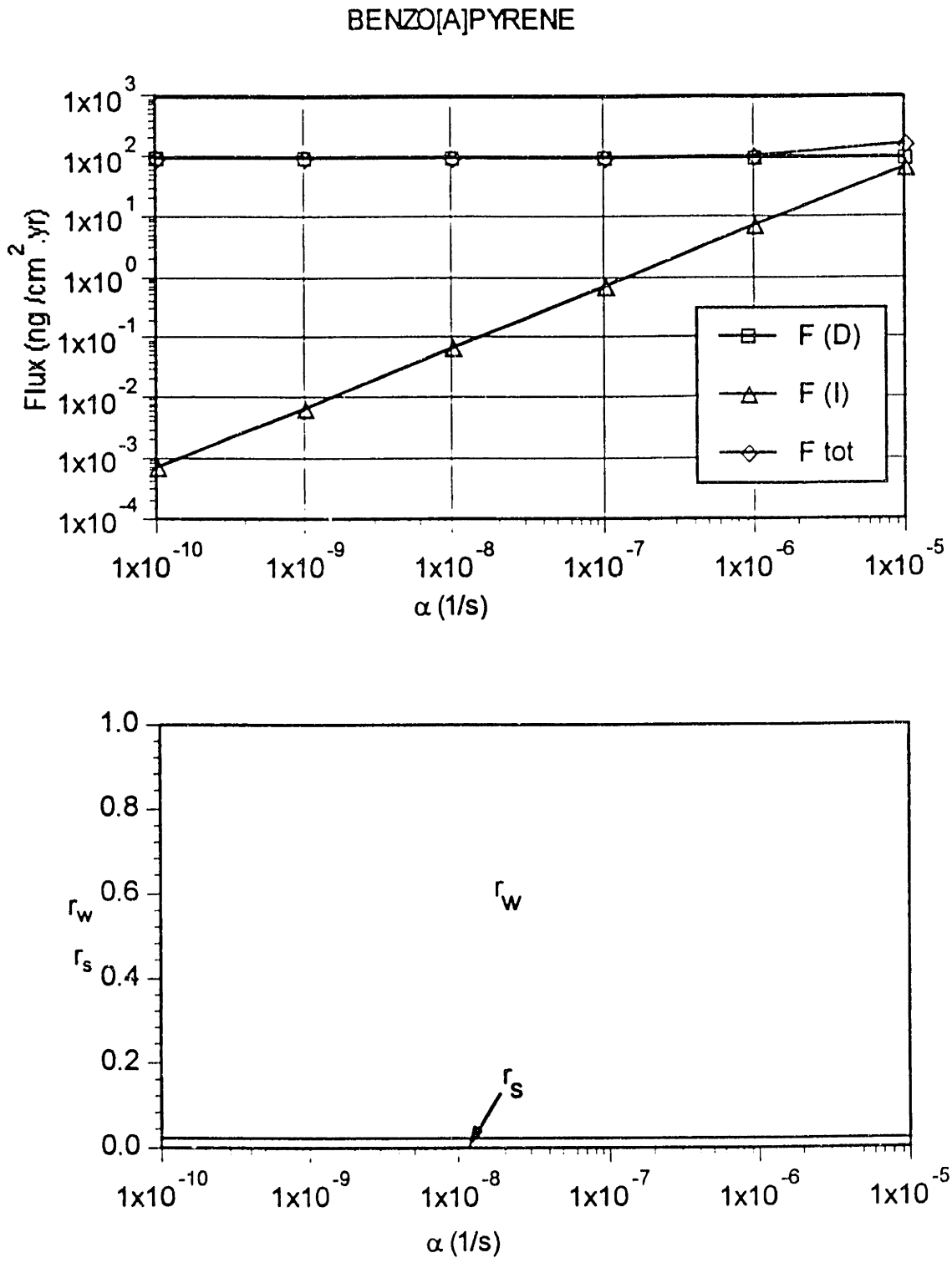

Figure 2.12b Sensitivities of fluxes and resistances to the irrigation rate constant (α) for benzo[a]pyrene

effect is not significant from the point of view of bed-water fluxes. The ratio of the amount of the chemicals in the colloidal phase to that in the dissolved phase is $K_c \cdot m_{coc}$. When the porewater colloids are not abundant, the amount of chemicals associated with colloids is negligible. The fluxes, the desorption enhancement, and the resistance in the sediment are not sensitive to the colloid concentration in the porewater (Figure 2.13, Table 2.9). Even when the organic colloid concentration in the porewater increases to the extent that the amount of the chemical in the colloidal phase is comparable to the amount of the dissolved chemical, the diffusive flux does not show a significant increase. The reason is that when the chemical concentration in the porewater, including the chemical in the colloidal phase, is high, the tendency for enhanced desorption decreases (see Table 2.9). The colloidal enhancement is canceled by the decreasing desorption enhancement. The overall effect slightly decreases the sediment resistance. Since the water resistance is larger than the sediment resistance for the base parameter values for the sensitivity analysis, the diffusive flux is not sensitive to the organic colloid concentration in the porewater. However, the irrigational flux, which is not influenced by the sediment resistance, shows a slight sensitivity (see Figure 2.13).

Similar to the organic colloid concentration in porewater (m_{coc}), the organic colloid concentration in the overlying water column ($m_{coc,w}$) has a negligible effect on the resistance in the water boundary layer when $m_{coc,w}$ is small (Figure 2.14, Table 2.10). Unlike the sediment resistance for m_{coc}, when $m_{coc,w}$ is large, there is no canceling factor for the water resistance, and the water resistance becomes small; therefore, the diffusive flux reflects the decrease of the water resistance and increases. In contrast, the

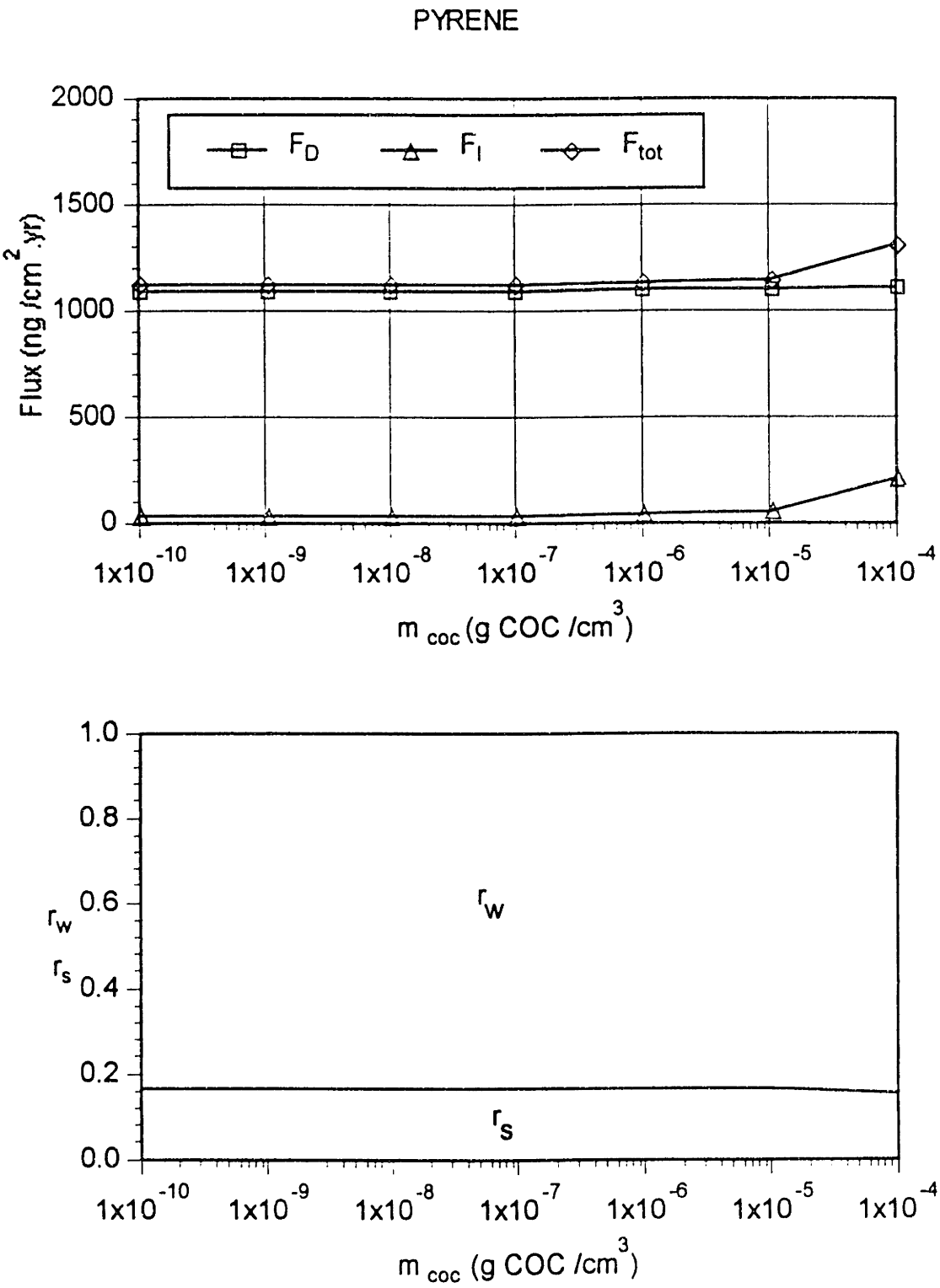

Figure 2.13a Sensitivities of fluxes and resistances to the concentration of colloidal organic carbon in porewater (m_{coc}) for pyrene

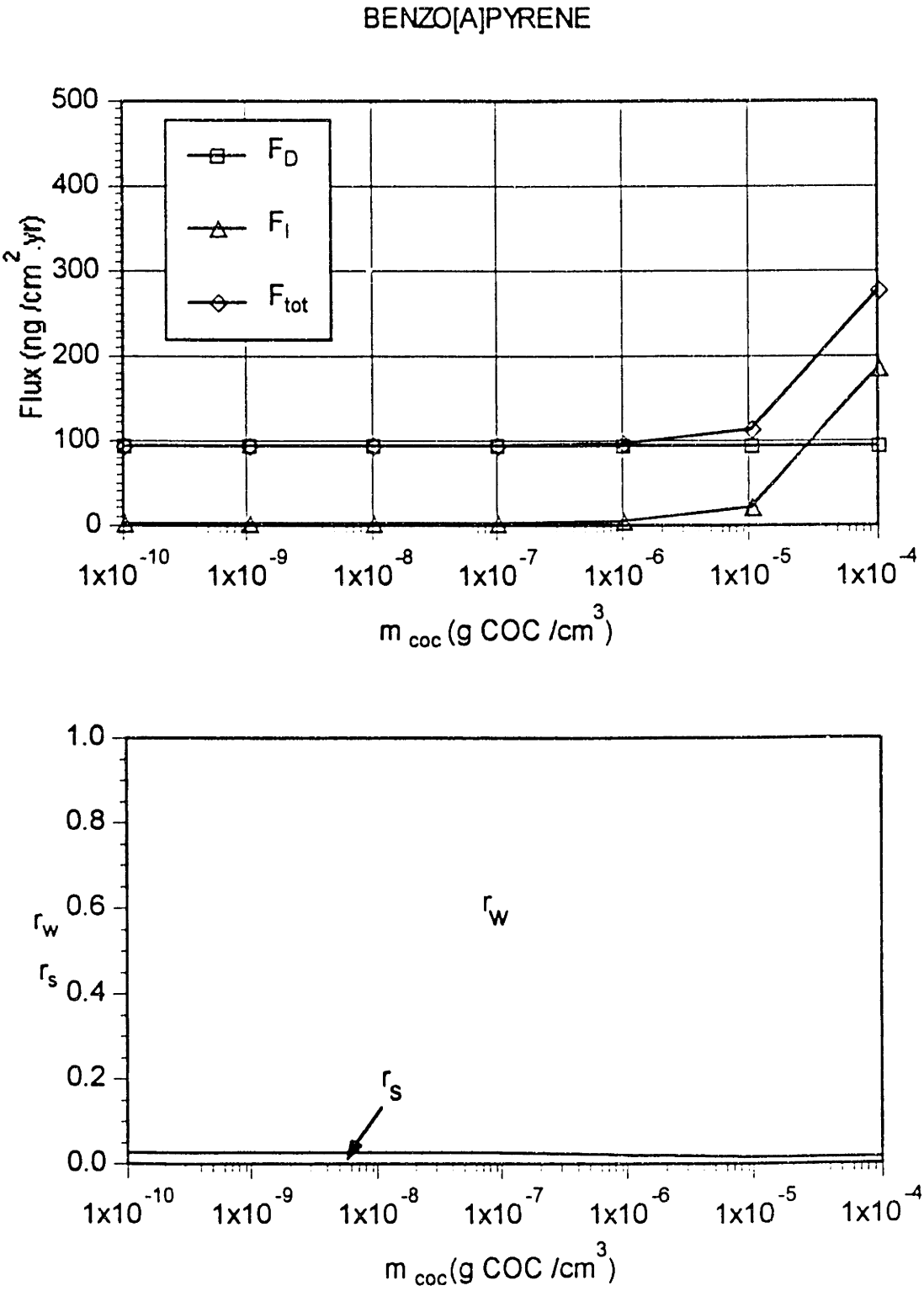

Figure 2.13b Sensitivities of fluxes and resistances to the concentration of colloidal organic carbon in porewater (m_{coc}) for benzo[a]pyrene

Table 2.9 Sensitivities of the enhancement factor (ψ) and resistances to the concentration of colloidal organic carbon in porewater (m_{coc})

PYRENE

m_{coc}	ψ	$1/v_s$	$1/v_w$	$1/v_{tot}$
g COC/cm^3		s/cm	s/cm	s/cm
10^{-10}	2900	670	3400	4100
10^{-9}	2900	670	3400	4100
10^{-8}	2900	670	3400	4100
10^{-7}	2900	670	3400	4100
10^{-6}	2800	670	3400	4100
10^{-5}	2000	650	3400	4000
10^{-4}	550	610	3400	4000

BENZO[A]PYRENE

m_{coc}	ψ	$1/v_s$	$1/v_w$	$1/v_{tot}$
g COC/cm^3		s/cm	s/cm	s/cm
10^{-10}	40000	50	2000	2100
10^{-9}	40000	50	2000	2100
10^{-8}	40000	50	2000	2100
10^{-7}	37000	48	2000	2100
10^{-6}	23000	42	2000	2100
10^{-5}	5100	32	2000	2100
10^{-4}	650	27	2000	2100

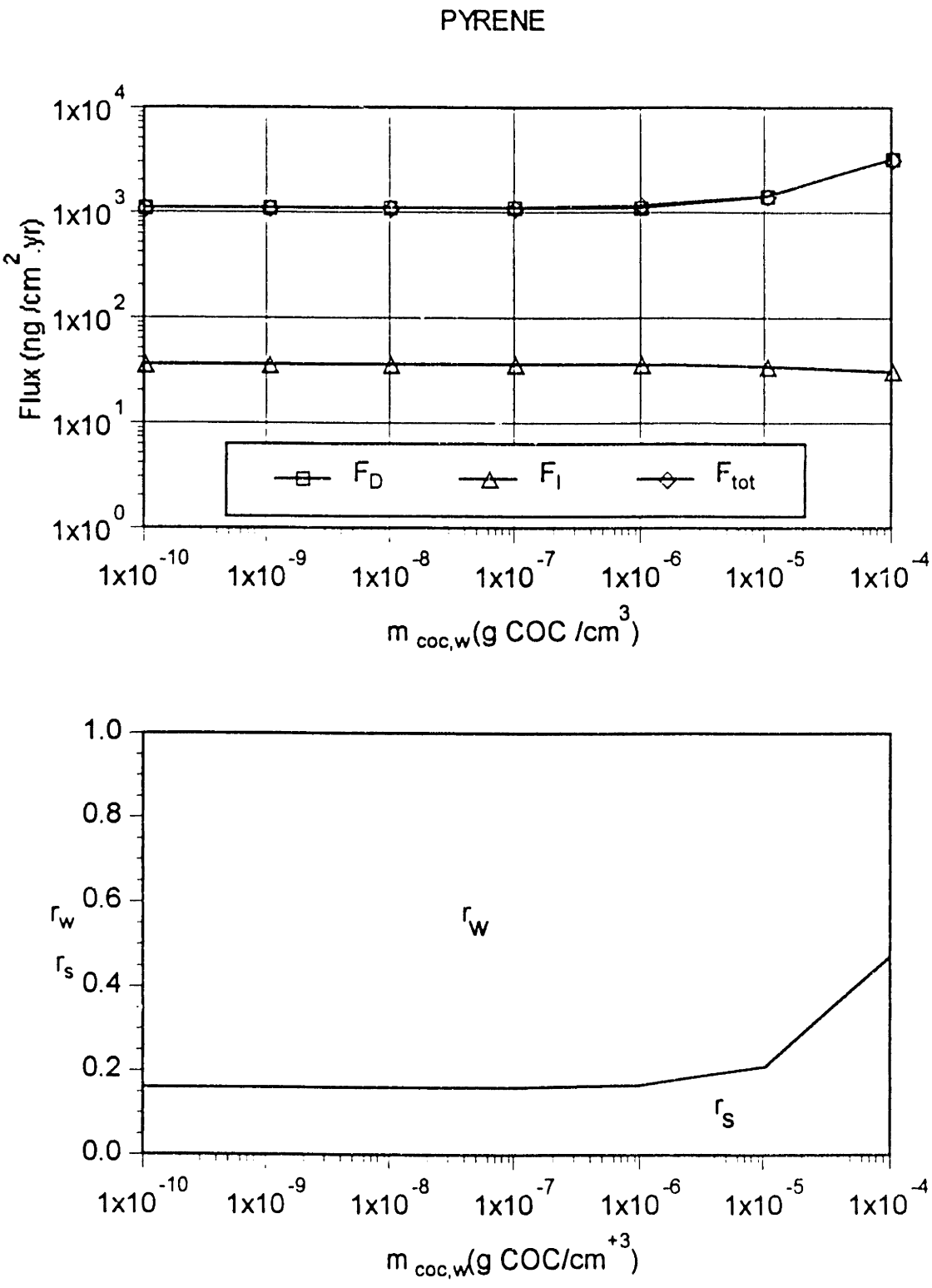

Figure 2.14a Sensitivities of fluxes and resistances to the concentration of colloidal organic carbon in seawater ($m_{coc,w}$) for pyrene

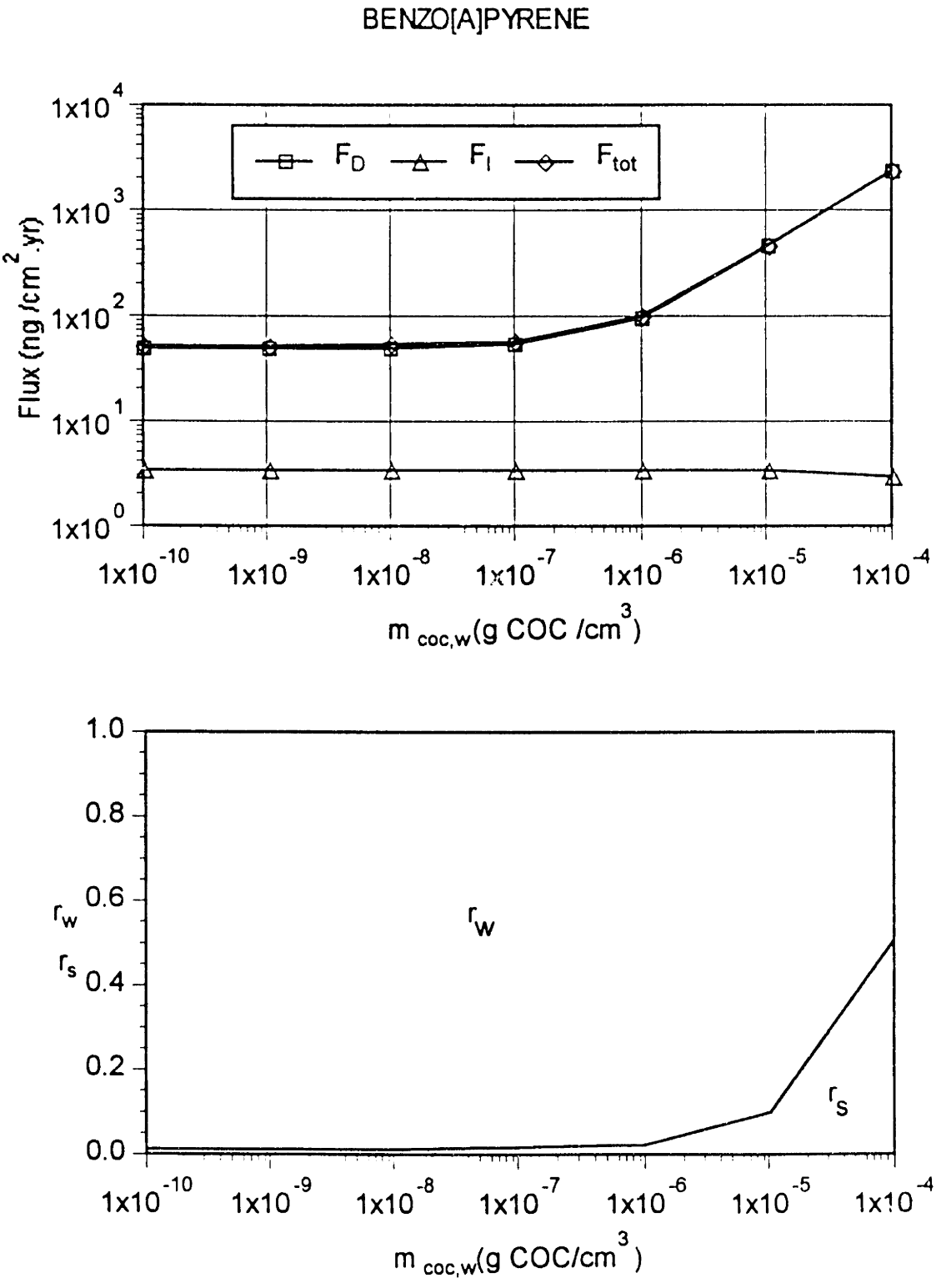

Figure 2.14b Sensitivities of fluxes and resistances to the concentration of colloidal organic carbon in seawater ($m_{coc,w}$) for benzo[a]pyrene

Table 2.10 Sensitivities of the enhancement factor (ψ) and resistances to the concentration of colloidal organic carbon in seawater ($m_{coc,w}$)

PYRENE

$m_{coc,w}$	ψ	$1/v_s$	$1/v_w$	$1/v_{tot}$
g COC/cm^3		s/cm	s/cm	s/cm
10^{-10}	2800	670	3500	4200
10^{-9}	2800	670	3500	4200
10^{-8}	2800	670	3500	4200
10^{-7}	2800	670	3500	4200
10^{-6}	2800	670	3400	4100
10^{-5}	2800	670	2600	3200
10^{-4}	2800	670	760	1400

BENZO[A]PYRENE

$m_{coc,w}$	ψ	$1/v_s$	$1/v_w$	$1/v_{tot}$
g COC/cm^3		s/cm	s/cm	s/cm
10^{-10}	23000	42	4000	4000
10^{-9}	23000	42	4000	4000
10^{-8}	23000	42	4000	4000
10^{-7}	23000	42	3600	3700
10^{-6}	23000	42	2000	2100
10^{-5}	23000	42	380	420
10^{-4}	23000	42	42	83

irrigational flux decreases because when the diffusive flux is larger, the concentration difference between the chemical in the sediments and the chemical in the overlying water column becomes smaller.

In addition to the sensitivities to the environmental factors discussed above, the sensitivities to properties of the chemical of interest were also analyzed. The properties of chemicals that can affect the fluxes are the aqueous solution molecular diffusivity (D_m), the organic carbon-water partition coefficient (K_{oc}) and the organic colloid-water distribution coefficient (K_c). The K_c values for pyrene and benzo[a]pyrene at site S1 reported by Chin and Gschwend (1992), which were used as the base values for this sensitivity analysis, were about three-tenths as great as the corresponding K_{oc} values (see Table 2.2). Therefore, for this sensitivity analysis, K_c is assumed to be three-tenths as much as K_{oc} .

When the chemical is more mobile (i.e., D_m is large), the resistances in both the sediments and the water boundary layer are smaller, and the diffusive flux is greater (Figure 2.15a). Hydrophobic chemicals, which have high K_{oc} and K_c, tend to be associated with the solid matrices and the colloids in the sediments. Similar to the effect of the organic content of the sediments, the sediment resistance is reduced by the extensive desorption enhancement (Table 2.11), and the water resistance is also lowered due to the high affiliation of hydrophobic chemicals with the colloids. However, for higher K_{oc} compounds, only a small fraction of the chemical is dissolved in the porewater and able to move across the sediment-water interface. The net result of the competition between the enhanced load of mobile species and the increased total resistance determines

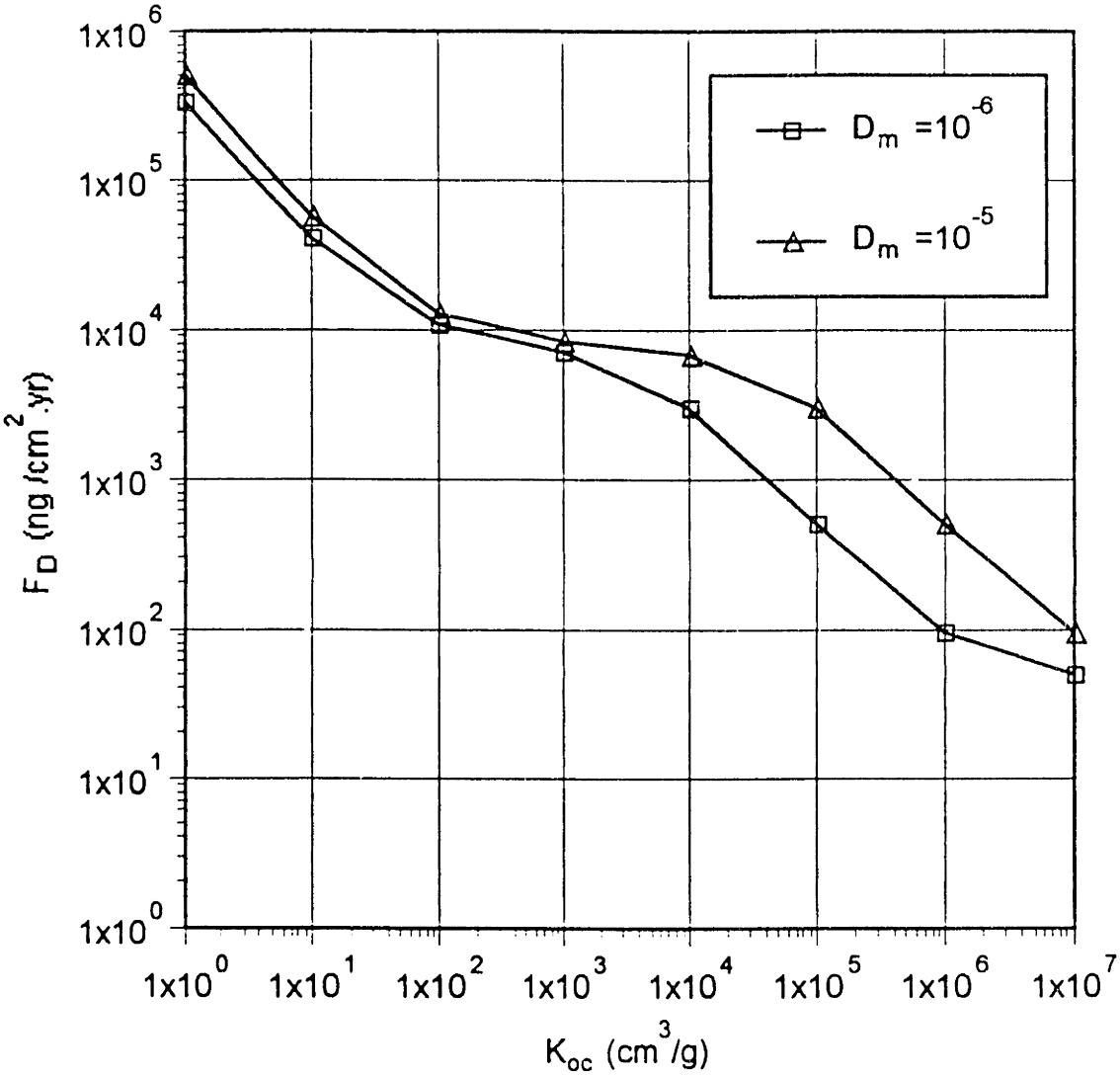

Figure 2.15a Sensitivity of diffusive fluxes to the organic carbon-water partition coefficient (K_{oc}). (D_m in cm^2/s)

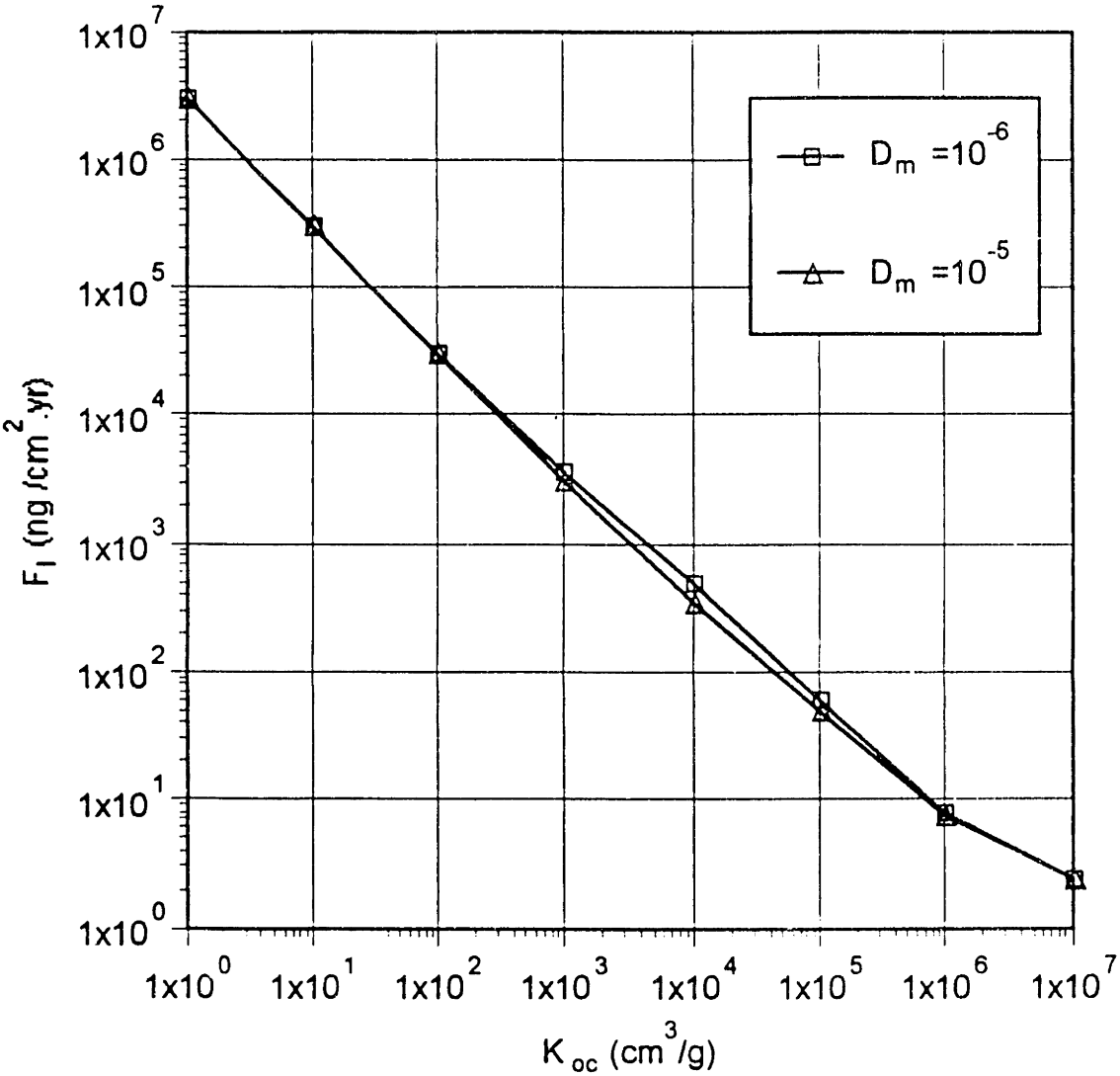

Figure 2.15b Sensitivity of irrigational fluxes to the organic carbon-water partition coefficient (K_{oc}). (D_m in cm^2/s)

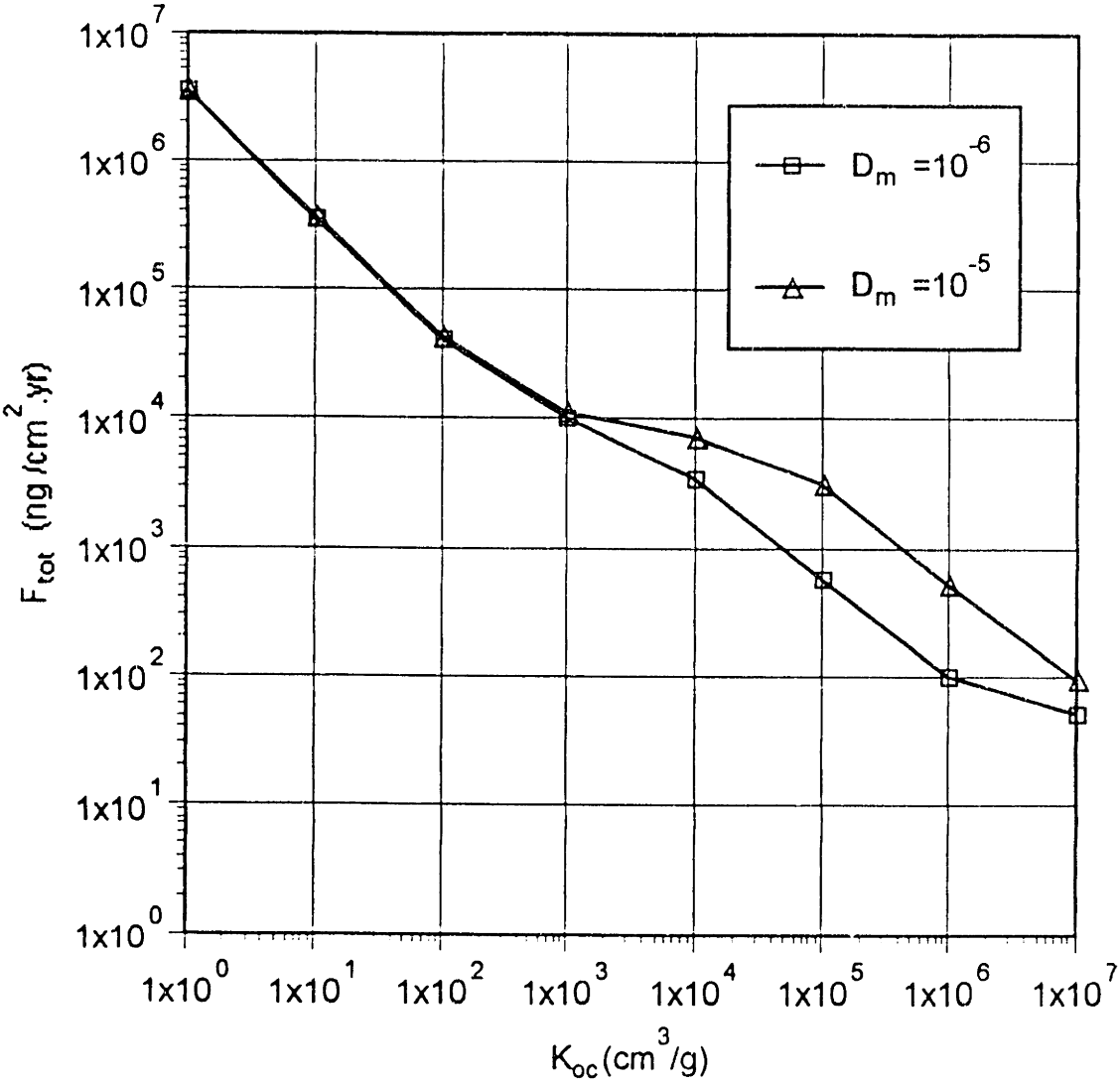

Figure 2.15c Sensitivity of total fluxes to the organic carbon-water partition coefficient (K_{oc}). (D_m in cm^2/s)

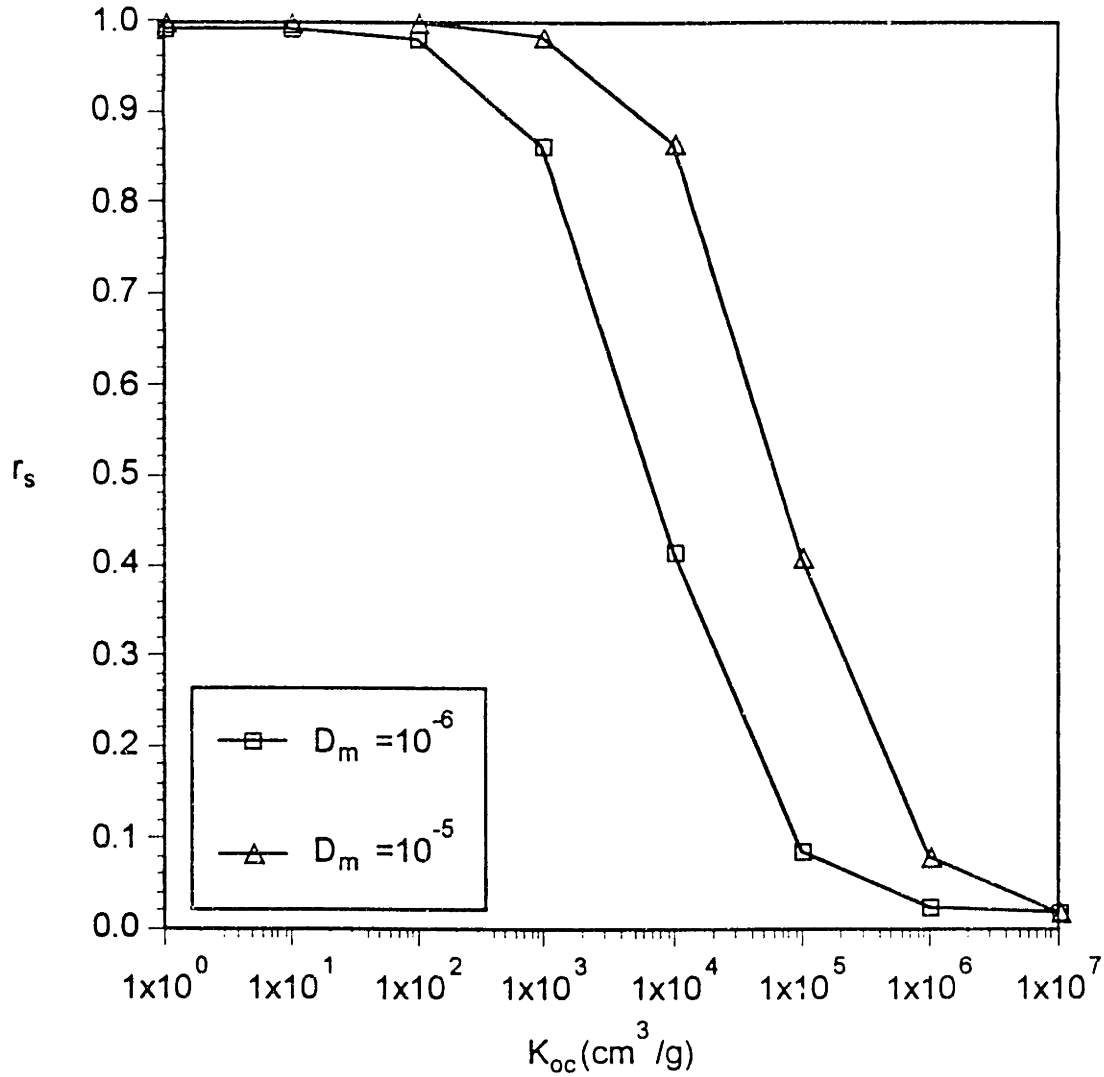

Figure 2.15d Sensitivity of resistances to the organic carbon-water partition coefficient (K_{oc}). (D_m in cm^2/s)

Table 2.11 Sensitivities of the enhancement factor (ψ) and resistances to the organic carbon-water partition coefficient (K_{oc})

$Dm = 10^{-6}$ cm^2/s

K_{oc} cm^3/g	ψ	$1/v_s$ s/cm	$1/v_w$ s/cm	$1/v_{tot}$ s/cm
10^0	1.0	2300000	15000	2300000
10^1	1.2	1900000	15000	1900000
10^2	3.4	680000	15000	700000
10^3	25	95000	15000	110000
10^4	220	11000	15000	25000
10^5	1800	1300	14000	15000
10^6	9500	190	7900	8100
10^7	21000	25	1500	1500

$Dm = 10^{-5}$ cm^2/s

K_{oc} cm^3/g	ψ	$1/v_s$ s/cm	$1/v_w$ s/cm	$1/v_{tot}$ s/cm
10^0	1.0	1500000	1500	1500000
10^1	1.2	1300000	1500	1300000
10^2	2.6	590000	1500	590000
10^3	17	90000	1500	92000
10^4	160	9700	1500	11000
10^5	1400	1000	1500	2500
10^6	10000	120	1400	1500
10^7	34000	14	790	800

the sensitivity of the diffusive flux to K_{oc} (see Figure 2.15a). In contrast to the diffusive flux, a high D_m slightly decreases the irrigational flux (Figure 2.15b) because the larger diffusive flux due to the large molecular diffusivity lowers the concentration differences between the chemical in the sediments and the chemical between the overlying water column. The irrigational flux is sensitive to K_{oc} because there is no counterbalancing factor like the desorption enhancement for the diffusive flux.

In summary, these sensitivity analyses indicate

(1) f_{oc}, Z_w, D_B, and K_{oc} are very important parameters;

(2) R and L are conditionally important; for R > 0.1 mm, the flux is sensitive to R; the flux of a soluble chemical is more sensitive to L than the flux of a hydrophobic chemical; and

(3) ϕ, α, m_{coc} ,and $m_{coc,w}$ are negligibly important factors for typically reported values.

These parameters are generally measured or estimated in studies concerning sediments. Efforts to quantify fluxes of organic pollutants at sites of interest need to focus on the estimation of the organic carbon content of the sediments, the thickness of the diffusive water boundary layer, the bioturbation coefficient, as well as the organic carbon-water partition coefficients of the organic pollutants of interest.

2.8 Discussion

This flux model is not applicable to all organic chemicals. It was assumed that $\bar{\alpha} << k_1 \rho K_d$ during the development of the flux model; however, this assumption may not be valid for hydrophilic organic chemicals or sediments composed of coarse aggregates.

It is necessary or compare $\bar{\alpha}$ and $k_1 \cdot \rho \cdot K_d$ before using the model, especially for hydrophilic organic chemicals.

The sensitivity analysis demonstrates that the diffusive flux is more significant than the irrigational flux in most cases. The irrigational flux can be comparable to the diffusive flux when

(1) the diffusive water boundary layer is thicker than 1 mm (see Figure 2.10). This indicates that when the surface of the sea bottom is very smooth, or the horizontal flow velocity of the overlying water column is very small, the irrigational flux can be greater than the diffusive flux.

(2) the bioturbation of the sediments is slower than 10^{-7} cm^2/s. When the bioturbation is very slow, the resistance of the sediments for the diffusive flux becomes so large that under the modeled condition: $\alpha = 5 \times 10^{-7}$ 1/s, the irrigational flux can be comparable to the diffusive flux (see Figure 2.11). Generally, slow bioturbation indicates that the sediments are heavily polluted. The biological irrigation should be slow as well, and the irrigational flux can still be smaller than the diffusive flux. Therefore, we can not conclude that the irrigational flux is more important than the diffusive flux for heavily polluted sediments.

(3) the biological irrigation is faster than 10^{-5} 1/s. Under this condition, even if bioturbation is as fast as 10^{-5} cm^2/s, the irrigational flux can not be neglected (see Figure 2.12).

It should be noted that even when the irrigational flux is larger than the diffusive flux under the conditions described above, irrigation remains negligible for the vertical distribution of the chemical concentration in most cases.

The sensitivity analysis shows that the resistance in the diffusive water boundary layer is usually the dominant resistance. This results from the significant reduction of the sediment resistance by the desorption enhancement (see Tables 2.3 - 2.11). The significance of desorption enhancement also indicates that desorption generally is not the step that limits the chemical exchange between the sediments and the overlying water column. The limiting step is the diffusion of chemicals across the water boundary layer. However, there are a few exceptions:

(1) When bioturbation is slow ($D_B < 10^{-7}$ cm^2/s), the sediment resistance is more important than the water resistance. Because the biologically active layer is extensively thicker than the water boundary layer, molecular diffusion alone is too slow to drive chemicals across the sediment bed in a shorter time than across the water boundary layer.

(2) For more hydrophilic organic chemicals ($K_{oc} < \sim 10^4$ cm^3/g, e.g. fluorene), the sediment resistance may become more important than the water resistance (see Figure 2.15d). Due to the small degree of desorption enhancement for relatively water-soluble chemicals, the sediment resistance exceeds the water resistance (see Table 2.11).

(3) The sediment resistance can be more important than the water resistance even for a chemical whose K_{oc} is larger than 10^4 cm^3/g (e.g. pyrene) (see Figure 2.10a).

When the overlying water column is very turbulent, or the surface of the sediment bed is very rough, the diffusive water boundary layer can be so thin that the water resistance becomes smaller than the sediment resistance.

2.9 Summary

This chapter presented a flux model for the transfer of organic chemicals between bed sediments and the overlying water column. The following summarizes the key results of this modelling effort.

1. The sediment-water environment was divided into three layers according to the chemical transport mechanisms: the turbulent water layer, the diffusive water boundary layer, and the biologically active sediment bed. In this study, seawater flushing was assumed to be very fast; thus, only the other two layers controlled the sediment-water exchange (Section 2.2).

2. The key transfer mechanisms in the sediments were molecular diffusion, bioturbation, biological irrigation, and desorption. In the diffusive water boundary layer, molecular diffusion was the dominant transport mechanism (Sections 2.3, 2.4, and 2.5).

3. Biological irrigation usually has negligible effects on the vertical distribution of the chemical concentration in the sediments (Section 2.6.1). Generally, the diffusive flux is more important than the irrigational flux when $Z_w < 1$ mm, $D_B > 10^{-7}$ cm^2/s, and $\alpha < 10^{-5}$ 1/s (Sections 2.7, 2.8).

4. The diffusive flux across the sediment-water interface can be quantified using the concentration difference between the sediments and the overlying water column

divided by the sum of the resistance of the sediment and the resistance of the water boundary layer (Section 2.6.2).

5. Among the model parameters, the organic carbon content of the sediments f_{oc}, D_B, Z_w, and K_{oc} are the ones that critically control the flux across the sediment-water interface. Therefore, people who are interested in investigating the flux of organic chemicals from sediments need to focus on the estimation of these critical parameters (Section 2.7).

6. Although colloids can carry organic chemicals across the sediment-water interface, the flux is not increased significantly by higher colloid concentrations (Section 2.7).

7. The resistance of the water boundary layer is usually more important than the sediment resistance because the desorption enhancement significantly reduces the sediment resistance (Sections 2.7, 2.8).

8. This flux model may not be applicable to hydrophilic organic chemicals or sediments composed of coarse aggregates. Before using this model to calculate the flux of organic chemicals from sediments, one must check if $\bar{\alpha} << k_1 \rho K_d$ (Sections 2.6.2, 2.8).

CHAPTER 3

APPLICATION OF THE FLUX MODEL: ESTIMATION OF THE FLUXES OF ORGANIC CHEMICALS FROM THE SEDIMENTS IN BOSTON HARBOR

3.1 Study Sites and the Analytical Data

The sediment samples for this study were taken from three sites in Boston Harbor (Figure 3.1). Large box cores (0.25 m^2) were taken, in conjunction with colleagues from the University of Massachusetts/Boston, outside the mouth of Fort Point Channel (FPC) on November 14, 1989, south of Peddocks Island (PI, 42°17′20″N, 70°55′44″W) on June 12, 1990, and northwest of Spectacle Island (SI, 42°19′46″N, 70°59′34″W) on October 10, 1990. FPC represents the inner harbor, into which contaminants are discharged from several sources including the largest untreated combined sewer overflows (CSOs) (Figure 3.2, Rex et al. 1991). Neither of the sites in the outer harbor (PI, SI) is near the outfalls of the sewage plants at Deer Island and Nut Island. However, SI is close to a large former CSO discharge on Moon Island and other Dorchester Bay CSOs (MWRA 1993). In addition, when the tide is ebbing, the water quality near SI is deteriorated by the heavily polluted water from the inner harbor. Unlike FPC and SI, PI is far from CSOs (see Figure 3.2).

The core samples were sectioned and analyzed for total organic carbon (Wong 1992), porosity (Susan McGroddy, unpublished), polycyclic aromatic hydrocarbon (PAH) concentrations (Susan McGroddy, unpublished), organic colloid concentrations (Yu-Ping Chin and Philip Gschwend, unpublished), ^{222}Rn (Wong 1992), and ^{234}Th (Gordon Wallace,

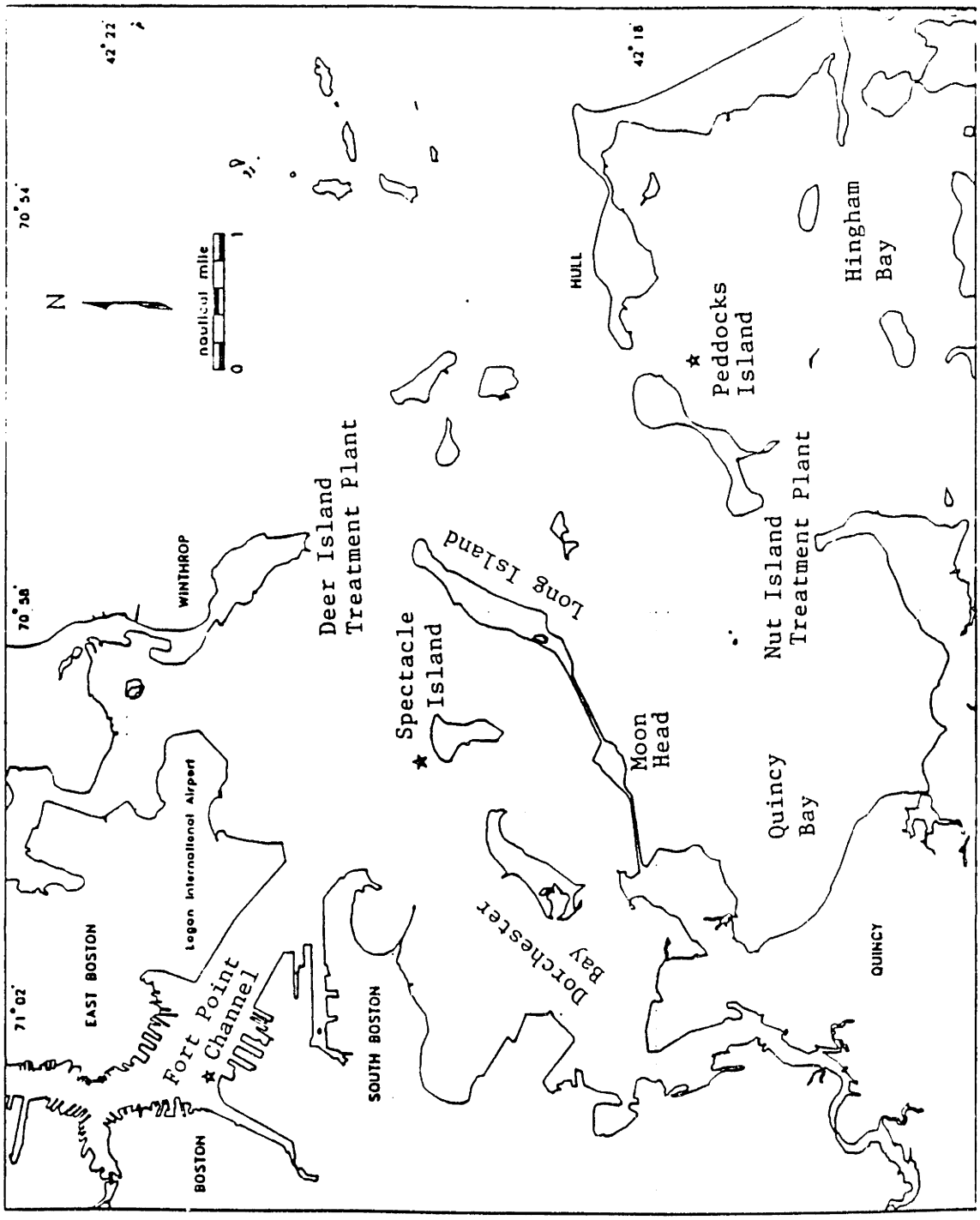

Figure 3.1 Location of the study sites in Boston Harbor (Wong 1992)

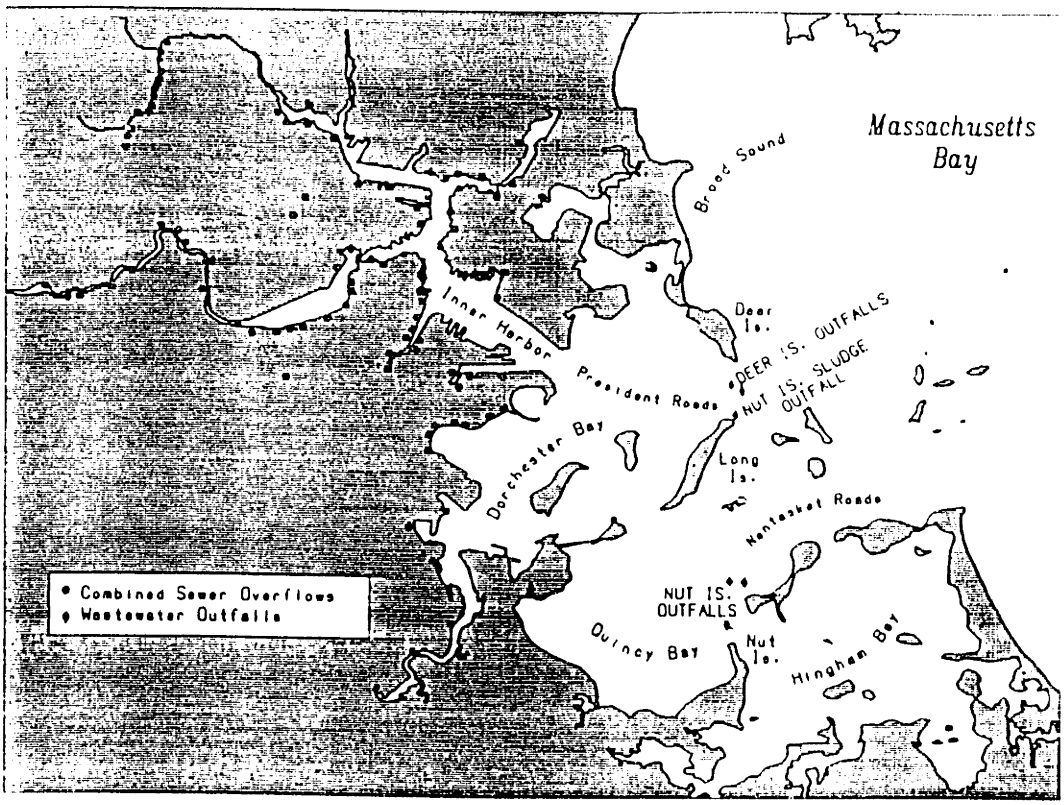

Figure 3.2 Locations of the combined sewer overflows and wastewater outfalls (Rex et al. 1991)

unpublished). The ^{222}Rn data were used to calculate the irrigational rates, and the ^{234}Th data were used to calculate the bioturbation coefficients.

The organic content of the sediments (f_{oc}) was determined by weight loss on ignition of dried sediments at 450°C overnight (Wong 1992). The values of f_{oc} were variable with depth, but averaged 5.1% at FPC and 4.2% at both PI and SI.

The porosity (ϕ) was calculated from the water content of the sediments measured by S. McGroddy (unpublished data), and the dry density of the sediments (ρ_s) was assumed to be 2.5 g/cm^3. The porosity of the sediments at each site was found to decrease with depth (Figure 3.3). The averages of the porosity at PI and SI were 0.77 and 0.71, respectively. The porosity of the sediments at the top centimeter at FPC was used to calculate the flux because it was assumed that only the top centimeter of the sediments was biologically active based on the fact that the excess activity of ^{234}Th was undetectable below 1 cm.

The concentrations of several PAHs in the sediments were measured at these sites (Figure 3.4, S. McGroddy, unpublished). These PAH concentrations irregularly varied with depth. The PAH concentrations at FPC and SI are much higher than the PAH concentrations at PI, which agrees with the fact that FPC and SI are near the CSO, whereas PI is not.

The organic colloid concentrations in the porewater (m_{coc}) were measured using the ultrafiltration method along with ultraviolet spectrophotometry and total organic carbon analysis described in Chin and Gschwend (1991) and Chin et al. (1991). The

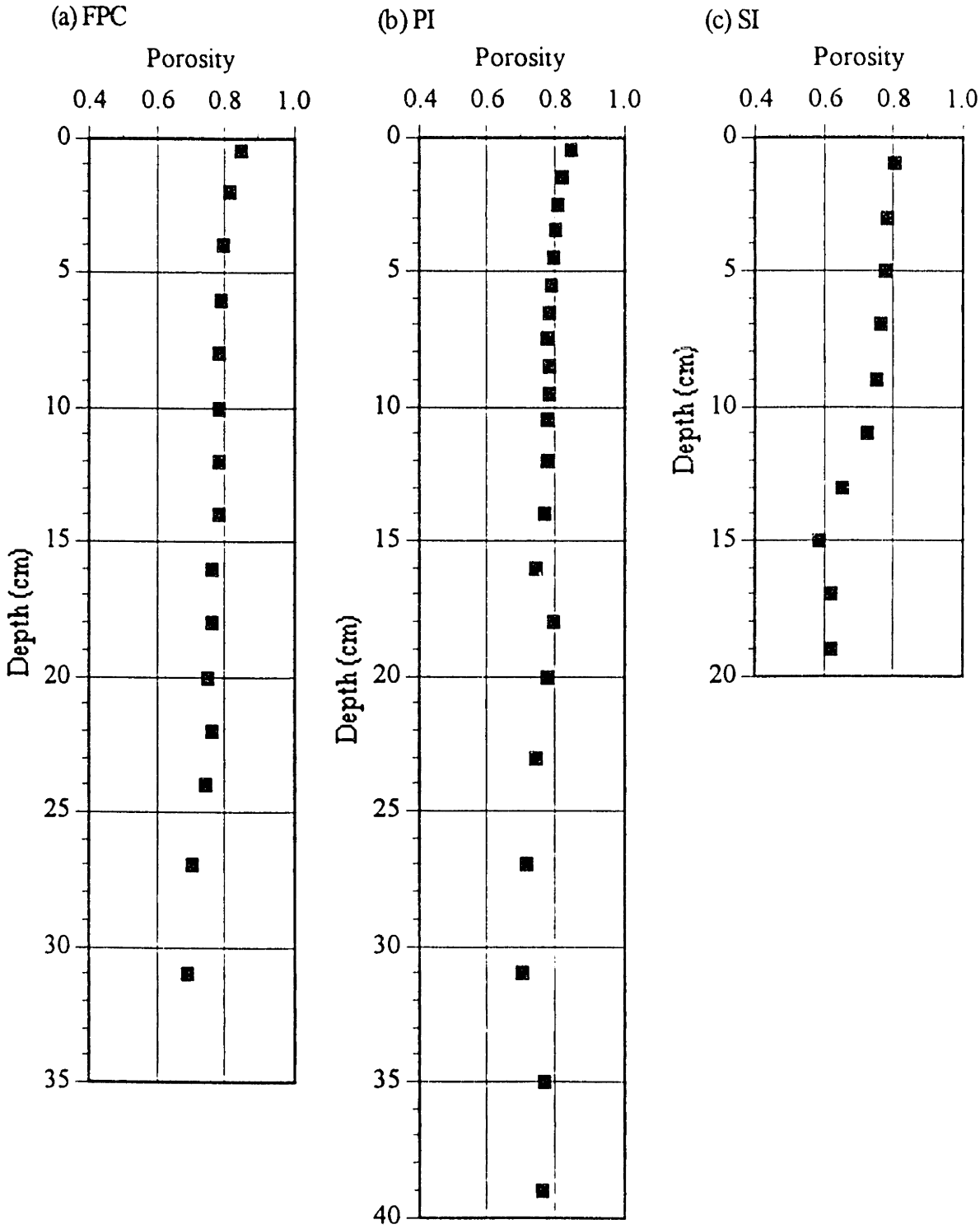

Figure 3.3 Porosity of the sediments at the (a) Fort Point Channel (b) Peddocks Island and (c) Spectacle Island sites (from McGroddy, unpublished data)

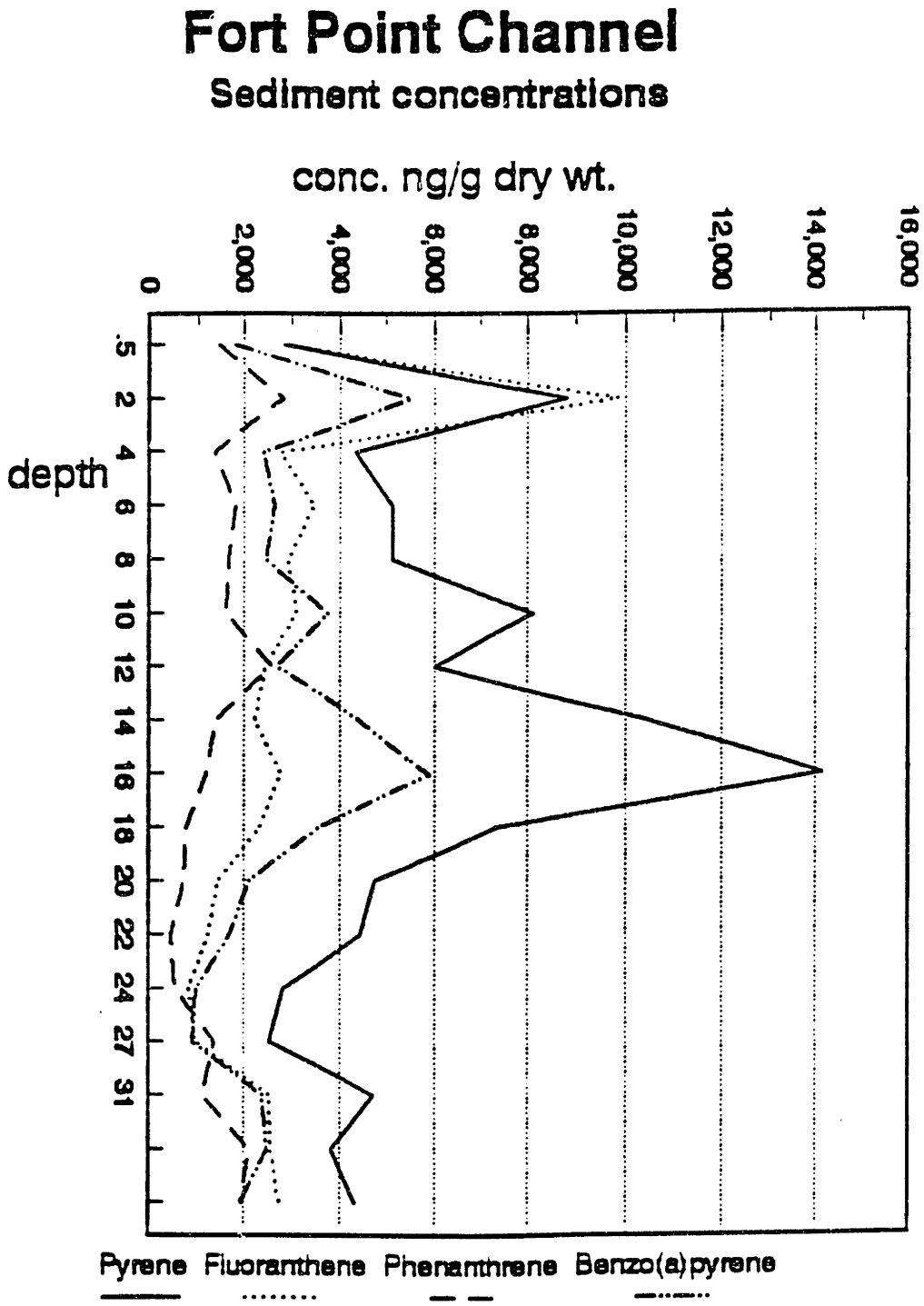

Figure 3.4a Concentrations of the PAHs sorbed in/on the solids of the sediments at the Fort Point Channel site (McGroddy, unpublished data)

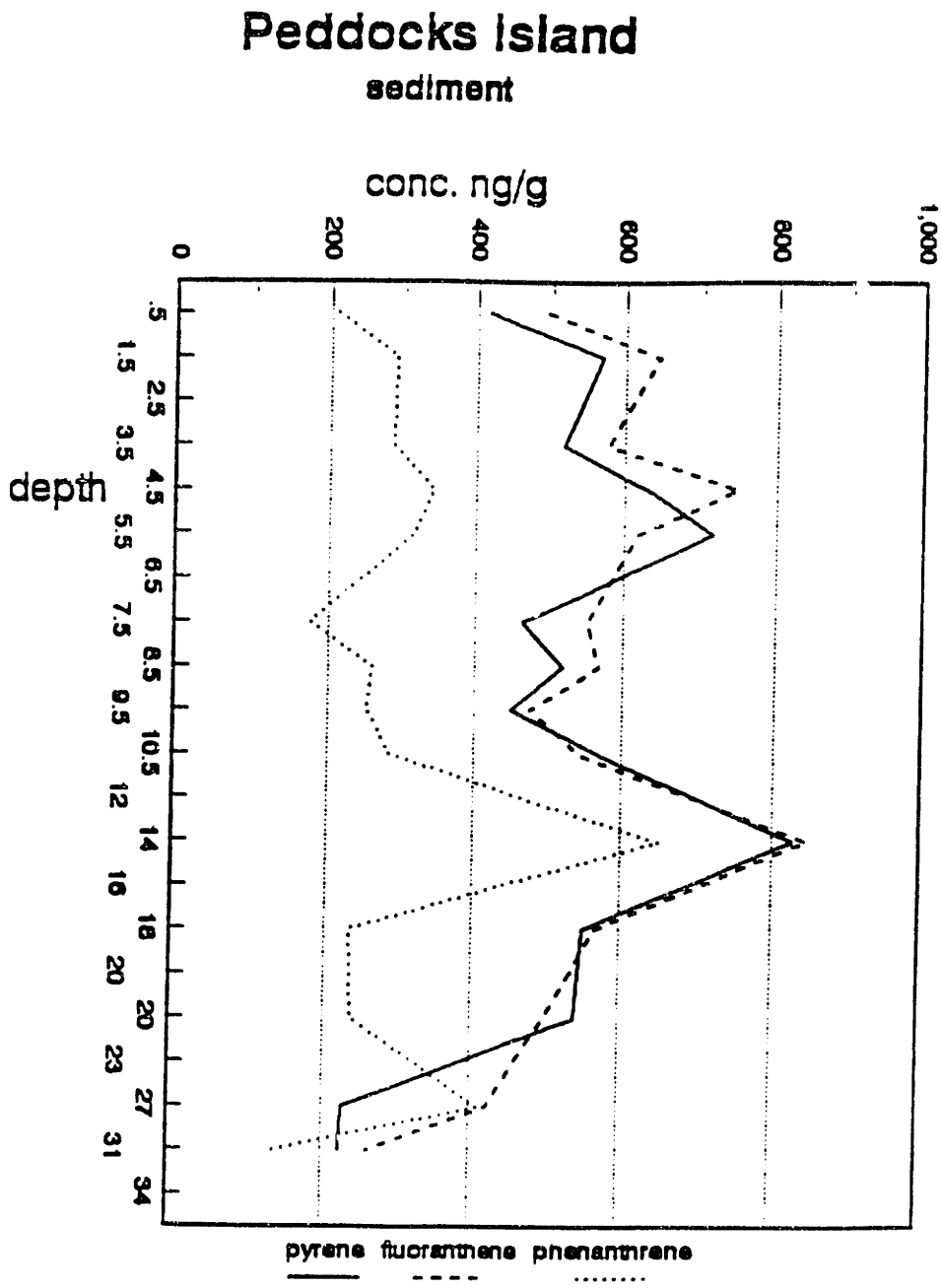

Figure 3.4b Concentrations of the PAHs sorbed in/on the solids of the sediments at the Peddocks Island site (McGroddy, unpublished data)

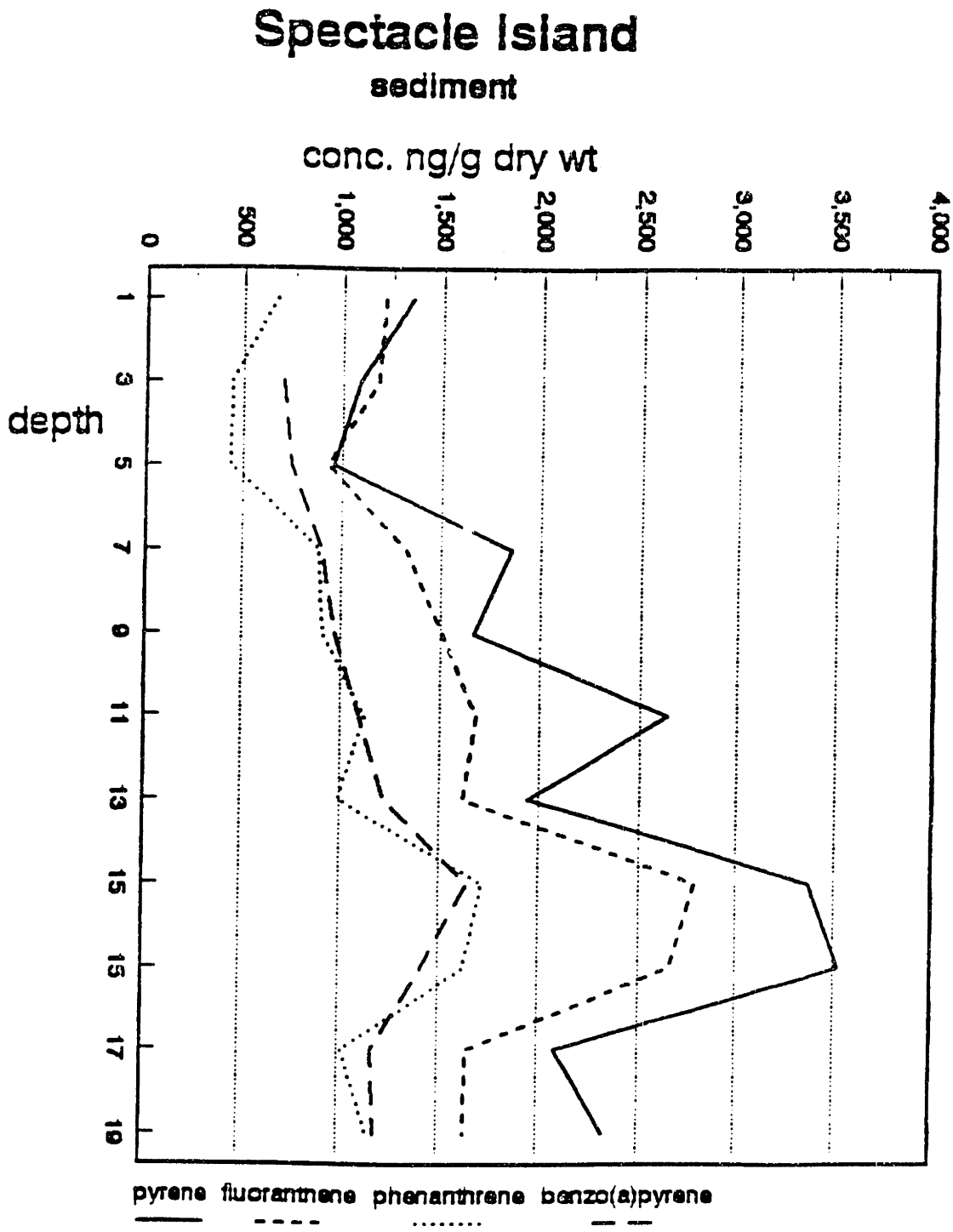

Figure 3.4c Concentrations of the PAHs sorbed in/on the solids of the sediments at the Spectacle Island site (McGroddy, unpublished data)

results are shown as Figure 3.5. The organic colloid concentration at the top sediments at each site was used to calculate the flux.

The measurement of the ^{222}Rn concentration was detailed in Wong (1992). The biological irrigation was then quantified with Equation 2-19 [$\alpha(x) = \alpha_0 \cdot \exp(-x/\alpha_1)$], by numerically fitting the deficit profiles of ^{222}Rn to optimize α_0 and α_1. The optimized values were $\alpha_0 = 1.81\times10^{-6}$ s^{-1} and $\alpha_1 = 12.45$ cm at PI, and $\alpha_0 = 6.99\times10^{-7}$ s^{-1}, $\alpha_1 = 9.93$ cm at SI (Wong 1992). The irrigation rate was assumed to be constant with depth for the flux model, and the average irrigation rate was computed from the following equation:

$$\alpha = \frac{\int_0^L \alpha_{(x)} dx}{L} = \frac{\alpha_0 \alpha_1 (1 - e^{-\frac{L}{\alpha_1}})}{L} . \qquad \textbf{(3-1)}$$

The average irrigation rates at PI and SI were 6.8×10^{-7} s^{-1} and 3.5×10^{-7} s^{-1}, respectively. These values were similar to those found in the studies discussed in Section 2.3. Because the sediments at FPC were more contaminated than the sediments at PI and SI, the irrigation rate at FPC was assumed to be smaller than the irrigation rate at PI or SI. The irrigation rate at SI was used to examine the applicability of the flux model to the sediments at FPC and to compare the irrigational flux with the diffusive flux at FPC.

The excess activity of ^{234}Th in the sediments (G. Wallace, unpublished) was used to calculate the bioturbation coefficients (D_B). D_B was assumed to be constant with depth,

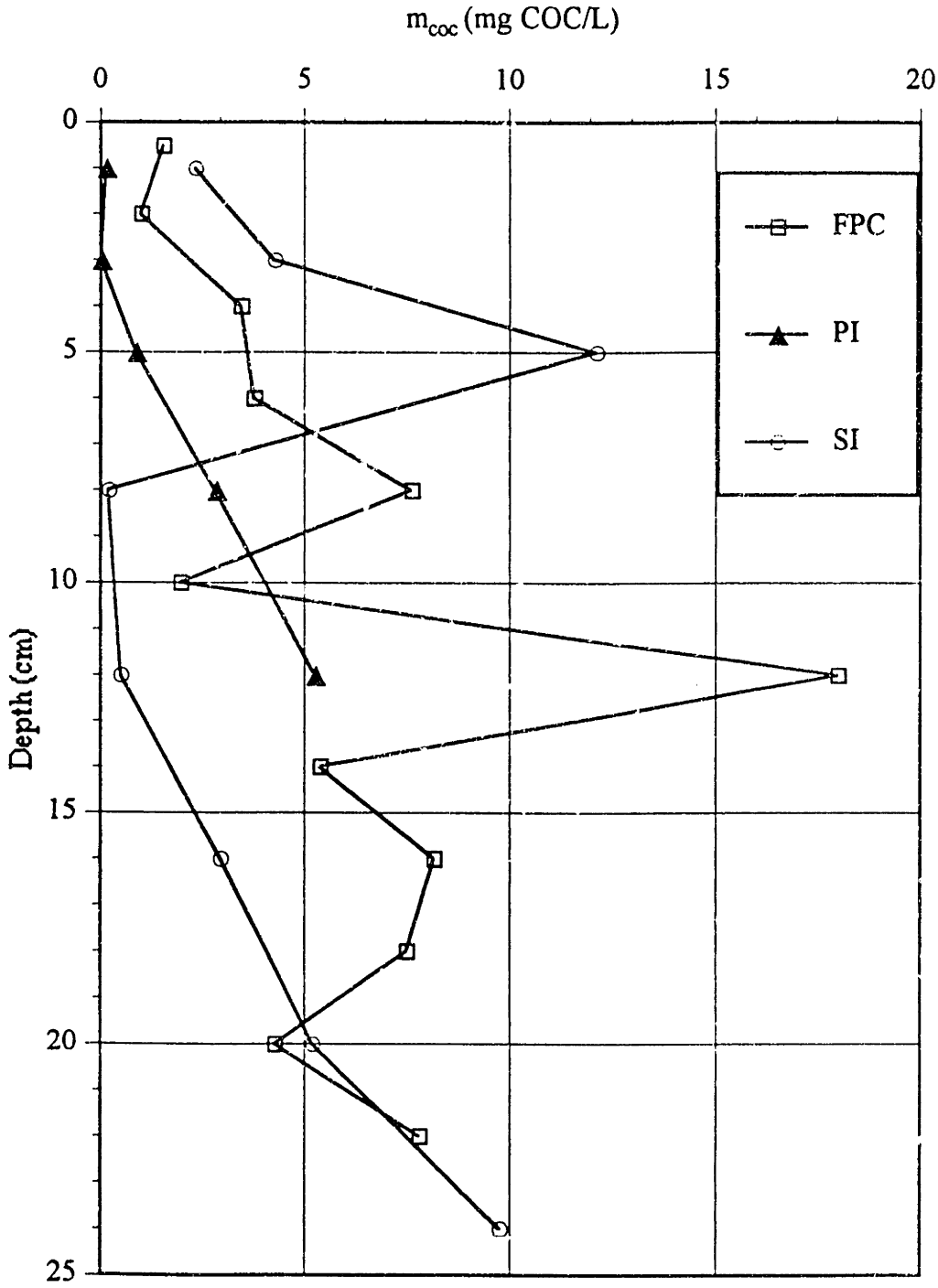

Figure 3.5 Organic colloid concentrations in the sediments at the study sites (from Chin and Gschwend, unpublished data)

and the ^{234}Th data were fitted to Equation 2-9 (Figure 3.6). D_B was found to be 1.2×10^{-5} cm^2/s and 6.3×10^{-6} cm^2/s for PI and SI, respectively. Compared with the D_B values reported in literature (10^{-6} ~ 10^{-11} cm^2/s, see Section 2.3), the biological activities at PI and SI were rather extensive. The excess activity of ^{234}Th in each section of the FPC core was undetectable except in the 0-1-cm section, which indicated that there was no bioturbation in the sediments below 1 cm. Based on this finding, the maximum bioturbation coefficient was estimated to be 1.7×10^{-7} cm^2/s. The observation of a higher irrigation rate and a higher bioturbation coefficient at PI is consistent with the presumption that the sediment bed at PI is less contaminated.

The colloid-water distribution coefficient (K_c) was measured by fluorescence quenching described in Chin et al. (1991). The observed K_c values for pyrene were 1.1×10^5 cm^3/g at FPC and 5.2×10^4 cm^3/g at SI (Chin and Gschwend 1992). The observed organic carbon-water partition coefficients (K_{oc}) for pyrene at FPC and SI were 1.6×10^5 cm^3/g and 1.7×10^5 cm^3/g, respectively (Chin and Gschwend 1992). The K_c and K_{oc} data for PI were assumed to be the same for SI.

A number of benthic organisms were found in the cores. Shrimps were seen in the top centimeter of the PI core, and worms could be found up to 30 cm deep of the PI core and 16 cm deep of the SI core. These depths were assumed to be the thicknesses of the biologically active layers of the sediments (L). As indicated previously, there was no bioturbation in the FPC sediments deeper than 1 cm; therefore, L was assumed to be 1 cm at FPC.

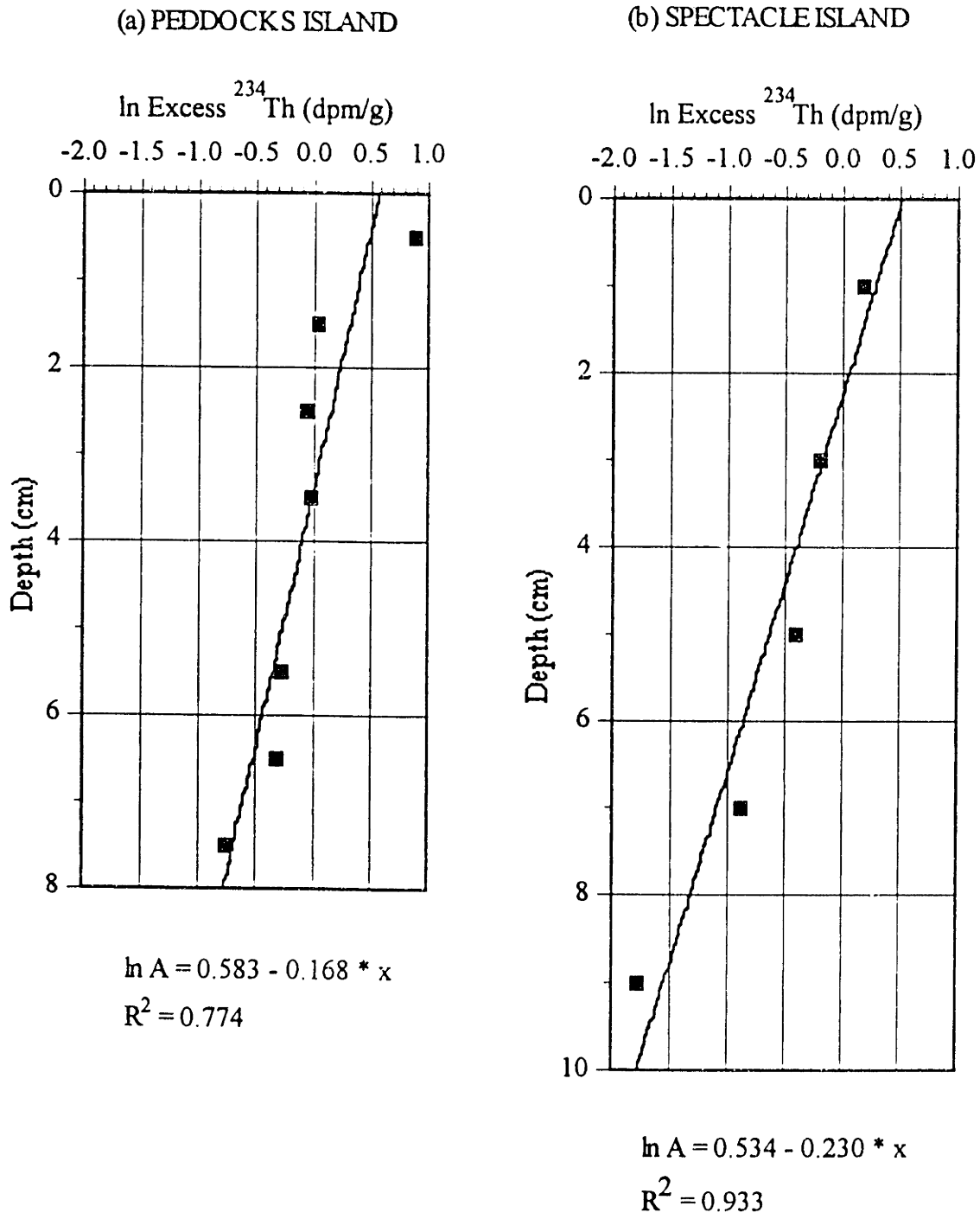

Figure 3.6 Excess ^{234}Th concentrations and the fitting curves at the (a) Peddocks Island and (b) Spectacle Island sites (from Wallace, unpublished data)

3.2 Fluxes of Pyrene and Benzo[a]pyrene from the Sediments

The fluxes of pyrene and benzo[a]pyrene from the sediments at the study sites were calculated. Pyrene represents the more water-soluble chemicals (K_{oc} on the order of 10^5 cm^3/g), and benzo[a]pyrene represents the more hydrophobic compounds (K_{oc} on the order of 10^6 cm^3/g). However, the benzo[a]pyrene concentration at PI was not available. The values of the model parameters used to estimate these fluxes are listed in Table 3.1. Some of them were obtained from the analyses described in Section 3.1. The others were assumed or calculated using the equations reviewed in Chapter 2.

The aqueous solution molecular diffusivity was calculated using Equation 2-2 under the assumption that the porewater temperature was 10°C. The sediment diffusion coefficients corrected for tortuosity and porosity were then calculated from Equation 2-6 using m = 3, suggested by Ullman and Aller (1982). The diffusivity of colloids (D_c) reported by Chin et al. (1991) ranged from 1.2×10^{-6} to 5.9×10^{-6} cm^2/s. In this thesis, 3×10^{-6} cm^2/s was chosen to calculate the flux.

The thickness of the diffusive water boundary layer (Z_w) was estimated using Equations 2-41 and 2-42 (Table 3.2). In Equation 2-42, the velocity for estimating the friction velocity should be the average velocity depth-wise; however, in the absence of the velocities at various depths, the velocity measured at a certain depth shown on the tidal current charts of Boston Harbor (National Ocean Survey 1977) was used to estimate Z_w. The velocity was measured at the time of spring tides, that is, during the time of new or full moon when the currents were stronger than average. Therefore, the velocity on the tidal current charts ought to be corrected by the correcting factor given in the charts.

Table 3.1 Parameter values for the estimation of the fluxes of pyrene and benzo[a]pyrene from the sediments at the study sites

	FPC		PI	SI		Reference
	Pyrene	B[a]p	Pyrene	Pyrene	B[a]p	
f_{oc}	5.1%	5.1%	4.2%	4.2%	4.2%	Wong, 1992
ϕ	0.84	0.84	0.77	0.71	0.71	McGroddy, unpubl.
ρ_s (g/cm^3)	2.5	2.5	2.5	2.5	2.5	(assumed)
ρ (g/cm^3)	0.47	0.47	0.74	1.04	1.04	
R (cm)	0.01	0.01	0.01	0.01	0.01	(assumed)
L (cm)	1	1	30	16	16	(assumed)
Z_w (cm)	0.029	0.028	0.022	0.010	0.010	
D_B (cm^2/s)	1.7×10^{-7}	1.7×10^{-7}	1.2×10^{-5}	6.3×10^{-6}	6.3×10^{-6}	Wallace, unpubl.
$\bar{D}_B$ (cm^2/s)	2.0×10^{-7}	8.8×10^{-7}	1.2×10^{-5}	7.1×10^{-6}	2.4×10^{-5}	
α (1/s)	3.5×10^{-7}	3.5×10^{-7}	6.8×10^{-7}	3.5×10^{-7}	3.5×10^{-7}	Wong, 1992
$\bar{\alpha}$ (1/s)	4.1×10^{-7}	1.8×10^{-6}	6.9×10^{-7}	3.9×10^{-7}	1.3×10^{-6}	
D_m (cm^2/s)	4.1×10^{-6}	3.7×10^{-6}	4.1×10^{-6}	4.1×10^{-6}	3.7×10^{-6}	
D'_m (cm^2/s)	2.9×10^{-6}	2.6×10^{-6}	2.5×10^{-6}	2.1×10^{-6}	1.8×10^{-6}	
D_c (cm^2/s)	3.0×10^{-6}	3.0×10^{-6}	3.0×10^{-6}	3.0×10^{-6}	3.0×10^{-6}	Chin et al., 1991
D'_c (cm^2/s)	2.1×10^{-6}	2.1×10^{-6}	1.8×10^{-6}	1.5×10^{-6}	1.5×10^{-6}	
$\bar{D}_m$ (cm^2/s)	3.3×10^{-6}	1.1×10^{-5}	2.5×10^{-6}	2.3×10^{-6}	6.1×10^{-6}	
D_w (cm^2/s)	4.6×10^{-6}	1.1×10^{-5}	4.3×10^{-6}	4.3×10^{-6}	7.2×10^{-6}	
m_{coc} (g COC/cm^3)	1.6×10^{-6}	1.6×10^{-6}	1.5×10^{-7}	2.4×10^{-6}	2.4×10^{-6}	Chin and Gschwend, unpubl.
$m_{coc,w}$ (g COC/cm^3)	1.0×10^{-6}	1.0×10^{-6}	1.0×10^{-6}	1.0×10^{-6}	1.0×10^{-6}	Chin and Gschwend, unpubl.
K_{oc} (cm^3/g)	1.6×10^{5}	3.7×10^{6}	1.7×10^{5}	1.7×10^{5}	3.9×10^{6}	Chin and Gschwend, 1992
K_c (cm^3/g COC)	1.1×10^{5}	2.5×10^{6}	5.2×10^{4}	5.2×10^{4}	1.2×10^{6}	Chin and Gschwend, 1992
K_d (cm^3/g)	8.2×10^{3}	1.9×10^{5}	7.1×10^{3}	7.1×10^{3}	1.6×10^{5}	
k_1 (1/s)	1.6×10^{-3}	1.4×10^{-3}	2.5×10^{-3}	3.5×10^{-3}	3.1×10^{-3}	
S_L (ng/g)	5500	3500	220	2800	1300	McGroddy, unpibl.
C_w (ng/cm^3)	0	0	0	0	0	(assumed)

Table 3.2a Estimation of the thickness of the diffusive water boundary layer (Z_w) at FPC: (i) the hourly current velocities measured 10 ft from the water surface (from National Ocean Survey, 1977); (ii) estimated Z_w.

(i)

Time	Spring tide velocity(knot)	Correcting factor	Corrected velocity	
			knot	cm/s
SFB[†]	0.1	0.6	0.06	3.08
SFB+1[††]	0.2	0.6	0.12	6.17
SFB+2	0.3	0.6	0.18	9.25
SFB+3	0.4	0.6	0.24	12.34
SFB+4	0.4	0.6	0.24	12.34
SFB+5	0.3	0.6	0.18	9.25
SEB[†]	0.2	0.5	0.10	5.14
SEB+1[††]	0.1	0.5	0.05	2.57
SEB+2	0.1	0.5	0.05	2.57
SEB+3	0.1	0.5	0.05	2.57
SEB+4	0.2	0.5	0.10	5.14
SEB+5	0.2	0.5	0.10	5.14
SEB+6	0.1	0.5	0.05	2.57
		Average velocity at 10 ft		6.01

(ii)

	Pyrene	Benzo[a]pyrene
Friction factor f	0.03	
Average velocity $\bar{u}$	6.01 cm/s	
Friction velocity u_*	0.37 cm/s	
Molecular diffusivity D_m	4.1×10^{-6} cm²/s	3.7×10^{-6} cm²/s
Kinematic viscosity ν	0.013 cm²/s	
Z_w	0.029 cm (290 μm)	0.028 cm (280 μm)

[†] SFB: Slack; Flood begins. SEB: Slack; Ebb begins.

[††] SFB+n: n hour(s) after SFB. SEB+n: n hour(s) after SEB.

Table 3.2b Estimation of the thickness of the diffusive water boundary layer (Z_w) at PI: (i) the hourly current velocities measured 20 ft from the water surface (from National Ocean Survey, 1977); (ii) estimated Z_w.

(i)

Time	Spring tide velocity(knot)	Correcting factor	Corrected velocity	
			knot	cm/s
SFB[†]	0.2	0.6	0.12	6.17
SFB+1[††]	0.2	0.6	0.12	6.17
SFB+2	0.4	0.6	0.24	12.34
SFB+3	0.3	0.6	0.18	9.25
SFB+4	0.3	0.6	0.18	9.25
SFB+5	0.4	0.6	0.24	12.34
SEB[†]	0.4	0.5	0.20	10.28
SEB+1[††]	0.3	0.5	0.15	7.71
SEB+2	0.3	0.5	0.15	7.71
SEB+3	0.3	0.5	0.15	7.71
SEB+4	0.3	0.5	0.15	7.71
SEB+5	0.2	0.5	0.10	5.14
SEB+6	0.1	0.5	0.05	2.57
		Average velocity at 20 ft		8.03

(ii)

Friction factor f	0.03
Average velocity $\bar{u}$	8.03 cm/s
Friction velocity u_*	0.49 cm/s
Molecular diffusivity D_m (pyrene)	4.1×10^{-6} cm²/s
Kinematic viscosity ν	0.013 cm²/s
Z_w	0.022cm (220μm)

[†] SFB: Slack; Flood begins. SEB: Slack; Ebb begins.

[††] SFB+n: n hour(s) after SFB. SEB+n: n hour(s) after SEB.

Table 3.2c Estimation of the thickness of the diffusive water boundary layer (Z_w) at SI: (i) the hourly current velocities measured 25 ft from the water surface (National Ocean Survey, 1977); (ii) estimated Z_w.

(i)

Time	Spring tide velocity(knot)	Correcting factor	Corrected velocity	
			knot	cm/s
SFB[†]	0.2	0.6	0.12	6.17
SFB+1[††]	0.4	0.6	0.24	12.34
SFB+2	0.6	0.6	0.36	18.50
SFB+3	0.7	0.6	0.42	21.59
SFB+4	1.0	0.9	0.90	46.26
SFB+5	0.9	0.8	0.72	37.01
SEB[†]	0.6	0.5	0.30	15.42
SEB+1[††]	0.2	0.5	0.10	5.14
SEB+2	0.3	0.5	0.15	7.71
SEB+3	0.5	0.5	0.25	12.85
SEB+4	0.7	0.6	0.42	21.59
SEB+5	0.6	0.5	0.30	15.42
SEB+6	0.3	0.5	0.15	7.71
		Average velocity at 25 ft		17.52

(ii)

	Pyrene	Benzo[a]pyrene
Friction factor f	0.03	
Average velocity $\bar{u}$	17.52 cm/s	
Friction velocity u_*	1.07 cm/s	
Molecular diffusivity D_m	4.1×10^{-6} cm²/s	3.7×10^{-6} cm²/s
Kinematic viscosity ν	0.013 cm²/s	
Z_w	0.010 cm (100 μm)	0.010 cm (100 μm)

[†] SFB: Slack; Flood begins. SEB: Slack; Ebb begins.

[††] SFB+n: n hour(s) after SFB. SEB+n: n hour(s) after SEB.

The flow velocity is linearly related to the friction velocity, which is linearly related to Z_w; therefore, the arithmetic mean of the velocities measured hourly in a tidal cycle can be used to estimate Z_w. The friction factor (f) was chosen to be 0.03, corresponding to a drag coefficient (C_f)[1] of 4.0×10^{-3} in a water depth of 5 m reported by Signell and Butman (1992). The kinematic viscosity was the viscosity at 10°C. The estimated Z_w values were 0.029 cm (290 μm) for pyrene and 0.028 cm (280 μm) for benzo[a]pyrene at FPC, 0.022 cm (220 μm) for pyrene at PI, and 0.010 cm (100 μm) for both pyrene and benzo[a]pyrene at SI. These values are within the range of the Z_w reported in literature (see Section 2.5).

Before applying the parameter values into the model, it is necessary to check if $\bar{\alpha} << k_1 \cdot \rho \cdot K_d$:

Table 3.3 Examination of the model applicability to the study sites

	FPC		PI	SI	
	pyrene	b[a]p	pyrene	pyrene	b[a]p
$\bar{\alpha}$	4.1×10^{-7}	1.8×10^{-6}	6.9×10^{-7}	3.9×10^{-7}	1.3×10^{-6}
$k_1 \cdot \rho \cdot K_d$	6.1	120	13	26	530

From Table 3.3, it is confirmed that the flux model is applicable to all of the study sites. The results of the flux estimation are shown in Table 3.4. The estimated total flux of

[1] $C_f = f/8 = n^2 g h^{-1/3}$ (Westerink et al. 1984); n is the Manning coefficient; g is the gravitational acceleration; h is the depth of the water column. Signell and Butman (1992) selected n = 0.0264 (SI units) to model the tidal exchange and dispersion in Boston Harbor. The corresponding drag coefficients were 2.5, 3.2, 4.0, 6.8 $\times10^{-3}$ in water depths of 20, 10, 5, 1 m, respectively.

Table 3.4 Fluxes of pyrene and benzo[a]pyrene from the sediments at FPC, PI, and SI

	FPC		PI	SI	
	Pyrene	B[a]p	Pyrene	Pyrene	B[a]p
F_D (ng/cm^2.yr)	**≤ 2500****	**≤ 230****	**170**	**4300**	**190**
F_I (ng/cm^2.yr)	**≤ 6.6*****	**≤ 0.87*****	**15**	**50**	**3.8**
F_{tot} (ng/cm^2.yr)	**≤ 2500**	**≤ 230**	**180**	**4300**	**190**
S_L/K_d - C_w* (ng/cm^3)	0.67	0.019	0.031	0.39	8.0×10^{-3}
(ng/L)	670	19	31	390	8.0
$1/v_w$ (s/cm)	6500	2500	5100	2300	1300
$1/v_s$ (s/cm)	2000	110	720	580	32
$1/v_{tot}$ (s/cm)	8500	2600	5800	2900	1400
$(1/v_w)/(1/v_{tot})$	0.76	0.96	0.88	0.80	0.98
$(1/v_s)/(1/v_{tot})$	0.24	0.04	0.12	0.20	0.02
F_D/F_{tot}	> 0.99	> 0.99	0.92	0.99	0.98
F_I/F_{tot}	< 0.01	< 0.01	0.08	0.01	0.02
Inventory (ng/cm^2)	2,200	1,400	3,800	3,300	15,000
Characteristic cleanup time (yr)	≥ 1	6	21	8	81

* C_w was assumed to be zero.

** The diffusive flux at FPC was calculated from the estimated maximum bioturbation coefficient.

*** The irrigational flux at FPC was calculated using the irrigation rate at SI, which was presumably higher than the irrigation rate at FPC.

pyrene from the sediments was 2500 ng/cm^2·yr at FPC, 180 ng/cm^2·yr at PI, and 4300 ng/cm^2·yr at SI; the flux of benzo[a]pyrene was 230 ng/cm^2·yr at FPC and 190 ng/cm^2·yr at SI. The "inventory" in Table 3.4 is the amount of the chemical within the biologically active layer per square centimeter. The "characteristic cleanup time" is the approximate time needed for the chemical in the biologically active layer to be totally released to the overlying water column at the releasing rate calculated from the flux model.

The diffusive flux is much greater than the irrigational flux at each site. At FPC the irrigational flux is negligible even though it was estimated from a presumably higher irrigation rate. PI has the greatest irrigational flux fraction because the biologically active sediment layer at PI is the thickest, which causes a greater irrigational flux (see Figure 2.9). Another cause is a thicker diffusive water boundary layer at PI, which causes a larger resistance for the diffusive flux.

As predicted in Chapter 2, the water resistance is more important than the sediment resistance at each site. It should be noted that at both FPC and SI, the fraction of the sediment resistance for pyrene is larger than that for benzo[a]pyrene, which is consistent with the conclusion from the sensitivity analysis (see Figure 2.15d).

Although the pollutant concentration at FPC is greater than the concentration at SI, the flux at FPC is smaller. One of the reasons is that the water boundary layer at FPC, which is located in the more tranquil inner harbor, is much thicker than the water boundary layer at SI, and hence, the water resistance at FPC is greater. The other reason

is that the bioturbation at FPC is slower than the bioturbation at SI; therefore, the sediment resistance at FPC is greater as well.

3.3 Significance of the fluxes of pyrene and benzo[a]pyrene

To determine the significance of the organic pollutant flux from the sediments in Boston Harbor, the loadings of pyrene and benzo[a]pyrene to the harbor water were estimated and compared with the loadings from other sources.

The fluxes of pyrene and benzo[a]pyrene from the sediments were calculated for additional sites: (1) where the concentrations of pyrene and benzo[a]pyrene in the sediments were reported by Shiaris and Jambard-Sweet (1986) (Table 3.5) and (2) which were in non-erosional areas according to the results of a sidescan-sonar survey conducted by Knebel et al. (1991). The outer harbor was divided along the Moon Island - Long Island line into the North Harbor and the South Harbor for estimating the loadings because the South Harbor was considered to be less contaminated (see Figure 3.2) with the exception of the Squantum site (SQ). SQ is close to a large former CSO discharge on Moon Island. Among the sites in the North Harbor, the sediment PAH concentrations at the Governor Island Flat site (GIF) are the greatest because it is close to the heavily contaminated inner harbor (Shiaris and Jambard-Sweet 1986). The properties of the sediments at the sites listed in Table 3.5 were assumed to be similar to those at SI (for the North Harbor sites) or PI (for the South Harbor sites) except for L and D_B. L and D_B at FPC, PI, and SI were related to the pyrene concentration in the sediments (S_{pyr}): $L = -5.49\times10^{-3}\times S_{pyr} + 31.27$, and $D_B = -2.2\times10^{-9}\times S_{pyr} + 1.25\times10^{-5}$. These relationships were

Table 3.5 Concentrations of pyrene and benzo[a]pyrene in Boston Harbor sediments (ng/g dry solids) (Shiaris and Jambard-Sweet 1986)

Site	Longitude	Latitude	Pyrene	B[a]p
Thompson Island (TI)	71°01′24″	42°19′01″	1783	1975
Governor Island Flats (GIF)	70°59′40″	42°20′59″	4686	3150
Deer Island Flats (DIF)	70°57′53″	42°20′47″	415	1156
Castle Island (CI)	71°00′05″	42°20′00″	1378	1259
Squantum (SQ)	70°59′44″	42°17′46″	10355	932
Seal Rock (SR)	70°58′29″	42°16′35″	621	683
Crow Point Flats (CPF)	70°53′30″	42°15′56″	163	321
Hull Bay (HB)	70°53′24″	42°17′08″	184	64
Hull Gut (HG)	70°55′05″	42°18′04″	2268	1577

used to estimate the L and D_B at the other sites. Z_w at these sites was estimated by the same way Z_w at PI and SI was estimated. The concentration in the seawater and the irrigational flux were assumed to be negligible. The results are summarized in Table 3.6 and Figure 3.7.

The loadings from the sediments in the North Harbor and the South Harbor were calculated by multiplying the average flux in each section by the non-erosional area. The flux at FPC was used to calculate the loading from the inner harbor sediments. The non-erosional area of Boston Harbor was estimated by MWRA (1993) from a sidescan-sonar survey conducted by Knebel et al. (1991). Table 3.6 shows the loading estimates. The amounts of pyrene and benzo[a]pyrene released from the sediments in the entire harbor per year were estimated to be 1400 kg and 96 kg, respectively.

MWRA (1993) estimated the loadings of pyrene and benzo[a]pyrene from stormwater, CSOs, the atmosphere, and rivers to Boston Harbor water (Table 3.7). For Boston Harbor, the sediment bed is the most important source for both pyrene and benzo[a]pyrene. The amount of contaminants from sediments greatly exceeds the amount from other sources. Therefore, to clean up Boston Harbor, the efforts need to focus on cleaning the sediments or impeding the release of organic pollutants from the sediments.

3.4 Discussion

The assumption that the chemical concentration in the seawater is negligible is acceptable for the study sites. The average pyrene concentrations in the seawater near Nut Island and Deer Island sewage outfalls, which were presumably higher than the

Table 3.6a Estimation of the loading of pyrene from Boston Harbor sediments: (i) fluxes from the outer harbor sediments; (ii) estimated loading.

(i)

NORTH HARBOR	SI	TI	GIF	DIF	CI	Ave.
F_D ($\approx F_{tot}$) (ng/cm^2.yr)	4300	2300	4700	490	1000	**2600**
S/K_d (ng/L)	392	250	656	58	193	
$1/v_{tot}$ (s/cm)	2900	3400	4400	3700	6000	

SOUTH HARBOR	PI	SQ	SR	CPF	HB	HG	Ave.
F_D ($\approx F_{tot}$) (ng/cm^2.yr)	170	1700	520	110	290	3600	**1100**
S/K_d (ng/L)	31	1450	87	23	26	316	
$1/v_{tot}$ (s/cm)	5800	28000	5200	6800	2800	2800	

(ii)

	Inner Harbor	North Harbor	South Harbor	Total
Non-erosional Area (km^2)*	8.0	27.7	40.4	76.1
Flux (ng/cm^2.yr)	2500	2600	1100	
Loading (kg/yr)	200	720	440	**1400**

* MWRA, 1993

Table 3.6b Estimation of the loading of benzo[a]pyrene from Boston Harbor sediments: (i) fluxes from the outer harbor sediments; (ii) estimated loading.

(i)

NORTH HARBOR	SI	TI	GIF	DIF	CI	Average
F_D ($\approx F_{tot}$)(ng/cm^2.yr)	190	230	280	120	78	**180**
S/K_d (ng/L)	8	12	19	7.1	7.7	
$1/v_{tot}$ (s/cm)	1400	1600	2200	1900	3100	

SOUTH HARBOR	SQ	SR	CPF	HB	HG	Average
F_D ($\approx F_{tot}$)(ng/cm^2.yr)	54	50	18	10	250	77
S/K_d (ng/L)	5.7	4.2	2.0	0.40	9.6	
$1/v_{tot}$ (s/cm)	3300	2600	3500	1300	1200	

(ii)

	Inner Harbor	North Harbor	South Harbor	Total
Non-erosional Area (km^2)*	8.0	27.7	40.4	76.1
Flux (ng/cm^2.yr)	230	180	77	
Loading (kg/yr)	18	50	31	**99**

* MWRA, 1993

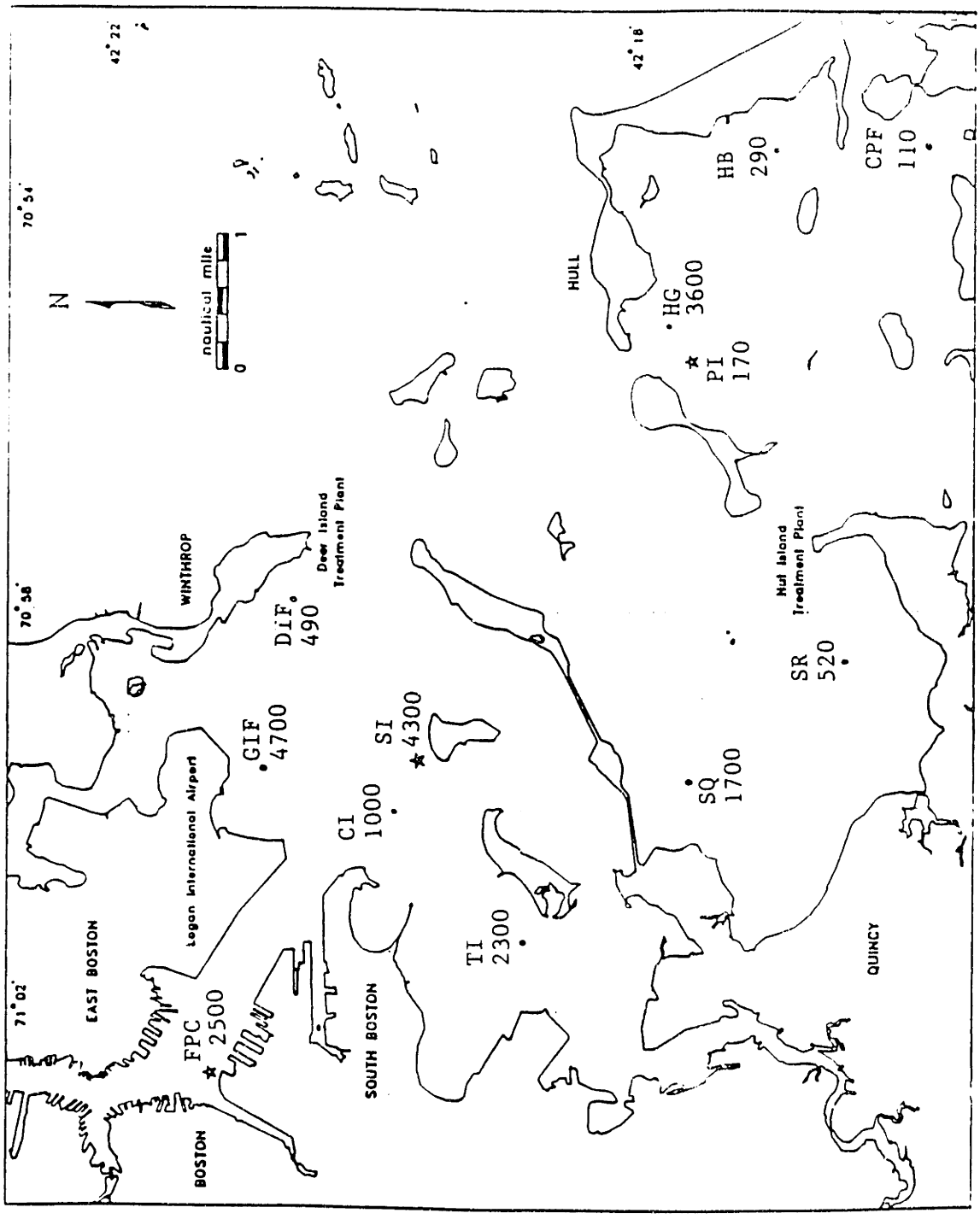

Figure 3.7a Estimated fluxes of pyrene from Boston Harbor sediments ($ng/cm^2.yr$)

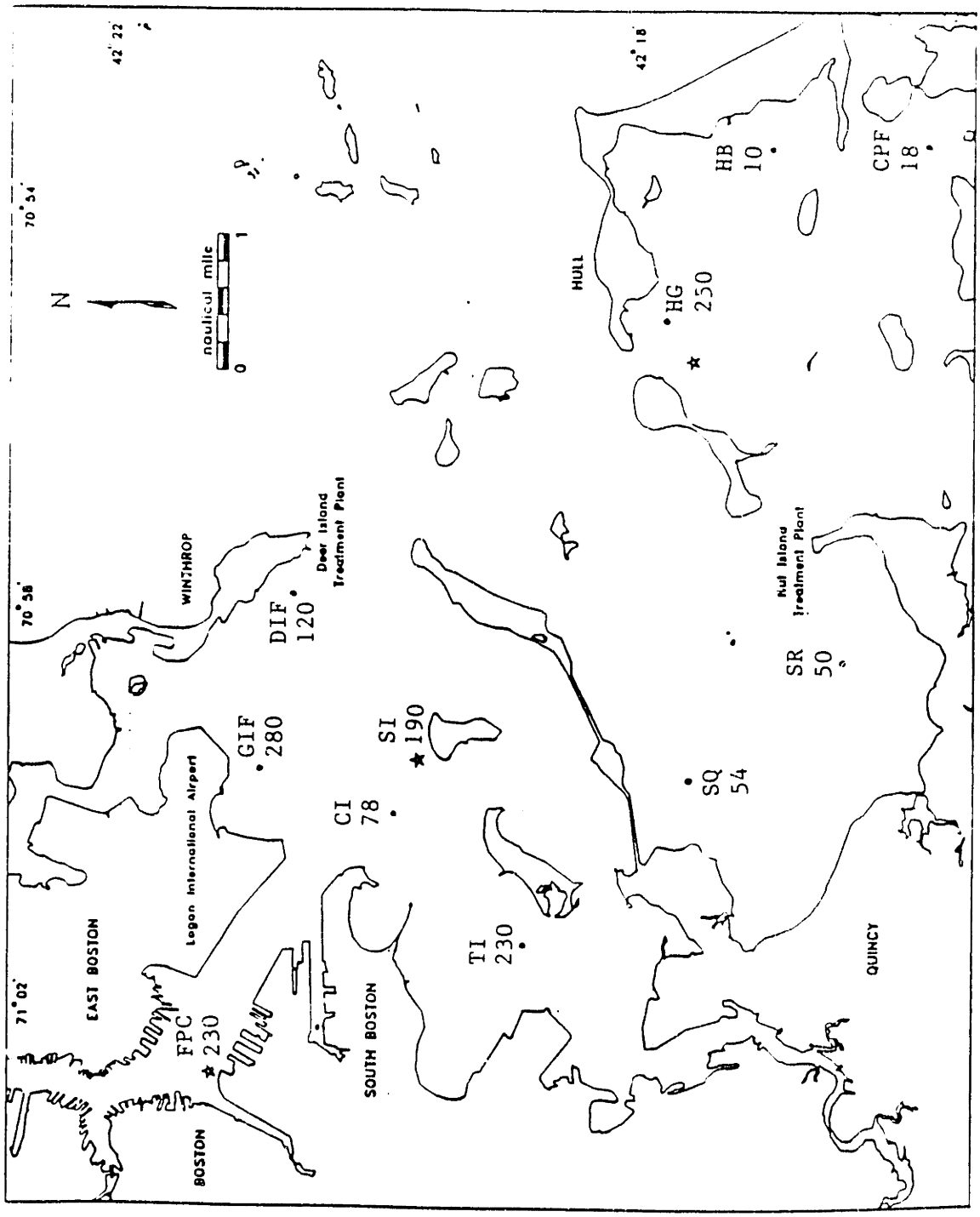

Figure 3.7b Estimated fluxes of benzo[a]pyrene from Boston Harbor sediments ($ng/cm^2.yr$)

Table 3.7 Estimated loadings of pyrene and benzo[a]pyrene to Boston Harbor (kg/yr)

Source	Pyrene	B[a]p
Stormwater*	1.7	0.68
CSOs*	4.6	1.3
Atmosphere*	NA	3.5
Rivers*	160	8.2
Sediments	**1400**	**96**

* MWRA, 1993

concentrations in other places in the harbor, were 4.1 ng/L and 7.6 ng/L, respectively, and benzo[a]pyrene was not detectable in most samples taken at these two sites (MWRA 1988). These concentrations are negligible compared with the pyrene concentrations in the porewater (see Table 3.6, S/K_d).

The estimation of the fluxes of pyrene and benzo[a]pyrene from the sediments in Boston Harbor described above was under the assumption that these chemicals were 100% available. However, S. McGroddy (pers. com.) has found evidence that part of the PAHs in the sediments in Boston Harbor is retained in soot in the sediment bed. Therefore, the chemical concentration in the porewater is not in equilibrium with the chemical concentration in the solids, and the chemicals are not entirely available. Assuming only 10% of each pollutant is available, the loading from the sediments to the harbor water is 140 kg/yr for pyrene and 9.6 kg/yr for benzo[a]pyrene, comparable to the loading from the rivers (see Table 3.7). If this assumption is correct, the sediment bed is still a major pollution source, although it is not a dominant one.

The results of the flux calculation confirm the conclusion of the sensitivity analysis that the diffusive flux is more significant than the irrigational flux. People who are interested in investigating the flux of organic chemicals such as PAHs and PCBs from sediments may be justified in omitting investigation of the irrigation rates assuming mixing organisms are present. The flux estimation also substantiates that the resistance of the diffusive water boundary layer is more important than the resistance of sediments for "real-world" conditions. Therefore, it is important to make a reliable estimate of the thickness of the water boundary layer, which includes the investigation of the friction

factor of the sediment bed surface and the measurement of the horizontal flow velocity of the overlying water column. The estimation of Z_w in this thesis is approximate because a single value for the friction factor was used for all of the study sites. In addition, the current velocity for the Z_w estimation was supposed to be the average velocity over the water column; however, due to lack of velocity data at various depths, the velocity at a single depth was used. Furthermore, the velocities at the study sites were not measured. The velocities used for Z_w calculation were estimated from the velocities measured near the study sites by the National Ocean Survey (1977). To estimate the organic chemical flux accurately, it is critical by a factor of two to obtain reliable surface friction factor data and current velocities at various depths.

The characteristic cleanup time for pyrene at FPC is estimated to be only a year (see Table 3.4). This may result from the very thin biologically active layer (1 cm). However, the pyrene flux estimated from the model developed by Wong (1992) was 625 ng/cm^2.yr at the first year and as great as 123 ng/cm^2.yr at the tenth year. Unlike the model presented in this thesis, Wong's model did not assume that the sediment and porewater concentrations were in steady state. For FPC, the steady-state assumption is not appropriate. While the pollutant in the top-centimeter sediments is driven out of the bed by bioturbation, the pollutant in the sediments below the biologically active layer is slowly diffusing in the undisturbed sediments. The sediment and porewater concentrations can not be in steady state at the top centimeter. This example indicates that the steady-state assumption is the weakness of this flux model. The flux estimated from this model is an instantaneous flux, which may be close to the real non-steady-state flux for a short

period of time; however, this model is not suitable for long-term flux estimation. Estimation of the flux as a function of time needs a non-steady-state model.

Another weakness of this flux model is the assumption that the model parameters are constant with depth. In the real world, most of the parameters vary with depth. The sensitivity analysis shows that the organic carbon content of sediments, bioturbation coefficient, and the organic carbon-water partition coefficient are critical parameters. It is necessary to consider them as functions of depth. However, if these parameters are treated as functions of depth, the governing differential equation system will be too complicated to be solved analytically. In addition, as discussed above, a non-steady state model is necessary for estimating the long-term flux, which makes the equation system more complicated. Therefore, it is necessary to develop a numerical model to estimate the flux more accurately.

3.5 Conclusions

The model presented in this thesis not only predicts fluxes of organic pollutants quantitatively, but also describes the fluxes qualitatively. This model demonstrates that the diffusive flux is usually more significant than the irrigational flux, and that the resistance that critically controls the diffusive flux is the resistance of the diffusive water boundary layer. This model also identifies that the organic carbon content of sediments, the bioturbation coefficient, the thickness of the diffusive water boundary layer, and the organic carbon-water partition coefficients of organic chemicals are the parameters to

which the flux is sensitive. When estimating the flux of organic pollutants from sediments, researchers need to focus on investigating these parameters.

In this chapter, the sediment bed has been identified as a likely major source of PAHs to the Boston Harbor water. Therefore, sediment pollution management should be the major issue of the Boston Harbor cleanup plan.

APPENDIX

SOLUTION OF THE GOVERNING EQUATION SYSTEM

From Section 2.6.1, the governing equation system consists of two differential equations:

$$\frac{d^2C_{pw}}{dz^2} - \frac{\bar{\alpha} + k_1 \rho K_d}{\bar{D}_B + \bar{D}_m} C_{pw} + \frac{k_1 \rho}{\bar{D}_B + \bar{D}_m} S = 0 \qquad \text{(A-1)}$$

and

$$\frac{d^2S}{dz^2} - \frac{k_1}{D_B} S + \frac{k_1 K_d}{D_B} C_{pw} = 0 \quad . \qquad \text{(A-2)}$$

To solve these equations, Equation (A-1) should be rearranged to express S as a function of C_{pw}:

$$S = -\frac{(\bar{D}_B + \bar{D}_m)}{k_1 \rho} \frac{d^2 C_{pw}}{dz^2} + \left(\frac{\bar{\alpha}}{k_1 \rho} + K_d\right) C_{pw} \; . \qquad \text{(A-3)}$$

Differentiating Equation (A-1) twice gives

$$\frac{d^4 C_{pw}}{dz^4} = \frac{\bar{\alpha} + k_1 \rho k_d}{\bar{D}_B + \bar{D}_m} \frac{d^2 C_{pw}}{dz^2} - \frac{k_1 \rho}{\bar{D}_B + \bar{D}_m} \frac{d^2 S}{dz^2} \; . \qquad \text{(A-4)}$$

Substituting Equation (A-3) into Equation (A-2) and then substituting Equation (A-2) into Equation (A-4) yields

$$\frac{d^4 C_{pw}}{dz^4} - \left(\frac{\bar{\alpha} + k_1 \rho K_d}{\bar{D}_B + \bar{D}_m} + \frac{k_1}{D_B} \right) \frac{d^2 C_{pw}}{dz^2} + \frac{k_1 \bar{\alpha}}{D_B (\bar{D}_B + \bar{D}_m)} C_{pw} = 0 \ . \qquad \text{(A-5)}$$

The general solution of Equation (A-5) is

$$C_{pw}(z) = a_1 e^{\epsilon_1 z} + a_2 e^{-\epsilon_1 z} + a_3 e^{\epsilon_2 z} + a_4 e^{-\epsilon_2 z} \qquad \text{(A-6)}$$

where

$$\epsilon_1^2 = \frac{\frac{\bar{\alpha} + k_1 \rho K_d}{\bar{D}_B + \bar{D}_m} + \frac{k_1}{D_B} - \sqrt{\left(\frac{\bar{\alpha} + k_1 \rho K_d}{\bar{D}_B + \bar{D}_m} + \frac{k_1}{D_B} \right)^2 - \frac{4 k_1 \bar{\alpha}}{D_B (\bar{D}_B + \bar{D}_m)}}}{2} \qquad \text{(A-7a)}$$

and

$$\epsilon_2^2 = \frac{\frac{\bar{\alpha} + k_1 \rho K_d}{\bar{D}_B + \bar{D}_m} + \frac{k_1}{D_B} + \sqrt{\left(\frac{\bar{\alpha} + k_1 \rho K_d}{\bar{D}_B + \bar{D}_m} + \frac{k_1}{D_B} \right)^2 - \frac{4 k_1 \bar{\alpha}}{D_B (\bar{D}_B + \bar{D}_m)}}}{2} \ . \qquad \text{(A-7b)}$$

Assuming $\bar{\alpha} << k_1 \rho K_d$, and $4 k_1 \bar{\alpha} / [D_B (\bar{D}_B + \bar{D}_m)] << [k_1 \rho K_d / (\bar{D}_B + \bar{D}_m) + k_1 / D_B]^2$, Equations (A-7a) and (A-7b) become

$$\epsilon_1^2 = 0 \tag{A-8a}$$

and

$$\epsilon_2^2 = \frac{k_1 \rho K_d}{\bar{D}_B + \bar{D}_m} + \frac{k_1}{D_B} . \tag{A-8b}$$

Therefore, the general solution of Equation (A-5) becomes

$$C_{pw}(z) = a_1 + a_2 z + a_3 e^{\epsilon z} + a_4 e^{-\epsilon z} \tag{A-9}$$

where

$$\epsilon = \sqrt{\frac{k_1 \rho K_d}{\bar{D}_B + \bar{D}_m} + \frac{k_1}{D_B}} . \tag{A-10}$$

The first- and the second-order derivatives of C_{pw} are

$$\frac{dC_{pw}}{dz} = a_2 + a_3 \epsilon e^{\epsilon z} - a_4 \epsilon e^{-\epsilon z} \tag{A-11}$$

and

$$\frac{d^2 C_{pw}}{dz^2} = a_3 \epsilon^2 e^{\epsilon z} + a_4 \epsilon^2 e^{-\epsilon z} . \tag{A-12}$$

By substituting Equation (A-10) into Equation (A-12) and substituting Equations (A-9) and (A-12) into Equation (A-3), the general solution for S may be written as

$$S(z) = a_1 K_d + a_2 K_d z - a_3 \frac{\bar{D}_B + \bar{D}_m}{\rho D_B} e^{\epsilon z} - a_4 \frac{\bar{D}_B + \bar{D}_m}{\rho D_B} e^{-\epsilon z} \qquad \text{(A-13)}$$

under the assumption that $\bar{\alpha}/k_1\rho << K_d$.

And the first-order derivative of S is

$$\frac{dS}{dz} = a_2 K_d - a_3 \frac{\epsilon(\bar{D}_B + \bar{D}_m)}{\rho D_B} e^{\epsilon z} + a_4 \frac{\epsilon(\bar{D}_B + \bar{D}_m)}{\rho D_B} e^{-\epsilon z} . \qquad \text{(A-14)}$$

The first boundary condition is that $C_{pw} = C_0$ at $z = 0$; therefore, Equation (A-9) reduces to

$$a_1 = C_0 - a_3 - a_4 . \qquad \text{(A-15)}$$

The second boundary condition is that $dS/dz = 0$ at $z = 0$. Thus, Equation (A-14) becomes

$$a_2 = \frac{\epsilon(\bar{D}_B + \bar{D}_m)}{K_D \rho D_B}(a_3 - a_4) . \qquad \text{(A-16)}$$

The third boundary condition is that $C_{pw} = C_L$ at z = -L; that is

$$C_L = a_1 - a_2 L + a_3 e^{-\epsilon L} + a_4 e^{\epsilon L} . \qquad \text{(A-17)}$$

Substituting Equations (A-15) and (A-16) into Equation (A-17) results

$$C_L = C_0 + a_3\left[e^{-\epsilon L} - \frac{\epsilon(\bar{D}_B + \bar{D}_m)L}{K_d \rho D_B} - 1\right] + a_4\left[e^{\epsilon L} + \frac{\epsilon(\bar{D}_B + \bar{D}_m)L}{K_d \rho D_B} - 1\right] . \qquad \text{(A-18)}$$

The last boundary condition is that $S = K_d C_{pw}$ at z = -L. S at z = -L can be obtained from Equation (A-13) by substituting -L for z. $K_d C_{pw}$ at z = -L is given by multiplying Equation (A-17) by K_d. Then this boundary condition yields

$$a_4 = -a_3 e^{-2\epsilon L} . \qquad \text{(A-19)}$$

By substituting Equation (A-19) into Equation (A-18), a_3 can be written as

$$a_3 = \frac{-(C_L - C_0)}{\frac{\epsilon(\bar{D}_B + \bar{D}_m)L}{K_d \rho D_B} + 1 + \frac{\epsilon(\bar{D}_B + \bar{D}_m)L}{K_d \rho D_B} e^{-2\epsilon L} - e^{-2\epsilon L}} . \qquad \text{(A-20)}$$

By multiplying the nominator and the denominator of Equation (A-20) by $e^{\epsilon L}$, a_3 becomes

$$a_3 = \frac{-(C_L - C_0)e^{\epsilon L}}{2\left[\frac{\epsilon(\bar{D}_B + \bar{D}_m)L}{D_B \rho K_d}\cosh(\epsilon L) + \sinh(\epsilon L)\right]} \qquad \text{(A-21)}$$

in which $\cosh(\varepsilon L) = \frac{1}{2}(e^{\varepsilon L}+e^{-\varepsilon L})$, and $\sinh(\varepsilon L) = \frac{1}{2}(e^{\varepsilon L}-e^{-\varepsilon L})$.

By substituting Equation (A-21) back into Equation (A-19), a_4 is found to be

$$a_4 = \frac{(C_L - C_0)e^{-\epsilon L}}{2\left[\frac{\epsilon(\bar{D}_B + \bar{D}_m)L}{D_B \rho K_d}\cosh(\epsilon L) + \sinh(\epsilon L)\right]} . \qquad \text{(A-22)}$$

Substituting Equations (A-21) and (A-22) into Equation (A-16) yields

$$a_2 = \frac{-(C_L - C_0)}{L + \frac{D_B \rho K_d}{\epsilon(\bar{D}_B + \bar{D}_m)}\tanh(\epsilon L)} \qquad \text{(A-23)}$$

in which $\tanh(\varepsilon L) = \sinh(\varepsilon L)/\cosh(\varepsilon L)$.

Then a_1 can be obtained by substituting Equations (A-21) and (A-22) into Equation (A-15):

$$a_1 = C_0 + \frac{(C_L - C_0)}{\frac{\epsilon(\bar{D}_B + \bar{D}_m)L}{D_B \rho K_d}\coth(\epsilon L) + 1} \qquad \text{(A-24)}$$

in which $\coth(\varepsilon L) = \cosh(\varepsilon L)/\sinh(\varepsilon L)$.

Finally, the solutions of Equations (A-1) and (A-2) are given by substituting Equations (A-21), (A-22), (A-23), and (A-24) into Equations (A-9) and (A-13):

$$C_{pw} = C_0 + \frac{C_L - C_0}{\frac{\epsilon(\bar{D}_B + \bar{D}_m)L}{D_B \rho K_d}\coth(\epsilon L) + 1} - \frac{C_L - C_0}{L + \frac{D_B \rho K_d}{\epsilon(\bar{D}_B + \bar{D}_m)}\tanh(\epsilon L)} z - \frac{(C_L - C_0)\frac{D_B \rho K_d}{\epsilon(\bar{D}_B + \bar{D}_m)}}{L\cosh(\epsilon L) + \frac{D_B \rho K_d}{\epsilon(\bar{D}_B + \bar{D}_m)}\sinh(\epsilon L)} \sinh\left[\epsilon(L + z)\right] \quad \text{(A-25)}$$

and

$$S = C_0 K_d + \frac{(C_L - C_0) K_d}{\frac{\epsilon(\bar{D}_B + \bar{D}_m)L}{D_B \rho K_d} \coth(\epsilon L) + 1}$$

$$- \frac{(C_L - C_0) K_d}{L + \frac{D_B \rho K_d}{\epsilon(\bar{D}_B + \bar{D}_m)} \tanh(\epsilon L)} z \qquad \text{(A-26)}$$

$$+ \frac{(C_L - C_0) \frac{K_d}{\epsilon}}{L \cosh(\epsilon L) + \frac{D_B \rho K_d}{\epsilon(\bar{D}_B + \bar{D}_m)} \sinh(\epsilon L)} \sinh[\epsilon(L + z)] \, .$$

REFERENCES

Aller, R. C. and J. K. Cochran. 1976. $^{234}Th/^{238}U$ disequilibrium in near-shore sediment: Particle reworking and diagenetic time scales. *Earth Planet. Sci. Lett.* 29:37-50.

Aller, R. C. and D. J. DeMaster. 1984. Estimates of particle flux and reworking at deep-sea floor using $^{234}Th/^{238}U$ disequilibrium. *Earth Planet Sci. Lett.* 67:308-18.

Aller, R. C. and J. Y. Yingst. 1978. Biogeochemistry of tube-dwellings: A study of the sedentary polychaete Amphitrite ornata (Leidy). *J. Mar. Res.* 26:201-54.

Aller, R. C., L. K. Benninger, J. K. Cochran. 1980. Tracking particle-associated processes in nearshore environments by use of $^{234}Th/^{238}U$ disequilibrium. *Earth Planet. Sci. Lett.* 47:161-75.

Aller, R. C., J. Y. Yingst, and W. J. Ullman. 1983. Comparative biogeochemistry of water in intertidal *Onuphis* (polychaeta) and *Upogebia* (crustacea) burrows: temporal patterns and causes. *J. Mar. Res.* 41:571-604.

Archer, D. and A. Devol. 1992. Benthic oxygen fluxes on the Washington shelf and slope: A comparison of *in situ* microelectrode and chamber flux measurements. *Limnol. Oceanogr.* 37:614-29.

Archie, G. E. 1942. The electrical resistivity log as an aid in determining some reservoir characteristics. *Trans. Am. Inst. Min. Metall. Pet. Eng.* 146:54-62.

Atkins, E. R., Jr. and G. H. Smith. 1961. The significance of particle shape in formation resistivity factor-porosity relationships. *J. Pet. Technol.* 13:285-91.

Atlan, Y., B. L. Minssieux, M. Quint, and P. Delvaux. 1969. Conductivité en milieu poreux argileux. Interpretation des diagraphies. In *Third Colloq. Assoc. Rech. Tech. Forage Prod.*, ed. C. R., Paris Ed. Tech.

Battelle Ocean Sciences. 1991. *CSO effect on contamination of Boston Harbor sediments.* MWRA Task Order No. 18. Boston: Massachusetts Water Resources Authority.

Berner, R. A. 1980. *Early Diagenesis: A Theoretical Approach.* Princeton: Princeton University Press, 241pp.

Bosworth, W. S. and L. J. Thibodeaux. 1990. Bioturbation: A facilitator of contaminant transport in bed sediment. *Environmental Progress* 9:211-17.

Boudreau, B. P. 1986. Mathematics of tracer mixing in sediments: II. Nonlocal mixing and biological conveyor-belt phenomena. *Am. J. Sci.* 286:199-238.

Boudreau, B. P. and N. L. Guinasso, Jr. 1982. The influence of a diffusive sublayer on accretion, dissolution, and diagenesis at the sea floor. In *The Dynamic Environment of the Ocean Floor*, ed. K. A. Fanning and F. T. Manheim, 115-42, Lexington: D. C. Heath and Co.

Boudreau, B. P. and M. R. Scott. 1978. A model for the diffusion-controlled growth of deep-sea manganese nodules. *Am. J. Sci.* 278:903-29.

Broman, D., C. Näf, I. Lundbergh, and Y. Zebühr. 1990. An *in situ* study on the distribution, biotransformation and flux of Polycyclic Aromatic Hydrocarbons (PAHs) in an aquatic food chain from the Baltic: An ecotoxicological perspective. *Environmental Toxicology & Chemistry* 9:429-42.

Brownawell, B. J. 1986. The Role of Colloidal Organic Matter in the Marine Geochemistry of PCBs. Dissertation, Massachusetts Institute of Technology-Woods Hole Oceanographic Institute Joint Program.

Butman, B., M. H. Bothner, J. C. Hathaway, H. L. Jenter, H. J. Knebel, F. T. Manheim, and R. P. Signell. 1992. *ContaminantTtransport and Accumulation in Massachusetts Bay and Boston Harbor: A Summary of U.S. Geological Survey Studies*. U.S. Geological Survey Open-File Report 92-202. Woods Hole: U.S. Department of the Interior, Geological Survey.

Chin, Y.-P. and P. M. Gschwend. 1991. The abundance, distribution, and configuration of porewater organic colloids in recent sediments. *Geochim. Cosmochim. Acta* 55:1309-17.

Chin, Y.-P. and P. M. Gschwend. 1992. Partitioning of polycyclic aromatic hydrocarbons to marine porewater organic colloids. *Environ. Sci. Technol.* 26:1821-26.

Chin, Y.-P. and P. M. Gschwend. Department of Civil and Environmental Engineering, Ralph M. Parsons Laboratory, Massachusetts Institute of Technology, Cambridge, Massachusetts.

Chin, Y.-P., A. P. McNichol, and P. M. Gschwend. 1991. Quantification and characterization of pore-water organic colloids. In *Organic Substances in Sediments and Water*, ed. R. A. Baker, 107-26.

Christensen, J. P., A. H. Devol, and W. M. Smethie, Jr. 1984. Biological enhancement of solute exchange between sediments and bottom water on the Washington continental shelf. *Conc. Shelf. Res.* 3:9-23.

Ciceri, G., S. Maran, W. Martinotti, G. Queirazza. 1992. Geochemical cycle of heavy metals in marine coastal area: Benthic flux determination from pore water profiles and in situ measurements using benthic chambers. *Hydrobiologia* 235-236:501.

Cochran, J. K. 1985. Particle mixing rates in sediments of the eastern equatorial Pacific: Evidence from ^{210}Pb, $^{239,240}Pu$ and ^{137}Cs distributions at MANOP sites. *Geochim. Cosmochim. Acta* 49:1195-210.

DeMaster, D. J. and J. K. Cochran. 1982. Particle mixing rates in deep-sea sediments determined from excess ^{210}Pb and ^{32}Si profiles. *Earth Planet. Sci. Lett.* 61:257-71.

Devol, A. H. 1987. Verification of flux measurements made with *in situ* benthic flux chambers. *Deep-Sea Res.* 34:1007-26.

Di Toro, D. M., J. S. Jeris, and D. Ciarcia. 1985. Diffusion and partitioning of hexachlorobiphenyl in sediments. *Environ. Sci. Technol.* 19:1169-76.

Emerson, S., R. Jahnke, and D. Heggie. 1984. Sediment-water exchange in shallow water estuarine sediments. *J. Mar. Res.* 42:709-30.

Goldberg, E. D. and M. Koide. 1962. Geochronological studies of deep-sea sediments by the ionium-thorium method. *Geochim. Cosmochim. Acta* 26:417-50.

Green, M. A., R. C. Aller, and J. Y. Aller. 1992. Experimental evaluation of the influences of biogenic reworking on carbonate preservation in nearshore sediments. *Marine Geology* 107:175-81.

Guinasso, N. L. and D. R. Schink. 1975. Quantitative estimates of biological mixing rates in abyssal sediments. *J. Geophys. Res.* 80:3032-43.

Hale, S. 1974. The Role of Benthic Communities in the Nutrient Cycles of Narragansett Bay. M.S. Thesis, Univ. Rhode Island.

Hammond, D. E. and C. Fuller. 1979. Use of Radon-222 to estimate benthic exchange and atmospheric exchanges in San Francisco Bay. In *San Francisco Bay, the Urbanized Estuary*, ed. T. J. Conomos, 213-30, San Francisco: Amer. Assoc. Adv. Sci.

Hammond, D. E., C. Fuller, D. Harmon, B. Hartman, M. Korosec, L. G. Miller, R. Rea, S. Warren, W. Berelson, and S. W. Hager. 1985. Benthic fluxes in San Francisco Bay. *Hydrobiologia* 129:69-90.

Hayduk, W. and H. Laudie. 1974. Prediction of diffusion coefficients for non-electrolytes in dilute aqueous solutions. *AIChE, J.* 20:611-15.

Imboden, D. M. 1981. Tracers and Mixing in the Aquatic Environment. Habilitation Thesis, Swiss Federal Institute of Technology (EAWAG-ETH).

Jørgensen, B. B. and D. J. Des Marais. 1990. The diffusive boundary layer of sediments: Oxygen microgradients over a microbial mat. *Limnol. Oceanogr.* 35:1343-55.

Jørgensen, B. B. and N. P. Revsbech. 1985. Diffusive boundary layers and the oxygen uptake of sediments and detritus. *Limnol. Oceanogr.* 30:111-22.

Kadko, D. C. 1981. A Detailed Study of Uranium Series Nuclides for Several Sedimentary Regimes of the Pacific. Ph.D. Thesis, Columbia University.

Kadko, D., K. Cochran, and M. Lyle. 1987. The effect of bioturbation and adsorption gradients on solid and dissolved radium profiles in sediments from the eastern equatorial Pacific. *Geochim. Cosmochim. Acta* 51:1613-23.

Kadko, D. and G. R. Heath. 1984. Models of depth-dependent bioturbation at Manop site H in the eastern equatorial Pacific. *Journal of Geophys. Res.* 89:6567-70.

Key, R. M., N. L. Guinasso, and D. R. Schink. 1979. Emanation of Radon-222 from marine sediments. *Mar. Chem.* 7:221-250.

Knebel, H. J. 1993. Sedimentary environments within a glaciated estuarine-inner shelf system: Boston Harbor and Massachusetts Bay. *Marine Geology* 110:7-30.

Knebel, H. J., R. R. Rendigs, and M. H. Bothner. 1991. Modern sedimentary environments in Boston Harbor, Massachusetts. *J. Sedim. Petrol.* 61:791-804.

Levich, V. G. 1962. *Physicochemical Hydrodynamics.* Prentice-Hall.

Lyman, W. J., W. F. Reehl, and D. H. Rosenblatt. 1991. *Handbook of Chemical Property Estimation Methods: Environmental Behavior of Organic Compounds.* Washington, D. C.: American Chemical Society.

Martin, W. R. and F. L. Sayles. 1987. Seasonal cycles of particle and solute transport processes in nearshore sediments: $^{222}Rn/^{226}Ra$ and $^{234}Th/^{238}U$ disequilibrium at a site in Buzzards Bay, MA. *Geochim. Cosmochim. Acta* 51:927-43.

Massachusetts Water Resources Authority. 1988. *Secondary Treatment Facility Plan.*

Massachusetts Water Resources Authority. 1993. *Contaminated Sediments in Boston Harbor.* Boston: U. S. Environmental Protection Agency Region I.

McCaffrey, R. J., A. C. Myers, E. Davey, G. Morrison, M. Bender, N. Luedtke, D. Cullen, P. Froelich, and G. Klinkhammer. 1980. The relation between pore water chemistry and benthic fluxes of nutrients and manganese in Narragansett Bay, Rhode Island. *Limnol. Oceanogr. 25:31-44.*

McGroddy, Susan. Environmental Science Program, University of Massachusetts, Boston.

Menzie-Cura & Associates, Inc. 1991. *Boston Harbor Estimates of Loadings.* Boston: Massachusetts Water Resources Authority.

National Ocean Survey. 1977 reprint. *Tidal current charts, Boston Harbor.* 4th ed., 1974. Rockville, MD: National Oceanic and Atmospheric Administration, U.S. Department of Commerce.

Noshkin, V. E. and V. T. Bowen. 1973. Concentrations and distributions of long-lives fallout radionuclides in open ocean sediments. In *Radioactive Contamination of the Marine Environment,* IAEA Symposium (SM-158/45), 671-86.

Nozaki, Y., J. K. Cochran, K. K. Turekian, and G. Keller. 1977. Radiocarbon and ^{210}Pb distribution in submersible-taken deep-sea cores from Project FAMOUS. *Earth Planet. Sci. Lett.* 34:167-173.

Oddson, J. K., J. Letey, and L. V. Weeks. 1970. Predicted distribution of organic chemicals in solution and adsorbed as a function of position and time for various chemical and soil properties. *Soil Sci. Soc. Am. J.* 34:412-17.

Peng, T. H., W. S. Broecker, and W. H. Berger. 1979. Rates of benthic mixing in deep-sea sediments as determined by radioactive tracers. *Quat. Res.* 11:141-149.

Reid, R. C., J. M. Prausnitz, and T. K. Sherwood. 1977. *The Properties of Gases and Liquids,* 3rd ed. New York: McGraw-Hill, pp. 544-601.

Rex, A. C., K. E. Keay, W. M. Smith, J. J. Cura, C. A. Menzie, M. S. Steinhauer, and M. S. Connor. 1991. *The State of Boston Harbor 1991.* MWRA Environmental Quality Technical Report No. 92-3. Boston: MWRA.

Santschi, P. H., P. Bower, U. P. Nyffeler, A. Azevedo, and W. S. Broecker. 1983. Estimates of the resistance to chemical transport posed by the deep-sea boundary layer. *Limnol. Oceanogr.* 28:899-912.

Santschi, P., P. Höhener, G. Benoit, and M. B. Brink. 1990. Chemical processes at the sediment-water interface. *Marine Chem.* 30:269-315.

Sarmiento, J. L. 1978. A Study of Mixing in the Deep Sea Based on STD Rn-222 and Ra-228 Measurements. Ph.D. Thesis, Columbia University.

Schwarzenbach, R. P., P. M. Gschwend, and D. M. Imboden. 1993. *Environmental Organic Chemistry*. New York: John Wiley & Sons, 681pp.

Shiaris, M. P. and D. Jambard-Sweet. 1986. Polycyclic aromatic hydrocarbons in surficial sediments of Boston Harbour, Massachusetts, USA. *Marine Pollution Bulletin* 17:469-72.

Signell, R. P. and B. Butman. 1992. Modeling tidal exchange and dispersion in Boston Harbor. *J. Geophysical Research* 97:15591-15606.

Smethie, W. M., C. A. Nittrouer, and R. F. L. Self. 1981. The use of radon-222 as a tracer for sediment irrigation and mixing on the Washington continental shelf. *Mar. Geol.* 42:173-200.

Stordal, M. C. and J. W. Johnson. 1982. Comparison of bioturbation rates determined by Pb-210 and plutonium in abyssal cores. *EOS* 63:113.

Streeter, V. L. and E. B. Wylie. 1985. *Fluid Mechanics*, 8th ed. New York: McGraw-Hill, pp. 214.

Sweerts, J.-P. R. A., V. St. Louis, and T. E. Cappenberg. 1989. Oxygen concentration profiles and exchange in sediment cores with circulated overlying water. *Freshwater Biol.* 21:401-09.

Thibodeaux, L. J. 1979. *Chemodynamics: Environmental Movement of Chemicals in Air, Water, and Soil*. New York: John Wiley & Sons, pp. 136-281.

Ullman, W. J. and R. C. Aller. 1982. Diffusion coefficients in nearshore marine sediments. *Limnol. Oceanogr.* 27:552-56.

van Genuchten, M. Th., J. M. Davidson, and P. J. Wierenga. 1974. An evaluation of kinetic and equilibrium equations for the prediction of pesticide movement through porous media. *Soil Sci. Soc. Am. J.* 38:29-35.

Wallace, Gordon. Environmental Science Program, University of Massachusetts, Boston.

Westerink, J. J., J. J. Connor, K. D. Stolzenbach, E. E. Adams, and A. M. Baptista. *1984. TEA: A linear frequency domain finite element model for tidal embayment analysis*. Energy Laboratory Report No. MIT-EL 84-012. Cambridge: Energy laboratory, Massachusetts Institute of Technology.

Wimbush, M. 1976. The physics of the benthic boundary layer. In *The Benthic Boundary Layer*, ed. I. N. McCave, 3-10, New York: Plenum.

Wimbush, M. and W. Munk. 1970. The benthic boundary layer. In *The Sea*, ed. A. E. Maxwell, v.4, 731-58, Wiley-Interscience.

Wong, C. S. 1992. Assessing the Flux of Organic Pollutants from the Sediments of Boston Harbor. S. M. thesis, Massachusetts Institute of Technology, 139 pp.

Wong, C. S., Y.-P. Chin, and P. M. Gschwend. 1992. Sorption of radon-222 to natural sediments. *Geochim. Cosmochim. Acta* 56: 3923-32.

Wu, S.-C., and P. M. Gschwend. 1986. Sorption kinetics of hydrophobic organic compounds to natural sediments and soils. *Environ. Sci. Technol.* 20:717-25.

Wu, S.-C., and P. M. Gschwend. 1988. Numerical modeling of organic compounds to soil and sediment particles. *Water Resources Research* 24:1373-83.